Dwarf Galaxies in Voids: Luminosity, Gas, and Star Formation Properties

A Thesis

Submitted to the Faculty

of

Drexel University

by

Crystal M. Moorman

in partial fulfillment of the

requirements for the degree

of

Doctor of Philosophy

July 2015

Dedications

To my family,

whose love and support

made this work possible.

Acknowledgments

I would first like to thank my advisor, Dr. Michael Vogeley for his support and patience over the years. His guidance throughout my time here made the completion of this work possible. I've really enjoyed the past few years and could not have hoped for a better advisor.

I would also like to thank my dissertation committee of Dr. Gordon Richards, Dr. Adam Lidz, Dr. Robert Gilmore, and Dr. Luis Cruz Cruz for the insight they provided throughout my research. Further, I would like to thank Martha Haynes and Riccardo Giovanelli for providing all of the ALFALFA data, showing me the ropes of radio astronomy, and teaching me to always ask. I thank the ALFALFA collaboration for observing, flagging, and extracting the HI signals used in this work.

I would also like to thank my fellow graduate students for all of their help and support over the years, as well as the much needed distractions. Erica, Austen, Frank, and Vish—From pushing me to work harder, to pulling me away from work when I most needed a break, I don't know what I would've done without all of you. I'd like to thank Erica Smith for editing the pages herein.

A special thank you goes to my entire family for the love and support they have given me throughout my life and for constantly encouraging me to follow my dreams. Mom, Dad, Kevin, and Kayla, you've been my biggest supporters since Day 1. From every softball game, to every concert, all the way up to my Ph.D. defense, you have always been there watching and cheering me on. I am so glad you all were able to be in the audience at my defense. I'm incredibly lucky to have the family I do. I couldn't possibly imagine a better one. Thank you all!

Finally, I'd like to thank Joey for...everything. I don't know what I could say here that would suffice, but I hope you can see what kind of impact you've had over the last 6 years reflected in these pages. And thank you, for your constant reminders that there are other things in life besides the Universe.

Table of Contents

List of Tables

List of Figures

Abstract

Dwarf Galaxies in Voids: Luminosity, Gas, and Star Formation Properties
Crystal M. Moorman
Prof. Michael S. Vogeley

We examine the first statistically-significant sample of dwarf galaxies in voids with matched optical (Sloan Digital Sky Survey), radio (Arecibo Legacy Fast ALFA Survey), and UV (GALEX) observations, which allows us to probe the impact of voids on the luminosity function, HI mass function, and star formation history of galaxies. Large-scale voids provide a unique environment for studying galaxy formation and evolution. Previous theoretical work predicts that galaxies residing in large-scale voids evolve as if they were in a universe with lower matter density, higher dark energy density, and larger Hubble constant. Environmental processes such as ram pressure stripping and galaxy-galaxy interactions should be less important for void galaxies than for galaxies in denser regions (wall galaxies). We measure the effects of environment on two fundamental tests of galaxy formation: the galaxy luminosity function (LF) and the HI mass function (HIMF). In both cases, we find a significant shift towards lower-mass, fainter galaxies in voids. However, we do not detect a dependence on environment of the low-mass/faint end slope of the HIMF and LF. We find that including low surface brightness dwarf galaxies from a blind H I survey steepens the r-band LF substantially, but not enough to reconcile the mismatch predicted low-mass slope of the dark matter halo mass function and the faint-end slope of the observed luminosity function. Utilizing optical, H I, and UV information of nearby galaxies, we determine that specific star formation rates of dwarf galaxies down to $M_r = -13$ are higher in voids than in walls. Furthermore, we downsample the ALFALFA wall galaxy distribution so that its stellar mass distribution matches the stellar mass distribution of void galaxies and determine the environmental dependence of star formation efficiency. We do not find strong evidence that star formation efficiency is dependent on large-scale environment, but this result is likely dependent on the requirements that all galaxies, regardless of environment, have high H I signal-to-noise flux and similar stellar mass distributions.

Chapter 1: Introduction

Large, deep redshift surveys, such as the 2dFGRS (Colless et al., 2001) and the SDSS (York et al., 2000; Abazajian et al., 2009), have allowed for a detailed three dimensional mapping of the Universe, revealing a large-scale structure, often referred to as the "Cosmic Web", containing: filaments, where galaxies live; clusters, where the filaments intersect; and voids, the vast majority of volume in between (Bond et al., 1996). In a redshift slice of the SDSS, depicted in Figure 1.1, we see evidence of the large-scale structure in the local Universe. Based on such detailed maps, theorists are able to reproduce the large-scale structure of the Universe in simulations such as the Millennium Simulation (Springel et al., 2005). Figure 1.2 displays a snapshot of the Millennium Simulation, in which we clearly see filaments, clusters, and large-scale voids predicted by our current cosmological model of the Universe. Voids are the largest-scale structures in the Universe, ranging on scales of 10-50 Mpc. These vast, underdense volumes formed from troughs in initial density perturbations in the early Universe, and gravitationally expel matter outward onto denser regions, forming sheet-like structures which gravitationally collapse forming the filamentary structures observed in the Universe.

Studies of the properties of these void regions estimate that they fill over 60% of the volume of the Universe (Pan et al., 2012; Sheth & van de Weygaert, 2004). Voids have an ellipsoidal shape with a preference for being slightly prolate. While the voids appear largely devoid of matter compared to the filaments and clusters, they are far from being empty. In fact, large-scale cosmic voids are predicted to contain a filamentary structural system similar to a small-scale Cosmic Web (van de Weygaert & van Kampen, 1993; Mathis & White, 2002; Benson et al., 2003; Gottlöber et al., 2003; Sheth & van de Weygaert, 2004; Aragon-Calvo & Szalay, 2013; Ricciardelli et al., 2013; Rieder et al., 2013). Figure 1.3 depicts the results of a dark-matter-only simulation of a single void region (Gottlöber et al., 2003). The simulation predicts intersecting filament structures that mimic the Cosmic Web on smaller scales within the void. Present-epoch voids are thought to form from smaller merging proto-voids. While most of the galaxies making up the walls of the proto-voids are expelled outwards from

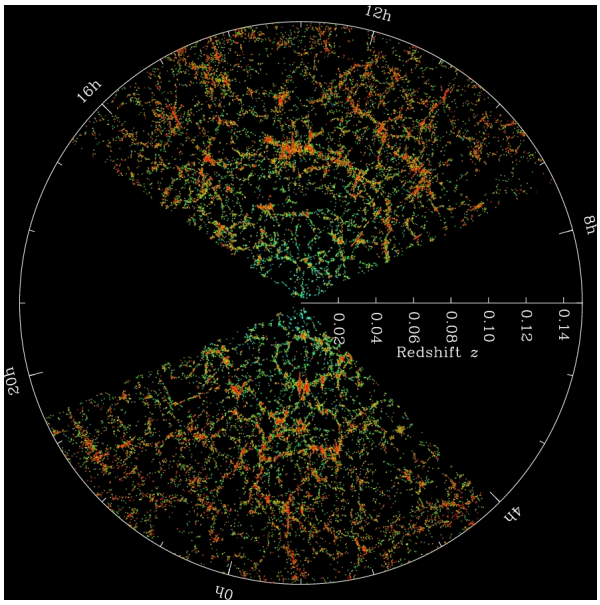

Figure 1.1 Redshift slice of the SDSS showing the large-scale structure of the nearby Universe. Each point represents a single galaxy detected by the SDSS.

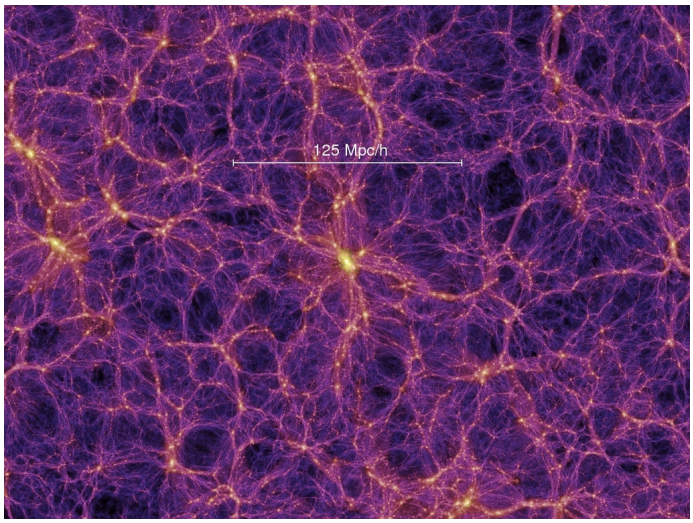

Figure 1.2 Snapshot of the dark-matter-based Millennium Simulation (Springel et al., 2005) showing the Cosmic Web structure predicted by ΛCDM cosmology. Brighter regions indicate regions of higher density, while dark regions are indicative of underdense regions.

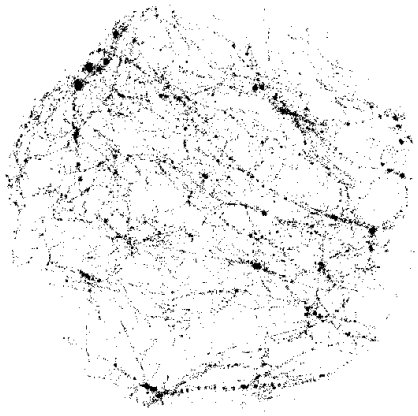

Figure 1.3 This image depicts a dark-matter-only simulation of a cosmic void from Gottlöber et al. (2003). This simulation predicts filament-like structures within the voids similar to the structure of the Cosmic Web.

the center of the merging void, the remainder of the proto-void walls gravitationally collapse into the filamentary structures predicted to reside within the large-scale cosmic voids we observe today (see, for example, Sheth & van de Weygaert (2004)). Evidence of such sub-structure has been observed in actual voids in Kreckel et al. (2012); Beygu et al. (2013), and Alpaslan et al. (2014) revealing that voids are not truly empty, but are simply very underdense. See, for example, Figure 1.4 from Stanonik et al. (2009) who find a set of three distinguishable galaxies in a void enveloped by a single H I cloud. The H I bridge connecting these galaxies points towards the possibility of substructure within voids.

An interesting aspect of cosmic voids is the galaxies residing within, and how their environment affects them. These "void galaxies" are bluer, fainter, and less massive than similar luminosity galaxies in average, higher density environments (Grogin & Geller, 1999; Rojas et al., 2004, 2005; Hoyle et al., 2012). Void galaxies are predicted to evolve as though in a universe with lower matter density, higher dark energy density, and larger Hubble constant (Goldberg & Vogeley, 2004). The drastic underdensities of voids allows void galaxies to evolve relatively undisturbed throughout their lifetimes. Thus, voids provide a unique testbed for galaxy formation simulations.

Simulations based on ΛCDM cosmology predict voids should have a density of 1/10th the mean cosmic density (Hoeft et al., 2006) for galaxies of all brightnesses. These simulations fairly accurately

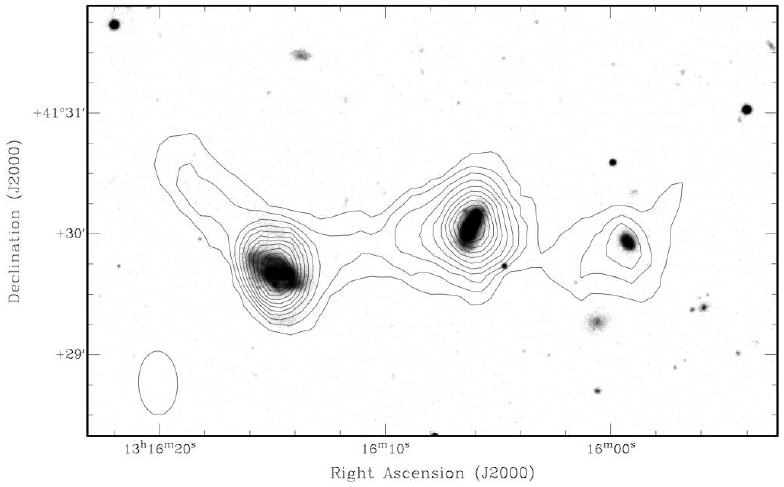

Figure 1.4 H I synthesis image from Stanonik et al. (2009) showing an H I bridge connecting three void galaxies. The H I intensity map, from the VGS, overplotted on a g-band image of three galaxies, from the SDSS, points to the possibility of substructure within voids.

reproduce the distribution of the brightest galaxies, but predict far more low mass, faint galaxies than are observed. Observations by Karachentsev et al. (2004) within the Local Void find the density of bright void galaxies is about 1/10th the mean, but the observed density of the faintest galaxies is closer to 1/100th the cosmic mean. Peebles (2001) describes this discrepancy, often called the "void phenomenon," saying that galaxies of all types respect the same voids.

A strong point of comparison between simulations and observations is through the dark matter halo mass function and the galaxy luminosity and mass functions: the number of galaxies per volume per unit luminosity or H I mass. Dark matter simulations predict the dark matter halo mass function follows a Schechter function of the form

$$\Phi(M) \propto \left(\frac{M}{M^*}\right)^{\alpha} e^{-\frac{M}{M^*}}, \tag{1.1}$$

with a steep slope ($\alpha \simeq -1.8$; e.g. Mathis & White 2002 and Boylan-Kolchin et al. 2009) at the low-mass end, implying a plethora of low mass halos. In Equation 1.1, M may represent e.g. halo mass, galactic mass, or galactic magnitude, and M^* is the characteristic turnover mass/magnitude. Under the assumption that light follows mass, one would expect steep low-mass/faint-end slopes for the

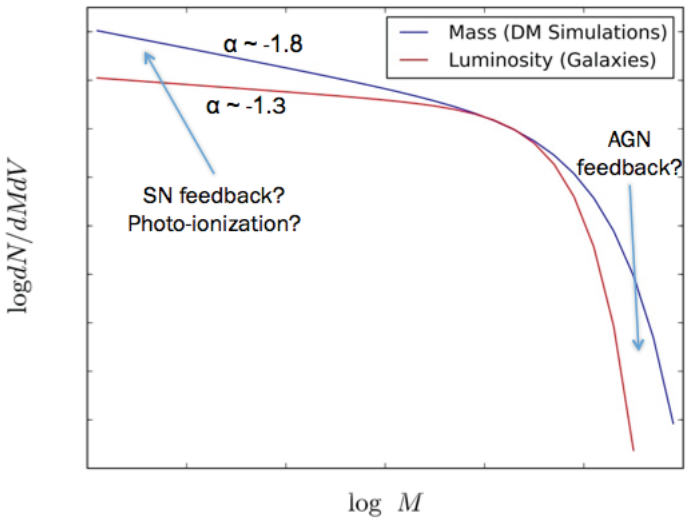

Figure 1.5 This cartoon helps to visualize the discrepancy between dark matter simulation predictions (blue line) and the observed galaxy luminosity function(red line). Star formation in simulated galaxies must be suppressed at the high mass end–likely due to AGN feedback–and low mass end–likely due to photoionization and supernovae feedback–for theory to match observations.

galaxy mass and luminosity functions. However, observations find much shallower ($\alpha \simeq -1.3$) slopes (e.g. Blanton et al. (2005b) and Martin et al. (2010)). This implies that star formation efficiency must decline at low masses and/or the ΛCDM mass function must be altered to accommodate, e.g., warm dark matter. A strong challenge to the ΛCDM cosmology is to explain why the predicted dark matter halo mass function has a different shape than galaxy mass and luminosity functions. See Figure 1.5 for a cartoon visualization of the problem. The discrepancy in predictions versus observations intensifies in voids where the mass function shifts towards lower masses.

In order for ΛCDM theory to match observations, star formation in simulated void dwarf galaxies must be strongly suppressed before and after reionization (Koposov et al., 2009). Two possible physical causes of this star formation suppression are photo-heating of gas in halos by UV radiation, which can cause cool gas to evaporate from the halos (Umemura & Ikeuchi, 1984), and supernova feedback, which could drive out a significant fraction of gas from dwarf galaxies (Couchman & Rees, 1986). Based on semi-analytic models, Benson et al. (2002) suggest that reionization itself could be responsible for the suppression of star formation in dwarf galaxies. Later simulations from Hoeft et al. (2006) find that adding in the effects of photo-heating from the UV background before and after

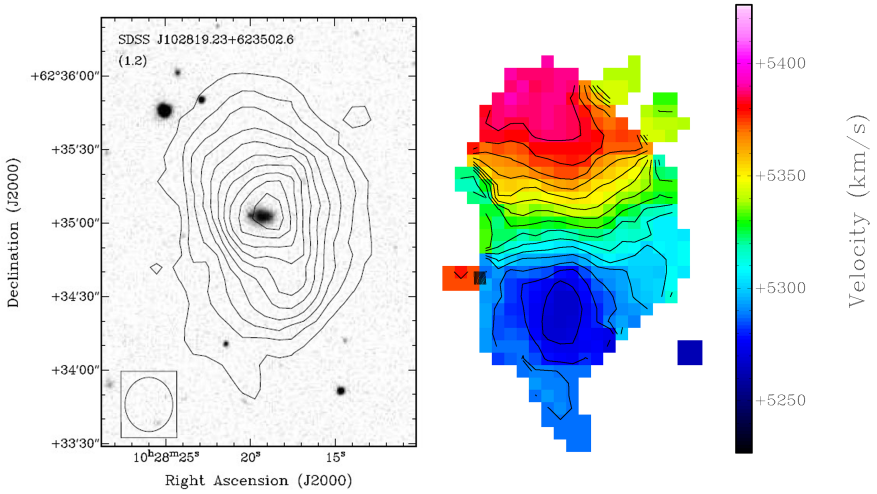

Figure 1.6 H I synthesis image of an SDSS void dwarf galaxy (Stanonik et al., 2009) with an undisturbed H I disk extending far beyond the optical, star forming disk. Left: H I intensity contours overplotted on the g-band image from SDSS. Right: H I velocity map revealing the H I cloud is rotating perpendicular to the plane of the optical disk.

reionization cannot be the sole cause of the lack of void dwarf galaxies. Tassis et al. (2008) simulate dwarf galaxies and find that most of their internal properties are reproduced without including the effects from supernovae feedback.

The strongest predictor of void dwarf galaxies, to date, is the high-resolution simulation of Cen (2011) who use an adaptive mesh refinement hydrodynamic simulation to simulate large void and cluster regions. They predict that galaxies in the local Universe will have higher specific star formation rates, due to the entropy of gas in void dwarfs being lower than the threshold at which the gas cooling time exceeds a Hubble time. Observations indicate that void galaxies indeed have higher star formation rates than galaxies of similar luminosity in denser regions (Rojas et al., 2005; Kreckel et al., 2012). A variety of methods of estimating star formation rates exist in the literature, with different methods probing star formation on different time scales. Two methods of estimating star formation utilized within this work use UV photometry from the Galaxy Evolution Explorer (GALEX Martin et al., 2005), and Hα spectroscopy from the SDSS. Active star formation seen in void dwarfs at late times implies a presence of cool gas around these galaxies. Therefore, the gas properties of dwarf galaxies in voids pose a crucial test.

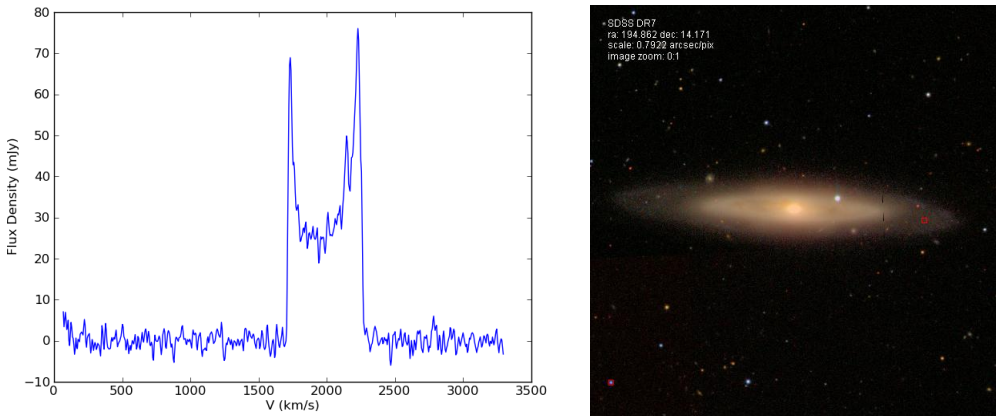

Figure 1.7 The 21cm-line profile of a H I cloud detected by ALFALFA (left) and an image of its optical counterpart from SDSS (right).

If star formation suppression and observational selection effects are indeed responsible for the lack of void dwarfs, we should observe a population of low-mass, optically dark, H I-rich galaxies at radio wavelengths. Kreckel et al. (2011) simulate a 30 Mpc radius void and predict an excess of ultra low luminosity galaxies in the void center using the adaptive mesh refinement hydrodynamic algorithm used in Cen (2011). The matter distribution of dwarf galaxies detectable by their H I (with high S/N ratios) is dominated by their neutral gas. For instance, Stanonik et al. (2009) identify a stellar-poor, void dwarf galaxy from the SDSS with an extended H I disk, shown in Figure 1.6 that remains unaffected due to its nearest known neighbor residing $\sim$ 4 Mpc away. The relatively shallow potentials of dwarf galaxies make them more fragile and thus more sensitive to the effects of interactions and feedback that affect the star formation rate. Dwarf galaxies residing in voids evolve with relatively undisturbed H I clouds because of the rarity of galaxy-galaxy interactions. Therefore, we expect to see a trend with the efficiency of star formation with stellar mass in voids, with optically dark galaxies at the low stellar mass end. While H I imaging surveys, such as the one used to detect the H I clouds in Figures 1.4 and 1.6, may detect previously unobserved H I clouds, H I imaging is costly in terms of telescope time and requires pointed observations. Quickly and efficiently detecting H I-rich sources over a wide, deep volume requires a blind H I survey. Blind H I surveys scan the sky for neutral gas sources via the 21cm emission line. The 21cm-line itself is

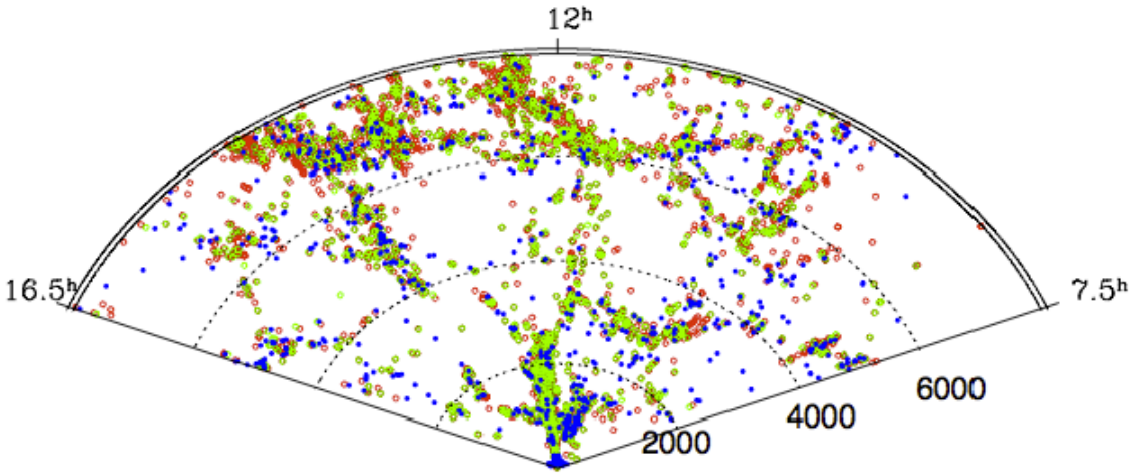

Figure 1.8 Cone diagram of galaxies detected in H I only (blue), optical only (red), and both (green) from Haynes (2008). Blind H I surveys trace the same large-scale structure as optical surveys.

an intrinsically narrow line broadened by galaxy kinematics and shifted in frequency due to galaxy recessional velocities typically resulting in a double horned profile. Within this work, we utilize the blind H I Arecibo Legacy Fast Arecibo L-band Feed Array (ALFALFA Giovanelli et al., 2005a,b) survey to obtain H I information. Figure 1.7 shows the H I profile of an ALFALFA detection with an image of its optical counterpart from the SDSS. Predictions for a population of very faint galaxies are further enhanced by Blanton et al. (2005b), who find that correcting for the effects of a population of low-surface brightness galaxies in the SDSS increases the faint-end slope of the optical luminosity function. Based on these results, the existence of a population of optically-dark, H I-rich galaxies seems likely; however, Basilakos et al. (2007) and Haynes (2008) find that a population large enough to reconcile theory with observations does not exist. That is, with the exception of only a few optically-dark galaxies (Giovanelli et al., 2013), evidence of a population of gas-rich, optically-dark, void dwarf galaxies numerous enough to reconcile dwarf galaxy counts with ΛCDM does not exist. H I detections respect the same voids identified in optical and IR surveys, as seen in Figure 1.8.

To estimate the number density of H I-rich dwarf galaxies, we turn to the H I mass function (HIMF) of ALFALFA detections. Previous measurements of the HIMF have focused primarily on

groups, clusters, and "field" galaxies leaving the shape of the void HIMF almost unknown (Rosenberg & Schneider, 2002; Springob et al., 2005; Zwaan et al., 2005; Stierwalt et al., 2009; Martin, 2011; Pisano et al., 2011). These studies used surveys that included only galaxies with H I masses down to $\sim 10^8 M_\odot$. Previous estimates of the HIMF vary depending on how environment is defined, where "void" ranges anywhere from locally isolated galaxies to large-scale structure underdensities. It is, therefore, imperative that we provide a clear definition of "void" as it is used in this work. Voids are dynamically-distinct regions which formed by gravity through the expansion of troughs in the initial density perturbations in the early Universe. They are extremely underdense ($\delta < -0.8$) regions with flat radial density profiles out to the void edges. We use the void catalog of Pan et al. (2012) who identify voids using the VoidFinder algorithm of Hoyle & Vogeley (2002) (also see El-Ad & Piran 1997). VoidFinder searches for voids by finding regions less dense than filaments and requires that the third nearest neighbor of an observed galaxy within a candidate void must be at least $7h^{-1}Mpc$ away. VoidFinder temporarily removes the potential void galaxies from the map and proceeds to grow spheres within the empty regions. A candidate void sphere is considered a true void if it has a minimum radius $r > 10h^{-1}$ Mpc. Where applicable, we combine overlapping spheres to form ellipsoidal voids, and we refer to the galaxies residing in these voids as "void galaxies". Galaxies residing outside of the voids are denoted "wall galaxies."

Much like the HIMF, we can test galaxy formation models down to the dwarf galaxy regime by investigating the environmental dependence of the optical luminosity function (LF) using optical data from the SDSS. Again, previous environmental results of the optical LF depend on how environment is defined. See, for example, Hoyle et al. (2005); Tempel et al. (2011) and McNaught-Roberts et al. (2014) for galaxy LFs with various definitions of "voids," Eke et al. (2004); Tully (2005) and Yang et al. (2009) for the LF of galaxy groups, and De Propris et al. (2003); Durret et al. (2011); McNaught-Roberts et al. (2014) and Martinet et al. (2014b) for the LFs of galaxy clusters. We discuss these previous results in more detail within the following chapters.

Regardless of definition, the trend of lower mass, fainter galaxies with decreasing density holds true for both the HIMF and LF. However, the faint and low-mass end slopes vary across the literature

depending on the sample used and the methods used to identify environment. Given the discrepancies between the expected dwarf galaxy density distribution in voids, based on ΛCDM simulations, and the observed dwarf galaxy density distribution in actual voids, the shape of the low luminosity/mass end of the LF and HIMF can provide good tests of models for formation and feedback in dwarf galaxies.

In the chapters that follow, we shed some light on the discrepancy between theory and observations of the number of dwarf galaxies in cosmic voids using the SDSS, ALFALFA, and GALEX Surveys. In Chapter 2, we present our methods and results for estimating the HIMF and velocity width function (WF) of void and wall detections in the ALFALFA Survey. We examine the impact of environment on the optical LF of optically selected galaxies down to $M_r = -13$ in Chapter 3. Furthermore, we present the environmental effects on the optical LF on H I selected galaxies and investigate the sample selection effects that lead to differing shapes of the LFs of H I vs. optically selected galaxies. In Chapter 4, we estimate the star formation efficiency of void dwarf galaxies and compare these estimates to those of similar-mass galaxies in denser regions. Finally, we present our conclusions in Chapter 5. Unless otherwise specified, we adopt the distances, D_i; H I masses, $M_{\rm HI}$; velocity widths, W_{50}; and integrated H I fluxes, $S_{\rm int}$ reported in the $\alpha.40$ catalogue (Haynes et al., 2011), as well as the ALFALFA adopted Hubble constant $h = H_0/100$ km s^{-1}Mpc$^{-1} = 0.7$. Where comoving coordinates are determined, we assume $\Omega_{\rm m} = 0.26$ and $\Omega_\Lambda = 0.74$.

Chapter 2: The H I Mass Function and Velocity Width Function of Void Galaxies in the ALFALFA Survey

Abstract

We measure the H I mass function (HIMF) and velocity width function (WF) across environments over a range of masses, $7.2 < \log(M_{\rm HI}/M_\odot) < 10.8$, and profile widths, $1.3\log(\mathrm{km\ s^{-1}}) < \log(W) < 2.9\log(\mathrm{km\ s^{-1}})$, using a catalog of ∼7,300 H I-selected galaxies from the ALFALFA Survey, located in the region of sky where ALFALFA and SDSS (Data Release 7) North overlap. We divide our galaxy sample into those that reside in large-scale voids (void galaxies) and those that live in denser regions (wall galaxies). We find the void HIMF to be well fit by a Schechter function with normalization $\Phi^* = (1.37 \pm 0.1) \times 10^{-2} h^3 \mathrm{Mpc}^{-3}$, characteristic mass $\log(M^*_{\rm HI}/M_\odot) + 2\log h_{70} = 9.86 \pm 0.02$, and low-mass-end slope $\alpha = -1.29 \pm 0.02$. Similarly, for wall galaxies, we find best-fitting parameters $\Phi^* = (1.82 \pm 0.03) \times 10^{-2} h^3 \mathrm{Mpc}^{-3}$, $\log(M^*_{\rm HI}/M_\odot) + 2\log h_{70} = 10.00 \pm 0.01$, and $\alpha = -1.35 \pm 0.01$. We conclude that void galaxies typically have slightly lower H I masses than their non-void counterparts, which is in agreement with the dark matter halo mass function shift in voids assuming a simple relationship between DM mass and H I mass. We also find that the low-mass slope of the void HIMF is similar to that of the wall HIMF suggesting that there is either no excess of low-mass galaxies in voids or there is an abundance of intermediate H I mass galaxies. We fit a modified Schechter function to the ALFALFA void WF and determine its best-fitting parameters to be $\Phi^* = 0.21 \pm 0.1 h^3 \mathrm{Mpc}^{-3}$, $\log(W^*) = 2.13 \pm 0.3$, $\alpha = 0.52 \pm 0.5$ and high-width slope $\beta = 1.3 \pm 0.4$. For wall galaxies, the WF parameters are: $\Phi^* = 0.022 \pm 0.009 h^3 \mathrm{Mpc}^{-3}$, $\log(W^*) = 2.62 \pm 0.5$, $\alpha = -0.64 \pm 0.2$ and $\beta = 3.58 \pm 1.5$. Because of large uncertainties on the void and wall width functions, we cannot conclude whether the WF is dependent on the environment.

2.1 Introduction

The advent of large redshift surveys has allowed for a detailed mapping of the nearby Universe, revealing a variety of environments within which galaxies reside: rich clusters, groups, filaments,

and the underdense regions filling the volume between. The starkly underdense regions filling most of our Universe, called "voids," are relatively pristine environments for studying galaxy evolution and formation, because gas-stripping galaxy interactions are exceptionally rare. The study of galaxies living in these dynamically distinct environments is therefore crucial to understanding the processes that affect galaxy formation.

A variety of definitions of "voids" exist in the literature (El-Ad et al., 1997; El-Ad & Piran, 1997, 2000; Plionis & Basilakos, 2002; Sheth & van de Weygaert, 2004; Hoyle & Vogeley, 2004; Rojas et al., 2004; Blanton et al., 2005a; Patiri et al., 2006; von Benda-Beckmann & Müller, 2008; Melnyk et al., 2009; Karachentseva et al., 2010; Park et al., 2012; Sutter et al., 2012; Elyiv et al., 2013) ranging anywhere from locally isolated galaxies to extreme large-scale underdensities. We wish to focus on large-scale structures and define voids as regions with density contrast $\delta < -0.8$ in optically selected bright galaxies ($\sim L^*$) with a minimum radius of $10h^{-1}$Mpc. That is, voids are not samples of "isolated" galaxies identified by visual inspection (e.g. Melnyk et al. 2009; Karachentseva et al. 2010). Large voids with density contrast $\delta < -0.8$ naturally arise via gravitational instability (Sheth & van de Weygaert, 2004). These large-scale voids may be identified using a variety of void-finding algorithms including Kauffmann & Fairall (1991); El-Ad & Piran (1997); Aikio & Maehoenen (1998); Schaap & van de Weygaert (2000); Hoyle & Vogeley (2002); Neyrinck (2008); Aragon-Calvo et al. (2010). A comparison of different void-finding techniques may be found in Colberg et al. (2008). Studies reveal that large-scale voids occupy approximately 60 percent of the volume of our Universe (Pan et al. 2012) and the galaxies within these voids form substructure that is evident in both simulations and observations (Mathis & White, 2002; Benson et al., 2003; Gottlöber et al., 2003; van de Weygaert et al., 2010; Aragon-Calvo & Szalay, 2013).

Simulations of the Λ cold dark matter (ΛCDM) cosmological model predict an abundance of low-mass dark matter halos (DMH) across all environments with a shift in the DMH mass function to lower masses in voids (Goldberg et al., 2005). If we assume a linear relationship between DMH mass, galaxy light, and baryonic mass, then we expect to see an abundance of low-mass, low-luminosity galaxies in voids and denser regions as well. We know this assumption to be false, because star

formation is suppressed at both high- and low-mass ends by e.g. AGN feedback and supernovae feedback, respectively. Given the phenomena affecting the low-mass ends, one might expect the low-mass slopes to vary across environment. For instance, ram pressure stripping removes cold gas from low-mass galaxies in clusters, but this phenomenon would not be as prevalent in void galaxies. One might also expect the effects from supernovae to set in at a particular mass, yet it seems to affect both the void and wall galaxies similarly, regardless of the shift in characteristic mass between environments. To date, there is no evidence for a difference between the low-mass slopes in voids versus denser regions, but we find this odd given the phenomena affecting the low-mass slopes. Critical points of comparison between the ΛCDM structure formation model and galaxy observations are found in the faint end of the galaxy luminosity function (LF) and the low-mass end of the neutral hydrogen mass function (HIMF). The global DMH mass function is predicted to follow a Schechter function (Press & Schechter, 1974) with a very steep low-mass end slope ($\alpha \simeq -1.8$; Mathis & White 2002), but measurements of the observed faint and low-mass end slopes of the global galaxy LF (e.g. Blanton et al. 2005b) and HIMF (e.g. Martin et al. 2010) are significantly shallower ($\alpha \simeq -1.3$). While Blanton et al. (2005b) note that selection effects of low-surface brightness galaxies could cause the slope to flatten, their estimate of the corrected slope is still too shallow ($\alpha \simeq -1.5$) to match DMH predictions.

Studies focusing on galaxies in large-scale voids indicate that void galaxies are generally bluer, fainter, later-type, and have higher star formation rates (SFRs) per stellar mass than their counterparts in denser regions (Rojas et al., 2004, 2005; Hoyle et al., 2005; Blanton et al., 2005a; Croton et al., 2005; Park et al., 2007; Croton & Farrar, 2008; Cen, 2011; Kreckel et al., 2011; Hoyle et al., 2012; Geha et al., 2012). Optical observations also reveal a discrepancy between the number of low-luminosity/low-mass (dwarf) galaxies and the predicted number of low-mass halos (e.g. Karachentsev et al. 2004). This discrepancy is part of the void problem mentioned in Peebles (2001) which states that all types of galaxies appear to respect the voids, whereas ΛCDM predicts that voids should contain an abundance of low-mass objects. ΛCDM simulations (Warren et al., 2006; Hoeft et al., 2006) predict that voids have a density of low-mass halos that is 1/10 that of the cosmic mean.

This is consistent with bright galaxies in large-scale voids (Hoyle & Vogeley, 2004; Conroy et al., 2005; Hoeft et al., 2006; Tinker et al., 2008); however, optical observations do not reveal a plethora of faint galaxies in voids (e.g. Karachentsev et al. 2004, in the Local Void). Among the attempts to identify an abundance of dwarf galaxies in voids are Grogin & Geller (1999); Blanton et al. (2003b); Hoyle et al. (2005); Croton et al. (2005) and Hoyle et al. (2012) who investigate the environmental dependence of the LF of optically selected galaxies. These results vary depending on the definition of environment used in the work, and none identifies an excess of dwarf galaxies in extreme voids. Koposov et al. (2009) propose that the lack of dwarf galaxies in voids found in optically selected samples could be due to strong star formation suppression of void galaxies, before and after reionization, as well as observational selection effects. If these effects are responsible, we would expect a population of low-mass, optically dark, yet H I-rich galaxies to exist. Such a population should be detectable by their gas.

The results of Basilakos et al. (2007) indicate that low-H I-mass galaxies seem to avoid underdense regions. To date, with only a handful of exceptions (e.g. Giovanelli et al. 2013), evidence of a population of gas-rich, optically dark galaxies large enough to reconcile dwarf galaxy counts with ΛCDM models does not exist (Haynes, 2008). The first generation of blind H I surveys were typically shallow and unable to detect H I clouds over a large range of masses. Small number statistics and uncertainties in distances of nearby galaxies (Masters et al., 2004) made determining large-scale environmental effects on galactic H I content difficult. Haynes et al. (1984) show that environment has an impact on the H I content of galaxies, where galaxies in clusters tend to be more H I deficient than "field" galaxies. Using the Arecibo Dual Beam Survey (Rosenberg & Schneider, 2000), Rosenberg & Schneider (2002) corroborate this work hinting at the influence of large-scale structure on the HIMF. These authors show that, for galaxies in the Virgo Cluster, the low-mass-end slope of the HIMF becomes shallower.

With the onset of deeper, large-area blind-H I surveys, we are able to better constrain the environmental impact on a galaxy's H I content. Headway has been made on determining the environmental dependence of the HIMF of H I clouds from second generation surveys by Zwaan et al. (2005) using

the H I Parkes All Sky Survey (HIPASS; Meyer et al. 2004) and by Springob et al. (2005), Stierwalt et al. (2009), and Martin (2011) using various data releases from the Arecibo Legacy Fast ALFA (ALFALFA) Survey (Giovanelli et al., 2005b,a). We find in the literature that the low-mass-end slope of the HIMF may become steeper or shallower with density depending on sample selection and the definition of environment. See, for example, Zwaan et al. (2005), Springob et al. (2005), Toribio et al. (2011a), and Martin (2011) who use either H I- or optically selected samples to define the environment of H I-selected galaxies on scales ranging from locally isolated galaxies to low-density environments on scales of ∼10Mpc. We discuss the conflicting HIMF results in more detail below in Section 2.4.1.

Another point of comparison between ΛCDM simulations and observations is through estimating corrections to the velocity width function (WF) to obtain a circular velocity function (CVF), although this comparison is less direct. CDM models predict the CVFs of halos to follow a power law with a steep slope of $\alpha \sim -3$ (Klypin et al., 1999; Zavala et al., 2009). Observations do not confirm this prediction. In fact, the observed velocity functions closely resemble Schechter functions with much shallower low-velocity slopes (e.g. Sheth et al. 2003; Zwaan et al. 2010; Papastergis et al. 2011). The observed velocity function of galaxies may be obtained indirectly through optical photometry or spectra using of the Tully–Fisher relation (Desai et al., 2004; Abramson et al., 2013) or through direct observations of the velocity width using H I surveys (Zwaan et al. (2010) with HIPASS; Papastergis et al. (2011) with ALFALFA).

A comparison of previous work on both optically selected void galaxies and H I-selected galaxies reveal similar characteristics between these two samples. Toribio & Solanes (2009) investigate properties of "isolated" H I-selected galaxies from ALFALFA and find that these remote objects tend to be blue, late-type, star-forming galaxies. Huang et al. (2012a) compare properties of H I- and optically selected samples found within the volume covered by both Sloan Digital Sky Survey Data Release 7 (SDSS DR7) and ALFALFA and find that for a given stellar mass, H I-selected galaxies generally have higher star formation rates (SFRs) and specific SFRs, yet lower star formation efficiencies. Rojas et al. (2004); Hoyle et al. (2005, 2012) find that optically selected void galaxies are generally

bluer, fainter, late-type, and have higher specific SFRs than galaxies in denser regions. Given the similarities in the characteristics of galaxies detected by blind H I surveys and void galaxies found using optically selected data, we would expect that H I surveys yield a higher fraction of void galaxy detections than that of galaxies found using optical surveys. As discussed in more detail below, we find that 35 percent of ALFALFA detections reside in large-scale voids, while in the same volume (out to $z \sim 0.5$) 26 percent of magnitude-limited SDSS detections are classified as void galaxies.

In this work, we study the HIMF and WF of ALFALFA galaxies that lie in deep large-scale voids. In Section 2.2 we discuss our void catalogue and H I-selected sample. In Section 2.3 we present our methods and results for the HIMF and WF of void galaxies. We compare our results to previous work in Section 2.4 and summarize our results in Section 2.5. Unless otherwise specified, we adopt the distances, D_i; H I masses, $M_{\rm HI}$; velocity widths, W_{50}; and integrated H I fluxes, $S_{\rm int}$ reported in the $\alpha.40$ catalogue (Haynes et al., 2011), as well as the ALFALFA adopted Hubble constant $h = H_0/100$ km s^{-1}Mpc$^{-1} = 0.7$. Where comoving coordinates are determined, we assume $\Omega_{\rm m} = 0.26$ and $\Omega_\Lambda = 0.74$.

2.2 Data

2.2.1 Finding A Void Galaxy Sample Using SDSS DR7

The SDSS DR7 (Abazajian et al., 2009) is a wide-field multi-band imaging and spectroscopic survey that uses drift scanning to map 8,032 deg^2 of the northern sky. SDSS utilizes the 2.5m telescope located at Apache Point Observatory in New Mexico, allowing it to cover $\sim 10^4$ deg^2 of the Northern hemisphere in the five band SDSS system – u, g, r, i, and z (Fukugita et al., 1996; Gunn et al., 1998). Galaxies with Petrosian r-band magnitude $r < 17.77$ are selected for spectroscopic follow up (Lupton et al., 2001; Strauss et al., 2002). Spectra obtained through the SDSS are taken using two double fiber-fed spectrographs and fiber plug plates covering a portion of the sky $1^\circ.49$ in radius with a minimum fiber separation of 55 arcsec (Blanton et al., 2003a).

The Korea Institute for Advanced Study Value-Added Galaxy Catalog (KIAS-VAGC) of Choi et al. (2010) is based on the SDSS DR7. This consists of 583,946 galaxies with $10 < r < 17.6$ from the NYU-VAGC Large Scale Structure Sample (brvoid0; Blanton et al. 2005c), 114,303 galaxies with

$17.6 < r < 17.77$ from NYU-VAGC (full0), and 10,497 galaxies from either UZC, PSCz, RC3, or 2dF which were excluded by SDSS. We omit 929 objects, mostly deblended outlying parts of large galaxies, for a total of 707,817 galaxies.

To create a void catalogue, Pan et al. (2012) employ the void-finding algorithm of Hoyle & Vogeley (2002), called VoidFinder – based on the El-Ad & Piran (1997) approach – on a volume limited sample of the KIAS-VAGC. The volume-limited sample we use consists of 120,606 galaxies within $z = 0.107$ corresponding to an absolute magnitude limit of $M_r < -20.09$. VoidFinder uses a nearest neighbors algorithm to identify volume-limited galaxies in low density regions. If a galaxy's third nearest neighbor is at least $6.3h^{-1}$ Mpc away, it is considered a potential void galaxy and is removed from the sample. VoidFinder then grows spheres in the empty spaces until the spheres are bounded by four remaining galaxies. If the sphere has a radius larger than $10h^{-1}$ Mpc it is considered a void, otherwise it is discarded. Each void is comprised of multiple spheres and we define the center of each void to be the center of the sphere with the maximal radius. The VoidFinder parameters were chosen to select void regions with density contrast $\delta < -0.8$. For a more detailed description of how VoidFinder works, see Hoyle & Vogeley (2002) and Pan et al. (2012).

Pan et al. (2012) identify 1,054 voids with radii greater than $10h^{-1}$ Mpc occupying approximately 60 percent of the volume covered by the SDSS DR7 out to $z = 0.107$. These voids have less than 10 percent of the average density out to the walls. They are ellipsoidal in shape with a preference for being prolate. The median effective void radius is $15h^{-1}$ Mpc with over half of the volume consisting of voids with effective radius greater than $17.8h^{-1}$ Mpc. Figure 2.1 shows a $10h^{-1}$ Mpc thick redshift slice of the volume-limited sample used to identify large-scale voids, centered at R.A.=12^h, Dec=10°. Wall galaxies in the volume-limited sample are shown as black points and void galaxies are shown as red crosses. The circles depict the intersection of the maximal spheres of each void with the center of the slice.

To account for the effects of the local peculiar velocity field, we apply the flow model of Masters (2005; hereafter, FlowModel) to the KIAS-VAGC galaxies. We then create a volume-limited sample with absolute magnitude limit $M_r < -20.09$. We apply the VoidFinder algorithm to this volume-

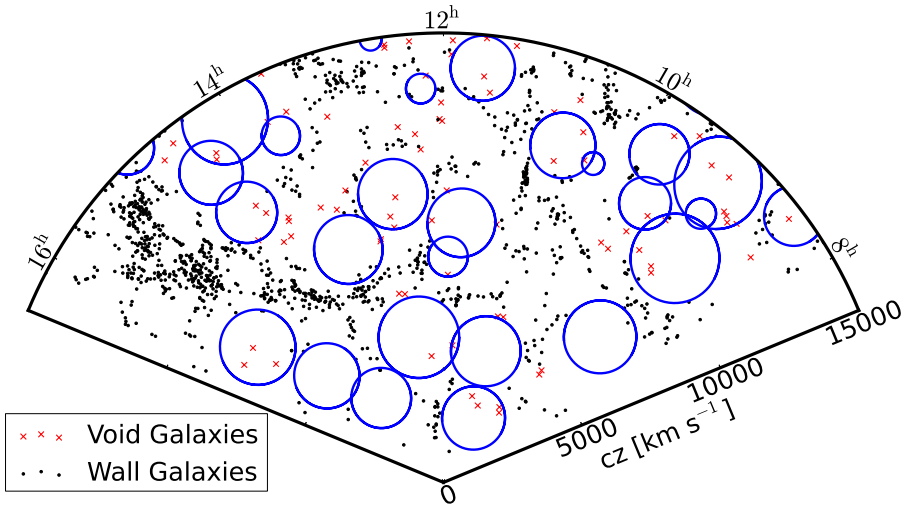

Figure 2.1 $10h^{-1}$Mpc slab of SDSS DR7 volume-limited sample. Void galaxies are displayed as red crosses, and wall galaxies are displayed as black points. The circles depict the intersection of only the maximal sphere of a void with the center of the slice. Note that voids tend to be ellipsoidal rather than spherical, thus void galaxies may appear outside of the maximal sphere drawn.

limited sample. See Figure 2.2 for the resulting void locations after applying the FlowModel to the KIAS sample compared to those of Pan et al. (2012). This figure depicts the same region of sky shown in Figure 2.1 with the intersection of the center of the slab with the modified void catalogue alongside the intersection of the slab with the Pan et al. (2012) void catalogue. Comparing galaxy locations to the void catalogue found using the FlowModel does not result in a significant difference in void and wall galaxy samples (see Figure 2.3). Because we do not notice a significant difference between the void catalogue of Pan et al. (2012) and our void catalogue, we use the void catalogue of Pan et al. (2012) for consistency.

2.2.2 The ALFALFA Sample

The ALFALFA Survey is a large-area, blind extragalactic H I survey that will detect >30,000 galaxies out to $cz \sim 18000$km s^{-1} with a median redshift of ∼8,000 km s^{-1}, over 7000 deg^2 of sky upon completion. ALFALFA has a 5σ detection limit of 0.72 Jy km s^{-1} for a source with a profile width of 200 km s^{-1} (Giovanelli et al., 2005b) and allows for the detection of galaxies with H I masses down to $M_{\rm HI} = 10^8 {\rm M}_\odot$ out to 40 Mpc. The most recent release of the ALFALFA Survey (Giovanelli et al.,

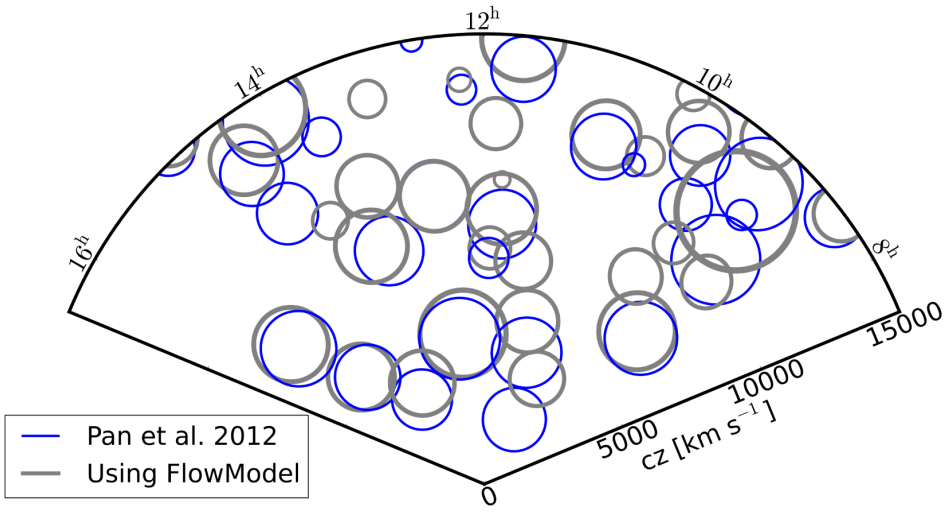

Figure 2.2 We process the KIAS data set through the FlowModel of Masters (2005) and obtain a new volume-limited sample to run through VoidFinder. This figure depicts the intersection of the center of a $10h^{-1}$Mpc slab centered at R.A.=12^h, Dec=10° with the resulting maximal spheres of this new set of voids (gray circles). For comparison, we also show the intersection of the slab with the maximal void spheres of the Pan et al. 2012 void catalogue (blue circles) found using an SDSS DR7 volume-limited sample.

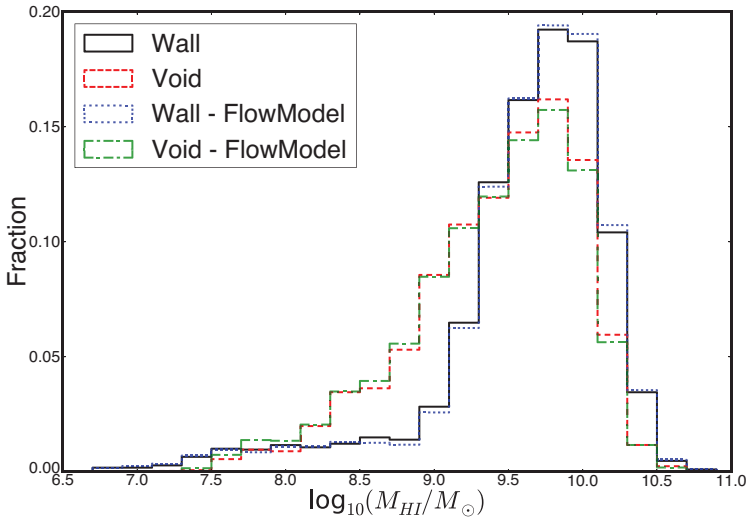

Figure 2.3 H I mass distribution of void (red dashed line) and wall (black solid line) galaxies as determined by the Pan et al. (2012) void catalogue and the H I mass distribution of void (green dash-dotted line) and wall (blue dotted line) galaxies as determined by the modified void catalogue obtained using the FlowModel of Masters (2005).

2005b,a), the $\alpha.40$ catalogue of Haynes et al. (2011), covers $\sim$2800 deg^2, approximately 40 percent of the final survey area. This catalogue, which consists of 15,041 H I detections and contains previously released catalogues (Giovanelli et al., 2007; Saintonge et al., 2008; Kent et al., 2008; Stierwalt et al., 2009; Martin et al., 2009), covers two regions in the Northern Galactic hemisphere, referred to as the Spring Sky, (07^h30^m <R.A.< 16^h30^m, 04° < Dec < 16° and 24° < Dec < 28°), and two in the Southern Galactic hemisphere, referred to as the Fall Sky, (22^h <R.A.< 03^h, 14° < Dec < 16° and 24° < Dec < 32°). Haynes et al. (2011) categorize the confidently detected H I sources of the $\alpha.40$ catalogue into one of the following three categories: Code 1 objects are reliable detections with high signal-to-noise ratio (S/N>6.5), Code 2 objects have lower S/N, but coincide with optical counterparts with known redshift similar to that of the H I detection, and Code 9 objects which correspond to high-velocity clouds.

Our interest lies in identifying reliable H I detections in voids. To identify $R > 10h^{-1}$Mpc voids, VoidFinder requires wide angular coverage in spectroscopy, which, for SDSS DR7, is only possible in the North. This region of sky corresponds to the ALFALFA Spring Sky; thus, we reduce our sample to objects included only in the Spring Sky. We further limit ourselves to Code 1 detections which lie within the redshift range $cz \leq 15000$km s^{-1}; beyond this redshift range, the FAA radar at the San Juan Airport interferes with ALFALFA's detection ability over a range of frequencies corresponding to a shell of thickness $\sim$10 Mpc. Our final sample contains 8,118 H I sources over an area of 2,077 deg^2 corresponding to $\sim$ 30 percent of the final projected survey area.

To ensure that we are using an unbiased H I-selected sample, we use the aforementioned subset of the full $\alpha.40$ data set to determine the HIMF and WF of void galaxies. However, certain tasks we would like to accomplish (namely those in Section 2.3.4) require that we cross-match the H I-detections with optical galaxies. Haynes et al. (2011) supply a cross-reference of 12,468 ALFALFA H I sources with the most probable optical counterpart from the SDSS DR7 where the two survey footprints overlap. Of the original 15,041 H I detections in the $\alpha.40$ catalogue, 201 have no assigned optical counterpart, 2312 lie outside the SDSS DR7 footprint, and 60 appear within the SDSS DR7 imaging survey but the galaxies' images are contaminated by bright foreground stars or other

artifacts. From the cross-referenced catalogue, we obtain photometric object IDs and query the SDSS DR7 database to obtain information regarding the apparent magnitude in each Sloan filter for every object in order to identify the objects' color and absolute r-band magnitude, M_r. Because we are comparing optically selected galaxy magnitudes to H I-selected galaxy magnitudes, we wish to remain consistent in how we determine absolute magnitudes; therefore, we K-correct the magnitudes and band-shift each H I source's M_r to $z = 0.1$ using KCORRECT Version 4.4 (Blanton & Roweis, 2007) as done in the KIAS-VAGC.

2.3 Methods and Results

2.3.1 Creating a Void H I-Selected Sample

We categorize the H I sources within our sample into void and wall galaxy samples by comparing the coordinates of each galaxy to the void catalogue of Pan et al. (2012). The void locations are found using comoving coordinates; to ensure we are consistent in finding the locations of H I clouds with respect to the voids, we use the redshift of each detection to obtain its comoving coordinates in h^{-1}Mpc. From our H I-detected sample, we identify $2,777$ ($\sim$35%) void galaxies and $4,857$ (60%) wall galaxies. The remaining 384 (5%) ALFALFA detections lie near the edges of the SDSS DR7 mask, so we cannot determine whether the galaxies live in a bona fide void. If we imagine there is a spherical void with radius $11h^{-1}$ Mpc lying only half in the survey, VoidFinder would be unable to fit a $10h^{-1}$ Mpc sphere within the survey in this region, so any galaxies in the spherical void would not be identified as void galaxies. Galaxies living all along the boundaries of the SDSS mask could be affected by such misclassifications; therefore, we remove these galaxies from our analysis so as not to contaminate our wall sample. Even with the removal of these edge galaxies, we are still sampling a cosmologically significant volume.

We encourage the reader to keep in mind that when we refer to "void" and "wall" galaxies in this paper, the names are not synonymous with "void" and "wall" galaxies referred to in other papers that have utilized VoidFinder as a means of identifying large-scale voids. The classification of voids and walls is the same as seen elsewhere, but the samples of galaxies within those environments differ because of the differences in H I-selected versus optically selected samples. In this paper, we are

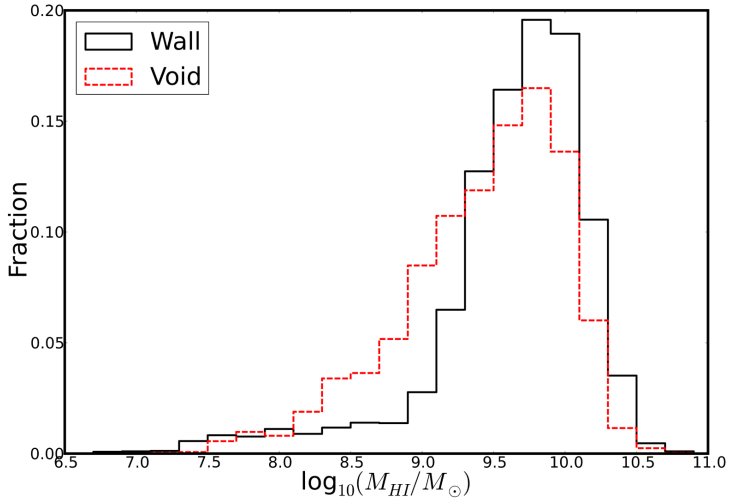

Figure 2.4 H I Mass distribution of void (red dashed line) and wall (black solid line) galaxies. The relatively small number of nearby structures makes it imperative that we use an inhomogeneity-independent method to estimate the H I mass function of this dataset. H I detections living in voids typically have lower H I masses than those in denser regions.

identifying the void and wall galaxies of a blind H I survey. The galaxy sample used here and those used elsewhere are very different; for example, blind H I detections residing in walls rarely populate the densest regions of the walls where we find a proliferation of galaxies in the optical. Optically selected wall samples typically consist of galaxies from the red sequence. By using an H I-selected sample, we lose a significant portion of the red sequence, and thus reduce the raw count of the wall population. This reduction of the wall population results in an increased void fraction for H I-selected samples. For comparison, within the same volume ($z \leq 0.5$), $\sim$ 26 percent of SDSS DR7 galaxies reside in voids. Note that one must be careful in computing the void fraction of a sample. Calculating the numerator is straight forward and is defined as simply the number of objects residing in voids, while the denominator must include only the galaxies accessible to VoidFinder. Excluded from the denominator are galaxies beyond a specified redshift (here, $z \leq 0.5$) and galaxies lying very near to the survey boundaries as discussed above.

We present the distribution of H I masses of void and wall galaxies of our ALFALFA sample in Figure 2.4. Here, we notice void galaxies tend to have lower H I masses than wall galaxies. Figure 2.5

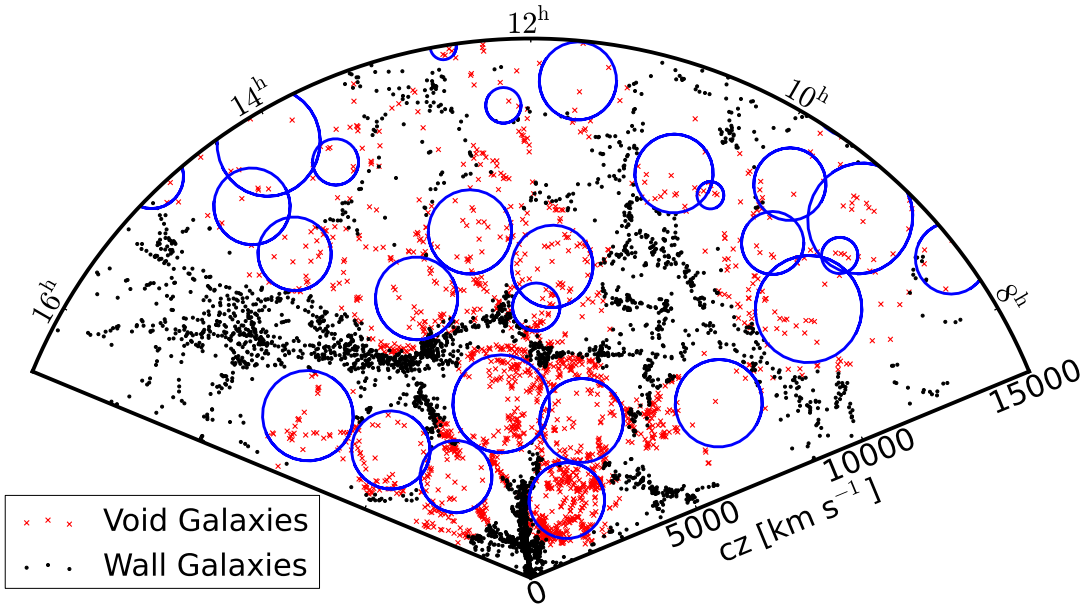

Figure 2.5 $10h^{-1}$Mpc slab of ALFALFA detections in the Spring Sky. Void galaxies are displayed as red crosses, wall galaxies are displayed as black points, and galaxies too close to the SDSS mask edge were not plotted. The circles depict the intersection of the maximal sphere of a void with the center of the slice. The voids appear highly populated, but the galaxies corresponding to the H I detections are fainter than the $M_r < -20.09$ galaxies used in our volume-limited catalogue. Refer to Figure 2.1 for the volume-limited sample used to produce the voids this slice.

shows our ALFALFA sample in a $10h^{-1}$ Mpc thick redshift slice centered at R.A.=12^h, Dec=10°. This is the same slice depicted in Figure 2.1 where, again, wall galaxies are shown as black points, void galaxies are shown as red crosses, and circles depict the intersection of the maximal spheres of each void with the center of the slice. The nearby voids appear highly populated by ALFALFA galaxies. The reader should keep in mind that Figure 2.5 plots an H I flux limited sample, whereas Figure 2.1 depicts an optical volume-limited sample; thus the majority of galaxies corresponding to these H I detections found in voids are fainter than our volume-limited cut of $M_r < -20.09$.

In addition to these physical boundary cuts, the method that we apply in this paper, the two dimensional stepwise maximum likelihood (2DSWML) method, requires that our sample be complete; therefore, we eliminate all galaxies that fall below the 50 percent completeness threshold in the flux–width plane reported in section 6 of Haynes et al. (2011). Figure 2.6 depicts the distribution of H I detections described in Section 2.2.2 with this completeness threshold in the flux–width

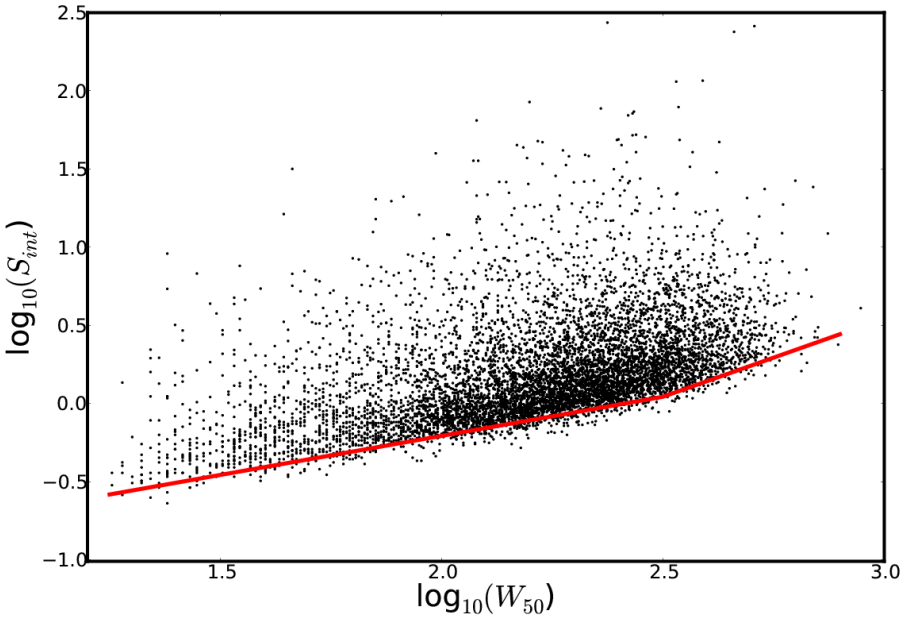

Figure 2.6 Distribution of H I detections used in this paper shown in integrated flux vs. velocity width space. The red line indicates our adopted completeness limit which is the 50 percent completeness threshold reported in Haynes et al. 2011.

plane. This cut eliminates 152 void galaxies and 240 wall galaxies. We provide a brief explanation of the completeness cuts here. Haynes et al. (2011) begin by separating the ALFALFA detections into H I line-width bins, then within each width bin the galaxies are binned again by integrated H I flux. A flux-limited sample from a uniform distribution of galaxies will produce a number count that approximately follows a power law with slope $-3/2$. The authors determine the onset of incompleteness when the binned integrated flux data deviate from this form. In Figure 2.7, we present the distribution of the final sample used in our analysis in the mass–width plane.

We make cuts to the ALFALFA–SDSS cross-referenced catalogue identical to the ones mentioned in Section 2.2.2. The resulting subsample is 305 H I detections fewer than the full sample mentioned above. We lose 54 H I detections from the void sample, 132 detections from the wall sample, and 119 from the edges where the survey region is inaccessible to VoidFinder. We further limit this sample to objects lying only in the ALFALFA Spring Sky. These reductions leave us with 7404 H I detections. 2571 of these live in voids, while 4485 reside in denser regions. The remainder of the galaxies lie

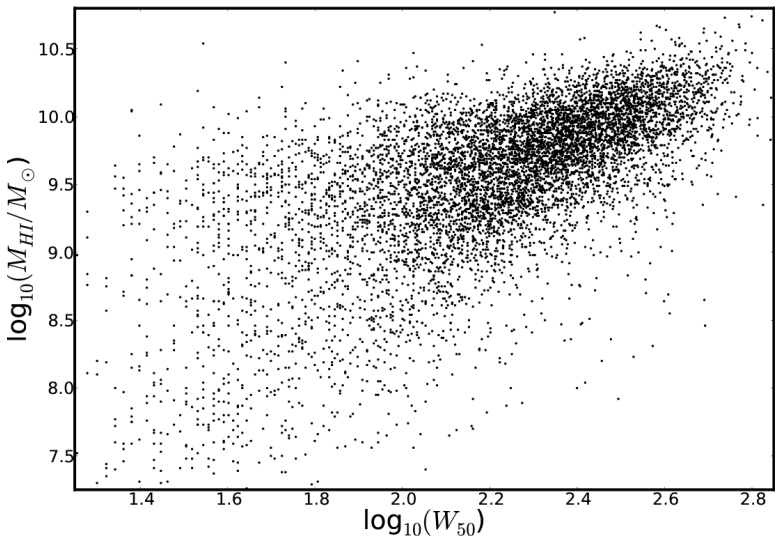

Figure 2.7 Distribution of our final sample in H I mass vs. velocity width space after all cuts have been made. The completeness limit of the sample in this space is dependent on the distance to each object and cannot be depicted using a single line.

along the edge of the SDSS DR7 survey mask in regions inaccessible to VoidFinder.

2.3.2 The 2DSWML Method

Because the ALFALFA survey's detection limit is dependent on both H I mass and velocity width (Giovanelli et al., 2005a), we estimate the HIMF and the velocity WF of our ALFALFA void and wall samples using an extension of the stepwise maximum likelihood method of Efstathiou et al. (1988) called the bivariate or two-dimensional stepwise maximum likelihood (2DSWML) method, introduced by Loveday (2000). We provide a brief overview of the 2DSWML method here. For more details of the direct application of this method to the $\alpha.40$ sample, see Martin et al. (2010, appendix B).

We obtain our estimates of the HIMF and WF by first splitting the bivariate distribution function $\phi(M_{\rm HI}, W_{50})$ into bins and define ϕ_{jk} as the maximum likelihood parameter of the distribution in logarithmic mass bin j and logarithmic velocity width bin k. We attain the maximum likelihood

solution via iteration of the following equation obtained by Efstathiou et al. (1988):

$$\phi_{jk} = \frac{n_{jk}}{\sum_i \frac{H_{ijk}}{\sum_m \sum_n H_{imn}\phi_{mn}}}. \tag{2.1}$$

Here, n_{jk} is the number of galaxies within each bin in the mass–width plane and H_{ijk} is a function that ensures the summation only goes over the area of bins accessible to galaxy i, where

$$H_{ijk} = \frac{1}{\delta M_{\rm HI}\delta W_{50}} \int_{W_k^-}^{W_k^+} \int_{M_j^-}^{M_j^+} C_i(M_{\rm HI}, W_{50}) {\rm d}M_{\rm HI}{\rm d}W_{50}. \tag{2.2}$$

Here, $C_i(M_{\rm HI}, W_{50})$ is an approximation of the completeness function described in Haynes et al. (2011) in the mass–width plane for galaxies at distance D_i. That is, if an object's integrated flux falls below the completeness limit, C=0, otherwise C=1. M_j^- and M_j^+ are the lower and upper limits on logarithmic mass bin j, and similarly, W_k^- and W_k^+ are the lower and upper limits on logarithmic width bin k.

2.3.3 HIMF

After obtaining the maximum likelihood bivariate distribution parameters, ϕ_{jk}, we marginalize over velocity width to measure the HIMF. Because the normalization is lost, we match the normalization of the void and wall galaxy HIMFs to the number density of void and wall galaxies within their respective volumes. We compare our measurements of the void and wall galaxy HIMFs over the mass range $7.2 < \log(M_{\rm HI}/{\rm M}_\odot) < 10.8$ with a Schechter function (Schechter, 1976) of the form

$$\Phi(M_{\rm HI}) = \frac{{\rm d}N}{{\rm d}V {\rm d}\log M_{\rm HI}} = \ln 10 \Phi^* \left(\frac{M_{\rm HI}}{M^*}\right)^{(\alpha+1)} \times \exp\left(-\frac{M_{\rm HI}}{M^*}\right). \tag{2.3}$$

We estimate the normalization factor Φ^*, the characteristic gas mass M^*, and the low-mass-end slope α using a least-squares estimator.

Here we present the global HIMF of the full $\alpha.40$ data set. It is well fitted by a Schechter function with estimated parameters ($\Phi^* = (6.3 \pm 0.3) \times 10^{-3}{\rm Mpc}^{-3}$, $\log(M^*/{\rm M}_\odot) + 2\log h_{70} = 9.96 \pm 0.02$, $\alpha = -1.33 \pm 0.02$) similar to those of Martin et al. (2010): $\Phi^* = (4.8 \pm 0.3) \times 10^{-3}{\rm Mpc}^{-3}$,

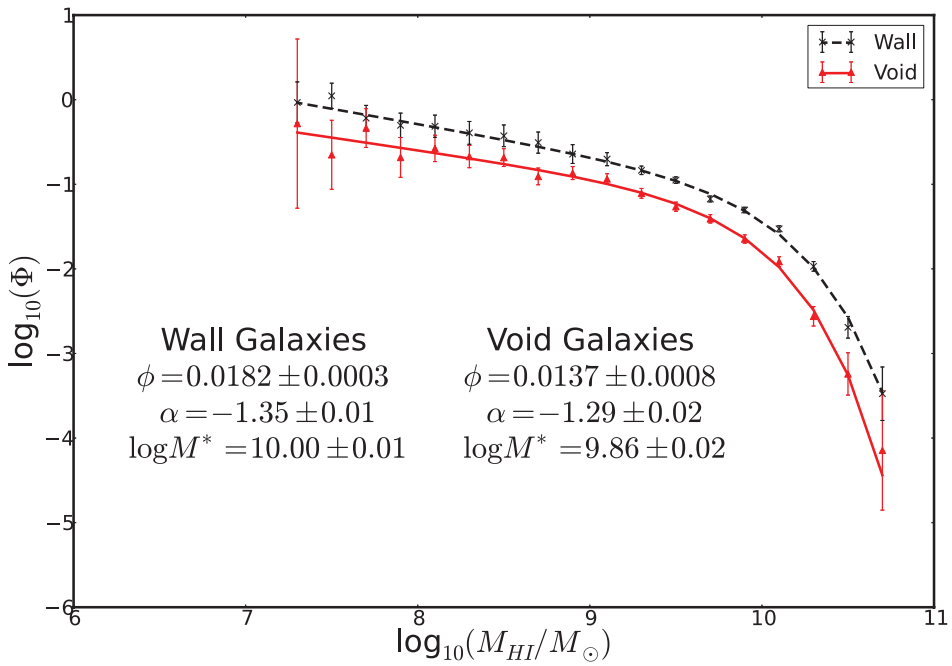

Figure 2.8 The HIMF of void (red) and wall (black) galaxies. The best-fitting Schechter functions for each sample are shown as solid (void) and dashed (wall) lines. We notice a shift towards lower masses as well as a small decrease in the low-mass slope for void galaxies.

$\log(M^*/\mathrm{M}_\odot) + 2\log h_{70} = 9.96 \pm 0.02$, $\alpha = -1.33 \pm 0.02$. Limiting the data set to H I detections located in the Spring Sky, we do not see a significant difference in the best-fitting parameters of the HIMF ($\Phi^* = (5.34 \pm 0.4) \times 10^{-3}\mathrm{Mpc}^{-3}$, $\log(M^*/\mathrm{M}_\odot) + 2\log h_{70} = 9.97 \pm 0.02$, $\alpha = -1.35 \pm 0.04$).

Dividing the Spring Sky into void and wall galaxies produce the following results: In Figure 2.8 we present the HIMF of both void and wall galaxy samples. For the void sample, we estimate the best-fitting Schechter parameters to be $\Phi^* = (1.37 \pm 0.1) \times 10^{-2}\mathrm{Mpc}^{-3}$, $\log(M^*/\mathrm{M}_\odot) + 2\log h_{70} = 9.86 \pm 0.02$, $\alpha = -1.29 \pm 0.02$. For the wall galaxy sample, we estimate $\Phi^* = (1.82 \pm 0.03) \times 10^{-2}\mathrm{Mpc}^{-3}$, $\log(M^*/\mathrm{M}_\odot) + 2\log h_{70} = 10.00 \pm 0.01$, $\alpha = -1.35 \pm 0.01$. See Section 2.3.5 for an explanation of uncertainties. The curves in Figure 2.8 show the Schechter functions associated with these best-fitting parameters.

We see that $\log(M^*)$ shifts towards lower H I masses in voids by $\log(M^*) = 0.14$. This characteristic mass is shifted by a factor of 1.4 and the direction of this shift is consistent with the shift in the DMH mass function of extended Press–Schechter theory (Goldberg et al., 2005). This direction

of the shift is also in agreement with the shift in the optical LF. We cannot quantitatively compare our HIMF shift with the shift found in the optically selected LF from voids to walls because of a difference in sample selection, but for completeness, Hoyle et al. (2005) find a shift in LF of the r-band magnitude towards lower magnitudes of $M_r^* \sim 1$ for void galaxies (a factor of 2.5). We also see only a slight dependence of the low-mass slope, α, on environment, with the slope steepening with increasing density. We compare our results to previous work more completely later in Section 2.4, but for now we will briefly compare our HIMF results to the HIMF of the Leo Group (Stierwalt et al., 2009), who estimate a low-mass slope of $\alpha = -1.41 \pm 0.04$ using ALFALFA. Given our findings, we conclude that the low-mass slope of the HIMF for ALFALFA galaxies in the Spring Sky is shallow for voids. The slope may increase with density to arrive at the steep Leo I Group slope, but the slope does not necessarily increase monotonically with density. Depending on how densely packed a particular galactic group or cluster is, the low-mass slope of the HIMF may vary drastically, ranging anywhere from the steep slope of the Leo Group (Stierwalt et al., 2009) to the very flat slopes found in loose groups (Pisano et al., 2011) and clusters (Verheijen et al., 2001; Rosenberg & Schneider, 2002; Martin, 2011) which, when combined, may give an intermediate low-mass slope similar to that of our wall galaxy sample.

2.3.4 WF

To determine the WF, we obtain our results from the bivariate distribution function of the 2DSWML method and marginalize over H I mass. As with the HIMFs, we must match the normalization of the void and wall WFs to their respective densities. To remain consistent with previously reported ALFALFA WF results (Papastergis et al. 2011 obtain observational results and translate theoretical results to the observed quantity rather than estimate corrections for the observations), we have corrected the velocity widths for Doppler broadening and make no other corrections, e.g. galaxy inclination. We compare the void and wall galaxy WFs over the width range $1.3 \log(\mathrm{km\ s^{-1}}) < \log(W_{50}) < 2.9 \log(\mathrm{km\ s^{-1}})$, where W_{50} is the velocity width measured at 50 percent of the peaks of the H I-line profile. The high-velocity width end falls off too quickly to be well fitted by a Schechter

function, so we fit the WFs to a modified Schechter function of the form

$$\Phi(W_{50}) = \frac{dN}{dV\, d\log W_{50}} = \ln 10 \Phi^* \left(\frac{W_{50}}{W^*}\right)^{\alpha} \exp\left(-\frac{W_{50}}{W^*}\right)^{\beta} \tag{2.4}$$

and estimate the normalization factor Φ^*, the characteristic velocity width $\log W^*$, and the low and high velocity width slopes α and β using a least-squares estimator.

Here we present the global WF of the full $\alpha.40$ sample. It is well fitted by a modified Schechter function where our 2DSWML-estimated parameters ($\Phi^* = (2.1 \pm 0.2) \times 10^{-2}\mathrm{Mpc}^{-3}$, $\log(W^*) = 2.56 \pm 0.03$, $\alpha = -0.73 \pm 0.02$, $\beta = 2.6 \pm 0.2$) match closely those of Papastergis et al. (2011): $\Phi^* = (1.1 \pm 0.2) \times 10^{-2}\mathrm{Mpc}^{-3}$, $\log(W^*) = 2.58 \pm 0.03$, $\alpha = -0.68 \pm 0.11$, $\beta = 2.7 \pm 0.3$. Limiting the data set to H I detections located in the Spring Sky, the WF remains well fit by a modified Schechter function although the parameters change somewhat: $\Phi^* = (1.3 \pm 0.3) \times 10^{-2}\mathrm{Mpc}^{-3}$, $\log(W^*) = 2.61 \pm 0.03$, $\alpha = -0.91 \pm 0.02$, $\beta = 3.44 \pm 0.2$. When we divide the Spring Sky sample into void and wall galaxies, our results of the 2DSWML method change drastically. In Figure 2.9 we present the WF of both void and wall galaxy samples. We see these functions are not as well fit by the modified Schechter function as the global $\alpha.40$ WF (see Figure 4 in Papastergis et al. 2011). For the void sample, we estimate the best-fitting modified Schechter parameters to be $\Phi^* = 0.21 \pm 0.1\mathrm{Mpc}^{-3}$, $\log(W^*) = 2.13 \pm 0.3$, $\alpha = 0.52 \pm 0.5$, $\beta = 1.3 \pm 0.4$. For the wall galaxy sample, we estimate $\Phi^* = 0.022 \pm 0.009\mathrm{Mpc}^{-3}$, $\log(W^*) = 2.62 \pm 0.5$, $\alpha = -0.64 \pm 0.2$, $\beta = 3.58 \pm 1.5$. We note here that two bins in both the void and wall WFs appear to be extreme outliers (void: $\log(W_{50}) = 1.8, 2.6$; wall: $\log(W_{50}) = 1.5, 2.0$); however, these bin heights are not caused by low-number statistics. The curves in Figure 2.9 show the modified Schechter functions associated with these best-fitting parameters.

We see that W^* shifts towards lower velocity widths in voids compared to walls; however, due to large uncertainties, we are unable to make any conclusive statements about the other parameters. It is our goal to ascertain whether there are any differences in the WF of void galaxies and wall galaxies. Looking at the poorly fit Schechter functions gives us no real insight, so we compute a Kolmogorov–Smirnov (K–S) test to compare the wall and void WF distributions. Including all

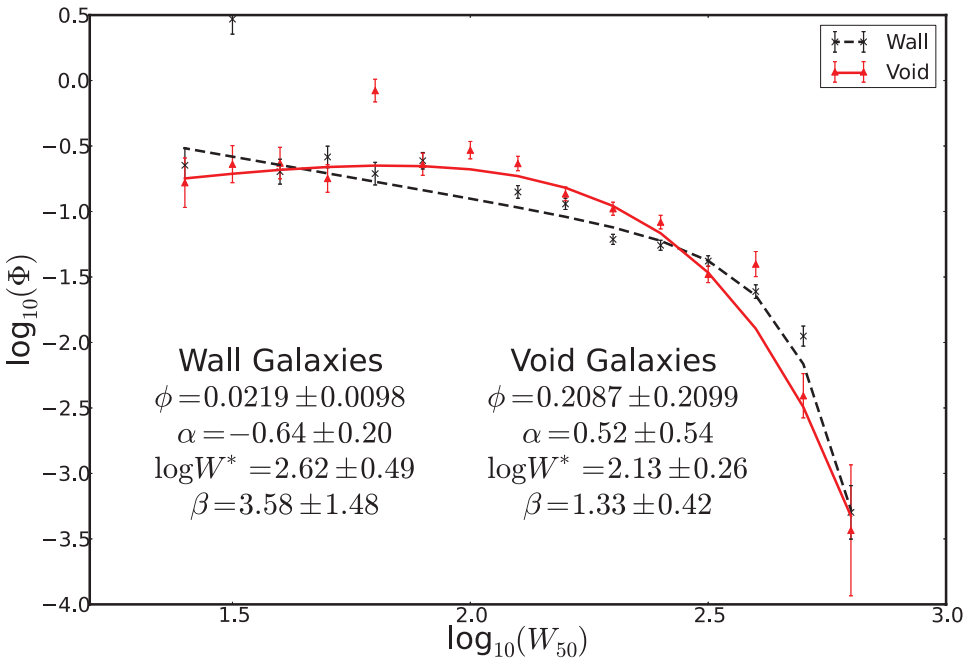

Figure 2.9 The WF of void (red) and wall (black) galaxies. The best-fitting modified Schechter functions for each sample are shown as solid (void) and dashed (wall) lines. Neither the void nor wall WF is well fit by a modified Schechter function.

points in the distributions (note the outlying points), we obtain a p-value of 0.05 from the K–S test. That is, 95 percent of the time we would correctly reject the hypothesis that the void and wall WFs are drawn from the same distribution. We have no reason to exclude the extreme outliers, but excluding the extreme outliers yields a p-value of 0.07. See Figure 2.10 for a comparison of the cumulative distribution functions (CDFs) of the two distributions with and without the outliers.

As mentioned above, galaxies in voids tend to be blue, late-type galaxies whereas red, dead, elliptical galaxies are primarily found in denser regions of the Universe. Therefore, we investigate the effects of color to shed some light on possible explanations as to why/if the WF differs between void and wall galaxies. For this sample, we use the ALFALFA-SDSS cross-reference catalogue provided by Haynes et al. (2011). This results in a few less galaxies than the sample we have been working with because we are dependent on the SDSS photometric pipeline for matches, and in some cases, the galaxy images may be contaminated by a foreground star or other artifact.

We split our H I cloud sample into groups based on color where we define galaxies with a color

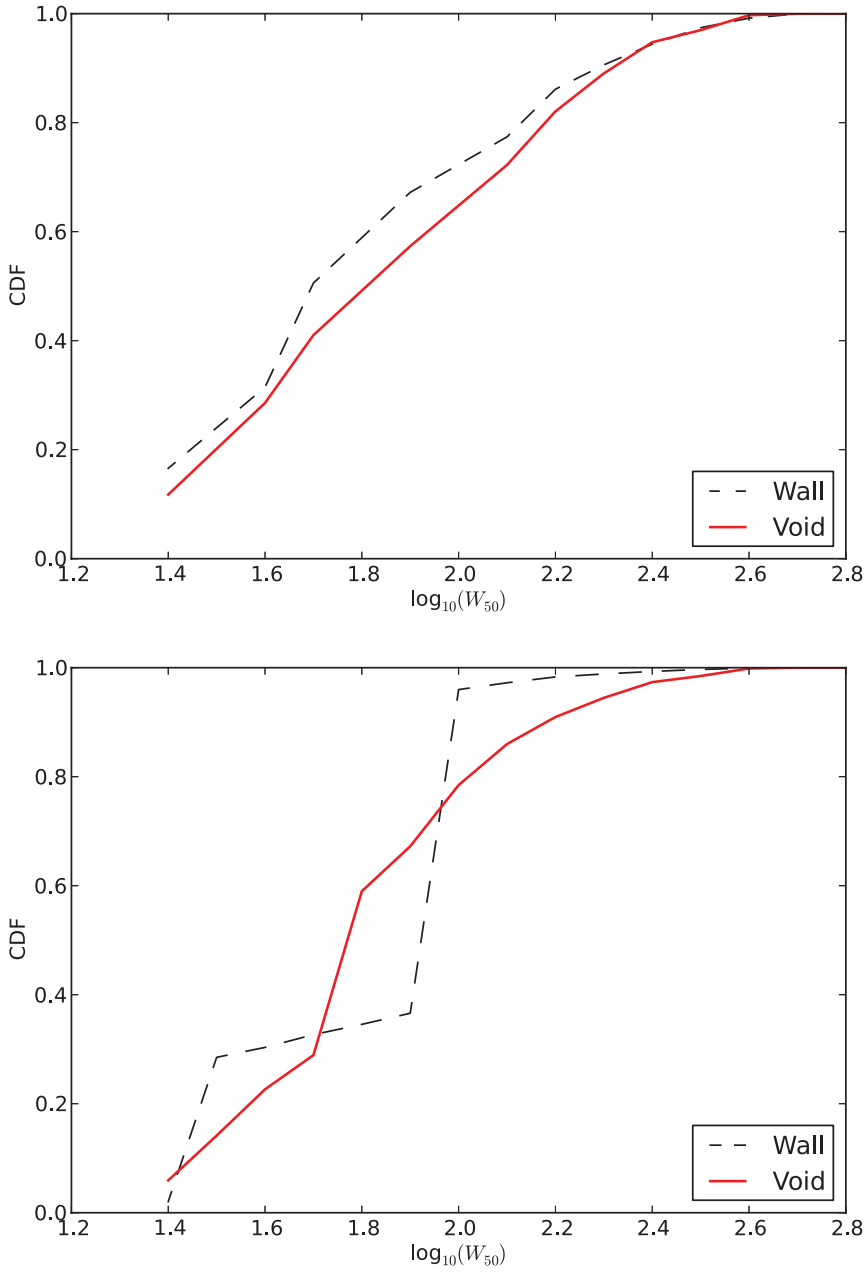

Figure 2.10 CDF of wall (black dashed) and void (red solid) WF. Top: Outlying points from the distributions have been removed. Bottom: Outlying distribution points are left in the CDF calculation.

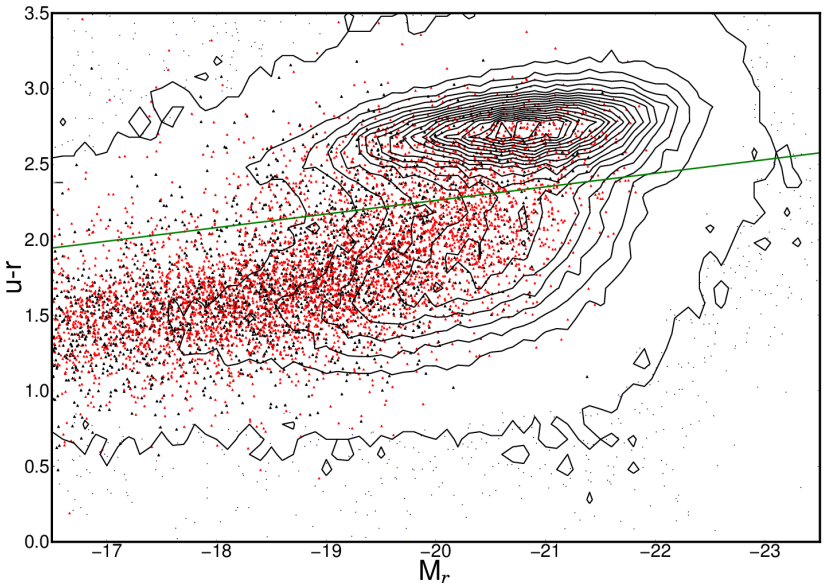

Figure 2.11 Color-magnitude diagram of optically-selected and H I-selected galaxies. Contours and black outlying points represent density of SDSS DR7 galaxies. Black and red triangles represent ALFALFA wall and void galaxies respectively. Green line shows the color cut mentioned in the text that splits the samples into a "red sequence" and a "blue cloud". The ALFALFA sample is lacking in the red sequence where we find our optical sample to be most dense.

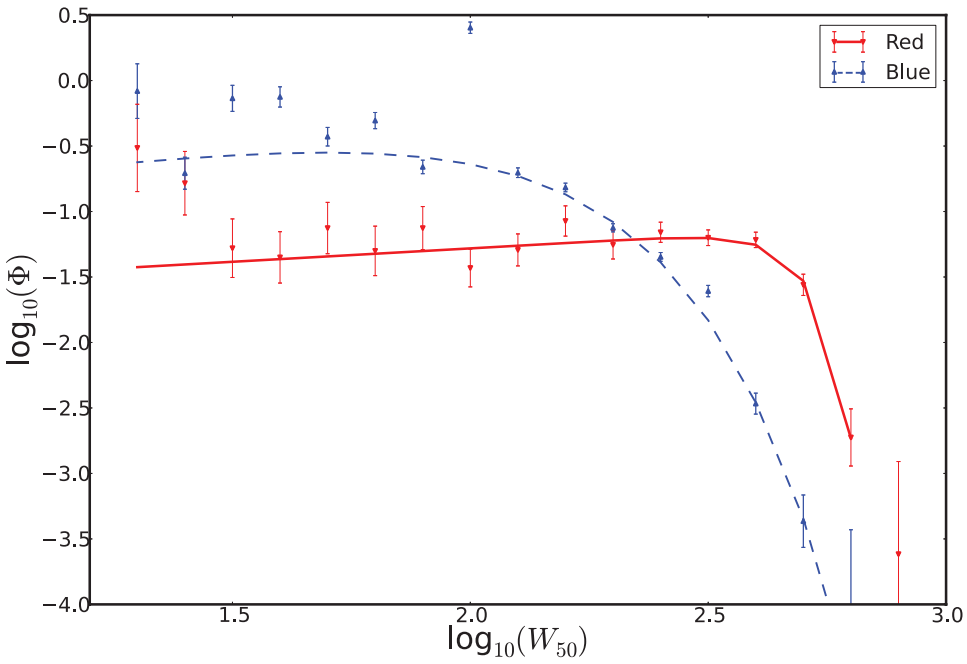

Figure 2.12 The WF of red (red triangles) and blue (blue triangles) galaxies. The best-fitting modified Schechter functions for each sample are shown as solid (red) and dashed (blue) lines. We see that the low-width slope of the red galaxy WF is substantially flatter than that of the blue sample.

$u - r < -0.09M_r + 0.46$ as blue and galaxies with color $u - r \geq -0.09M_r + 0.46$ as red. Here, M_r is the r-band magnitude of the object's optical counterpart given by the SDSS DR7. See Figure 2.11 for the location of this definition of color as shown on a color–magnitude diagram; this cut divides the sample into a "red sequence" and a "blue cloud". Our resulting subsamples contain $\sim 6,000$ blue galaxies and $\sim 1,400$ red galaxies. Figure 2.12 depicts the resulting WFs of the blue and red subsamples along with the best-fitting modified Schechter functions. We see that the low-width slope of the red galaxy WF is substantially flatter than that of the blue galaxies. Because a blind-H I survey is more likely to identify a blue, late-type galaxy (e.g. Huang et al. 2012a), it is understandable that the low-width slope of the red galaxy WF would be flat or even turn over, because only the most massive red elliptical galaxies will contain enough H I to be detected, therefore boosting the high-width end.

2.3.5 Error Analysis

We account for a number of sources of error which we add in quadrature; the first is from Poisson counting errors. We also take into account the error in each bin of our bivariate distribution introduced from the 2DSWML method which we estimate via the inverse of the information matrix as described in Efstathiou et al. (1988). This method uses the fact that the maximum likelihood estimates of ϕ_{jk} are asymptotically normally distributed.

We also account for cosmic variance, or the effects of the inhomogeneity of large-scale structure, by using the jackknife resampling method (Efron, 1982) to estimate the uncertainties in our HIMF/WF measurements. We do so by dividing the Spring Sky into N subregions, and calculating the HIMF/WF of a subsample of galaxies which omits a different $1/N$th of the surveyed area each time. After measuring the HIMF/WF of each of the N regions, we estimate the variance of the value of the distribution function in each H I mass/width bin as

$$\mathrm{Var}(x) = \frac{N-1}{N} \sum_{i=1}^{N} (x_i - \bar{x})^2 \,. \tag{2.5}$$

For our analysis, we divide our sample volume into $N = 18$ subregions, equally spaced in R.A.

For the HIMF, we need to account for errors in distance measurements. The calculation of the H I mass of a galaxy is proportional to the square of the distance to the galaxy; thus, errors in distance estimates could lead to large errors in mass and cause a galaxy to be moved from one mass bin to another. We account for this by creating 300 realizations of the void and wall HIMFs, where we estimate errors on $M_{\rm HI}$ using reported $S_{\rm int}$ errors and estimated distance errors. We give each galaxy i in our sample, at a distance D_i, a random H I mass assuming a Gaussian random error, and calculate the HIMF of each of these realizations.

We use a similar approach to account for the error in velocity widths, which can shift a galaxy from one width bin to another, by creating 150 realizations of the void and wall WFs using the reported W_{50} and ΔW_{50} values. The published W_{50} errors, ΔW_{50}, from the $\alpha.40$ catalogue take into account distortion of the spectral profile due to noise and the systematic effect of a guess at the locations of the spectral boundaries.

2.4 Comparison with Previous Observations

2.4.1 Comparing the HIMF

Previous studies on the environmental impact of the HIMF come to varying conclusions depending on the H I sample used or the method of determining galaxy density. Table 2.1 presents a comparison of the best fitted Schechter function parameters of the HIMF of various galaxy samples. These samples consist of HI detections from an HI-selected or optically selected survey and measure environment based on nearest-neighbor algorithms, PSCz density maps, well-known groups and clusters, or VoidFinder. We briefly describe the results of these studies here.

Springob et al. (2005) compare the HIMF of a complete optically selected sample across environments. The sample consists of H I-selected galaxies with integrated H I flux $S_{\rm int} > 0.6$ within -2° <Dec< 38° with an optical apparent diameter $a > 1.0$ arcmin, Galactic latitude $|b| > 15^\circ$, and morphological type Sa-Irr. The authors define environment based on ranges of galaxy densities (local density: $n < 1.5, 1.5 < n < 3.0, n > 3.0$) defined via a Point Source Catalog Redshift Survey (PSCz) density reconstruction map, and find, with low-significance, that α flattens with increasing density while M^* shifts to lower masses (within a range of $\log(M^*) < 0.16$). This trend is consistent

with the theory that galaxies in clusters are H I deficient (Giovanelli & Haynes, 1985); however, the decrease in M^* with increasing density contradicts our findings. While these findings are of low statistical significance, and the authors report that better statistics are needed to conclusively determine whether the HIMF varies across environments, differences between our results and theirs could be due to the difference in samples – optically selected versus H I-selected samples. The authors also do not isolate "void" galaxies as we have defined them.

Zwaan et al. (2005) compute the HIMF in several density regions using n-th nearest neighbor distances to define density for $n = 1, 3, 5, 10$. They find that the best-fitting Schechter function for low-density environments has a flat low-mass-end slope α that steepens with increasing density when defined on small and large scales. They find no environmental dependence of the characteristic turnover mass M^*. This is counterintuitive given that we would expect galaxies in extremely overdense areas to have their gas stripped away during mergers or other galactic interactions. One possible reason for Zwaan et al. (2005) finding such a contrasting result is that the authors define local density using the H I galaxies themselves via nearest neighbor distances. Galaxies living in extremely high-density environments defined by an optical sample may undergo mergers or other astrophysical effects causing most, if not all, H I to be stripped from low-mass galaxies, resulting in a very different density map from those found using optical surveys.

Martin (2011) uses both the full $\alpha.40$ dataset as well as the Spring Sky portion of the data to estimate the HIMF of galaxies living in several different density regions. She uses two methods to determine local density: first, by using two PSCz density reconstruction maps (a coarse and fine grid), and second, by applying an nth nearest neighbors method to a volume-limited sample of galaxies from SDSS DR7 over a range of n values, and thus, over a range of density scales. The latter of these methods was only applied to the Spring Sky portion of the dataset where the $\alpha.40$ and SDSS DR7 footprints overlap. Using these methods, Martin (2011) finds that M^* increases with increasing density on all scales, whereas the trend of the low-mass-end slope varies depending on the scale on which environment is defined. When density is defined on larger scales, α steepens with density until some threshold density, after which it flattens out. The author suggests that when density is defined

on the largest scales, the HIMF will have a flattened low-mass slope, in the extreme high- and low-density regions, whereas the not-so-extreme environments will have a relatively steeper slope that increases with density. Martin (2011) proposes the lowest density regions maintain an abundance of intermediate-mass galaxies – possibly due to an increased sensitivity to reionization in voids (Hoeft et al., 2006) – which boosts the intermediate regions of the HIMF thus flattening the slope. In the highest density regions, the lowest mass galaxies have their cool gas stripped away, thus flattening the low-mass slope.

Pisano et al. (2011) use the HICAT (Meyer et al., 2004) catalogue and the Lyons Group Galaxies to determine the HIMF of six loose groups of galaxies with properties similar to those of the Local Group. These authors find a very flat low mass slope for loose galactic groups. Stierwalt et al. (2009) use the ALFALFA survey to calculate the HIMF of the Leo I Group which has a higher density than the groups used in Pisano et al. 2011. They find a steep low-mass slope of $\alpha = -1.41$. Kovac (2007), on the other hand, finds a very flat low-mass slope of the high-density CV group. There does not seem to be a clear trend with environment at least on the group level.

In the Spring Sky, we investigate the HIMF parameters of true voids – extreme underdensities on the largest scales – and find the characteristic turnover mass M^* is shifted towards lower masses compared to M^* in denser environments. In conjunction with the findings of Stierwalt et al. (2009), who find a relatively steep ($\alpha = -1.41$) low-mass-end of the HIMF for objects in the Leo I Group, our findings of the low-mass slope of void galaxies ($\alpha = -1.29$) indicate that the low-mass slope of the HIMF of ALFALFA detections steepens with density. This result is in agreement with the findings of Martin (2011). A number of things could be responsible for the somewhat flatter low-mass slope of void galaxies than wall galaxies. The higher specific SFRs of low-mass galaxies in voids may cause them to burn their fuel faster than their counterparts in walls, thereby flattening the low-mass slope. Given the shift in characteristic H I mass to lower masses in voids, and assuming (again, naively) that the baryonic mass is directly proportional to the DMH mass, void galaxies will have shallower potential wells and could much more easily lose their cool gas, causing their low-mass slope to flatten. Another, more likely, candidate for the cause of the flattened low-mass slope is supernova

Table 2.1 Schechter function fits to the HIMFs of different galaxy samples across environments. Each sample contains either H I-selected or optically selected galaxies, and galaxy environment was determined using either nearest-neighbor algorithms (using optical or H I samples), PSCz density maps, well-known groups/clusters, or VoidFinder.

Author	Sample	Density measured	Φ^* $\times 10^{-2}h^3\mathrm{Mpc}^{-3}$	$M^* + 2\log h$	α
Rosenberg	ADBS	Full sample	0.58	9.88	-1.53
		Virgo Cluster			-1.2
Springob	Optically selected galaxies	PSCz DM – lowest ρ	0.32	10.07	∼-1.37
		– intermediate ρ		9.91	∼-1.13
		– highest ρ		9.96	∼-1.25
Zwaan	HIPASS	H I 10th NN – lowest ρ	0.60	9.80	-1.0
		– intermediate ρ			-1.4
		– highest ρ			-1.55
Martin	ALFALFA	SDSS 10th NN – lowest ρ	0.31	9.80	-1.15
		– intermediate ρ		10.05	-1.37
		– highest ρ		10.05	-1.2
Martin	ALFALFA	Coarse PSCz DM – lowest ρ		9.93	-1.0
		– higher ρ		10.05	-1.45
Stierwalt	ALFALFA	Leo I Group	∼3.0	∼10.7	-1.41
		Full sample			
Pisano	HICAT	Optically selected		∼9.8	-1.0
		Loose Groups			
This work	ALFALFA	VoidFinder – void	1.37±0.08	9.86±0.02	-1.29±0.02
		VoidFinder – wall	0.28±0.03	10.00±0.03	-1.35±0.03

feedback. While a comparison of optical and infrared redshift surveys (Fisher et al., 1995; Saunders et al., 2000; Strauss et al., 2002; Jones et al., 2004) might reveal similar large-scale structure (Hoyle & Vogeley, 2004), local density maps revealing large-scale structure in H I would differ drastically (e.g. Papastergis et al. 2013; Waugh et al. 2002). Therefore, we cannot quantitatively compare our results to Zwaan et al. (2005), because they measure local density using an H I sample. We also cannot quantitatively compare our results to those of Springob et al. (2005), because they determine the HIMF using an optically selected sample.

2.4.2 Comparing the WF

Little work has been done to determine the environmental effects on purely observed velocity WFs, specifically in the most underdense regimes. Desai et al. (2004) compare the Galaxy Circular Velocity

Function (GCVF) of clusters grown in a ΛCDM simulation with the GCVF of clusters from the SDSS obtained using galaxy photometry and the Tully–Fisher relation (Tully & Fisher, 1977). They find that both the observed and simulated GCVFs are well fitted by a power law, with the observed cluster GCVF having only a slightly shallower slope, although they mention the difference in slope is not significant. They also determine the GCVF of "field" galaxies and find that, compared to the predicted power law, these galaxies display a much shallower slope at low velocities and a much steeper slope at higher velocities with a turnover velocity of $\sim 200\text{km s}^{-1}$ – a shape well described by a Schechter function.

Abramson et al. (2013) report their findings on the CVF of galaxies in groups using three different samples from the NYU Value Added Galaxy Catalog (Blanton et al., 2005c). In contrast to ΛCDM predictions, these authors find that the group galaxy CVF is consistent with, if not shallower than, the observed field galaxy CVF at the low-velocity end. They find that the shape of the CVF depends primarily on the morphological types of galaxies included in the samples, with an increase in the fraction of late-type galaxies steepening the low-velocity slope; they suggest the flattened slope of the group CVF is due primarily to the depression of late-type galaxies in groups. Sigad et al. (2000) find similar results using a ΛCDM simulation. Assuming a linear relation between halo mass and luminosity, the authors populate the halos with "galaxies," identify group and isolated "galaxies," and report that the isolated "galaxies" have a steeper low-velocity slope than grouped "galaxies."

Although we cannot directly compare an observed WF with a CVF, at first glance, our findings on the environmental dependence of the WF appear to be in contrast with Abramson et al. (2013) and Sigad et al. (2000), and indicate that galaxies in voids exhibit a shallower low-velocity slope than their counterparts in denser regions; however, large uncertainties weaken our conclusions. On the other hand, assuming color and morphology go hand in hand, our results are in agreement with those of Abramson et al. (2013) in that blue galaxies seem to have a steep low-velocity width slope and red galaxies tend to have a much shallower low-velocity width slope. See Figure 2.12 for a comparison of the blue and red WFs.

2.5 Conclusions

Using the void catalogue obtained by Pan et al. (2012) and the $\alpha.40$ catalogue from Haynes et al. (2011), we measure the HIMF of 2,300 void galaxies with H I masses ranging from $7.2 < \log(M_{\rm HI}/{\rm M}_\odot) < 10.8$. We find that the HIMF of void galaxies is well fitted by a Schechter function with parameters $\Phi^* = (1.37 \pm 0.1) \times 10^{-2} h_{70}^3 {\rm Mpc}^{-3}$, $M_{\rm HI}^* + 2\log h_{70} = 9.86 \pm 0.02$, and $\alpha = -1.29 \pm 0.02$. For galaxies residing in higher density regions, we find the best-fitting Schechter parameters to be $\Phi^* = (1.82 \pm 0.03) \times 10^{-2} h_{70}^3 {\rm Mpc}^{-3}$, $M_{\rm HI}^* + 2\log h_{70} = 10.00 \pm 0.01$, and $\alpha = -1.35 \pm 0.01$. We also measure the WFs across environments and, while the void and wall WFs are not well fitted by a modified Schechter function, we estimate the best-fitting parameters of a modified Schechter function to be $\Phi^* = 0.21 \pm 0.1 h^3 {\rm Mpc}^{-3}$, $\log(W^*) = 2.13 \pm 0.3$, $\alpha = 0.52 \pm 0.5$, and $\beta = 1.3 \pm 0.4$ for the void sample, and $\Phi^* = 0.022 \pm 0.009 h^3 {\rm Mpc}^{-3}$, $\log(W^*) = 2.62 \pm 0.5$, $\alpha = -0.64 \pm 0.2$, and $\beta = 3.58 \pm 1.5$ for the wall sample.

We conclude the following:

1. The ALFALFA $\alpha.40$ catalogue yields a higher fraction of void galaxies (35%) than the optically selected (26%) SDSS DR7 magnitude-limited sample over the same volume. Because these surveys are magnitude limited, the fraction of void galaxies varies with redshift. We know blind-H I surveys preferentially detect blue, late-type galaxies and void regions are also predominantly filled with these blue, spiral galaxies. The red luminous galaxies, typical in the wall sample of an optical survey, are lost when we use an H I-selected sample. This reduction of red galaxies caused by moving from an optically selected sample to an H I-selected sample, therefore, decreases the raw count of the wall sample, and increases the void fraction for H I-selected samples.

2. Our findings suggest that the characteristic turnover mass of the HIMF is marginally dependent on environment. The characteristic H I mass, M^*, shifts to lower masses in voids by a factor of 1.4; while this shift is small, it is significant. The shift is consistent with extended Press–Schechter theory which states that the mass function should shift to lower masses in underdense regions.

3. We see only a slight difference in the low-mass slopes of void and wall galaxy HIMFs. We believe something may be gleaned from combining our void results with others' results investigating

large-scale, non-void environments. When we couple our void galaxy HIMF with other H I-selected samples from optically selected environments, such as the Stierwalt et al. (2009) HIMF of the Leo I Group, and Rosenberg & Schneider's HIMF of galaxies in the Virgo Cluster, we find that the low-mass end slope α varies with environment on the largest scales. This indicates a possible trend with environment (as mentioned in Martin 2011) where the low-mass slope is flat in voids, and increases with density up to some turnover density, where the galaxies within clusters become H I deficient through e.g. galaxy–galaxy interactions.

Our wall HIMF is neither as steep as that found in Stierwalt et al. (2009) nor as flat as the extremely overdense (cluster) HIMFs suggested by Rosenberg & Schneider (2002) and Martin (2011), because we are effectively averaging all non-void densities. Our wall regions cover a combination of high-density groups made up of early-type galaxies, low-density groups made up of late-type galaxies, and clusters which tend to be H I deficient, to name a few. This conglomeration of vastly different environments yields a wall HIMF with a low-mass slope somewhere inbetween the flattest and steepest group/cluster slopes reported in the literature (Pisano et al., 2011; Martin, 2011; Stierwalt et al., 2009; Zwaan et al., 2005; Rosenberg & Schneider, 2002).

4. We do not find a statistically significant difference in the WF distribution of wall and void galaxies. These distributions are not well fitted by a modified Schechter function.

5. We find that the WF varies with galaxy color with bluer galaxies increasing the low velocity slope. The WF of the blue and red galaxies are also not well fitted by a modified Schechter function.

Acknowledgements

The authors would like to acknowledge the work of the entire ALFALFA collaboration team in observing, flagging, and extracting the catalog of galaxies used in this work. We thank the referee for helpful comments and suggestions. The ALFALFA team at Cornell is supported by NSF grants AST-0607007 and AST-1107390 to RG and MPH and by grants from the Brinson Foundation.

Funding for the creation and distribution of the SDSS Archive has been provided by the Alfred P. Sloan Foundation, the Participating Institutions, the National Aeronautics and Space Administration, the National Science Foundation, the U.S. Department of Energy, the Japanese Monbuka-

gakusho, and the Max Planck Society. The SDSS Web site is http://www.sdss.org/.

The SDSS is managed by the Astrophysical Research Consortium (ARC) for the Participating Institutions. The Participating Institutions are The University of Chicago, Fermilab, the Institute for Advanced Study, the Japan Participation Group, The Johns Hopkins University, the Korean Scientist Group, Los Alamos National Laboratory, the Max-Planck-Institute for Astronomy (MPIA), the Max-Planck-Institute for Astrophysics (MPA), New Mexico State University, University of Pittsburgh, Princeton University, the United States Naval Observatory, and the University of Washington.

Chapter 3: The Optical Luminosity Function of Void Galaxies in the SDSS and ALFALFA Surveys

Abstract

We measure the r-band galaxy luminosity function (LF) across environments over the redshift range $0 < z < 0.107$ using the SDSS. We divide our sample into galaxies residing in large scale voids (void galaxies) and those residing in denser regions (wall galaxies). The best fitting Schechter parameters for void galaxies are: $\log \Phi^* = -3.40 \pm 0.03$ log(Mpc^{-3}), $M^* = -19.88 \pm 0.05$, and $\alpha = -1.20 \pm 0.02$. For wall galaxies, the best fitting parameters are: $\log \Phi^* = -2.86 \pm 0.02$ log(Mpc^{-3}), $M^* = -20.80 \pm 0.03$, and $\alpha = -1.16 \pm 0.01$. We find a shift in the characteristic magnitude, M^*, towards fainter magnitudes for void galaxies and find no significant difference between the faint-end slopes of the void and wall galaxy LFs. We investigate how low surface brightness selections effects can affect the galaxy LF. To attempt to examine a sample of galaxies that is relatively free of surface brightness selection effects, we compute the optical galaxy LF of galaxies detected by the blind H I survey, ALFALFA. We find that the global LF of the ALFALFA sample is not well fitted by a Schechter function, because of the presence of a wide dip in the LF around $M_r = -18$ and an upturn at fainter magnitudes ($\alpha \sim -1.47$). We compare the H I selected r-band LF to various LFs of optically selected populations to determine where the H I selected optical LF obtains its shape. We find that sample selection plays a large role in determining the shape of the LF.

3.1 Introduction

A critical measurement of the distribution of galaxies, that may be compared to galaxy formation and evolution models, is the galaxy luminosity function (LF): the number of galaxies per volume per luminosity. The shape of a LF is typically fit by a Schechter (1976) function described as a power law with faint-end slope, α, and an exponential drop-off at the characteristic magnitude, M^*. With the

advent of deep, wide optical surveys, we now have sufficiently large samples of galaxies that allow us to study the LF of complete samples of galaxies across environments, colors, and morphological types.

Deep redshift surveys have allowed measurements of the evolution of the LF with cosmic time (Ramos et al., 2011; Loveday et al., 2012; McNaught-Roberts et al., 2014; Martinet et al., 2014a). Measuring how the LF changes with galaxy morphology and color can support or reject theories on galaxy formation and evolution. For instance, the LF results of Driver et al. (2007) suggest that galaxies begin their lives with a pseudo-bulge-like structure and evolve into disc galaxies before becoming classic elliptical galaxies. Madgwick et al. (2002), Driver et al. (2007), Yang et al. (2009), and Tempel et al. (2011) find that the galaxy LF varies with both color and morphological type. Early-type galaxies typically have larger characteristic magnitudes and flatter faint-end slopes than late-type galaxies. Similarly, red galaxies tend to have flatter faint-end slopes and slightly larger characteristic magnitudes than blue galaxies. They also find that the bright end of the LF is characteristically determined by red and elliptical galaxies, while the faint end is dominated by blue and spiral galaxies.

Determining how LFs split based on color and type vary with environment gives us insight as to how large-scale structure affects the evolution of galaxies. For example, Tempel et al. (2011) find that the shape of the spiral galaxy LF is independent of environment. This implies that spiral galaxies in voids evolve no differently than spiral galaxies in denser regions. They also find that the faint-end of the elliptical galaxy LF steepens with increasing density. This effect is likely due to the presence of satellite galaxies that formed in the early Universe and have since been tidally stripped quenching star formation at later times. However, these authors only probe the environmental effects on the LF of galaxies down to $M_r = -17$.

Previous measurements of the galaxy LF dependence on large-scale structure range from void regions (Grogin & Geller, 1999; Hoyle et al., 2005; Tempel et al., 2011), to groups (Eke et al., 2004; Yang et al., 2009), to clusters (De Propris et al., 2003; Durret et al., 2011; McNaught-Roberts et al., 2014; Martinet et al., 2014b). The environmental effects on the characteristic magnitude

remain consistent across the literature: M^* becomes fainter with decreasing large-scale density. The environmental dependence of α varies in the literature depending on the survey, redshift limits, magnitude limits, and methods used.

Previous estimates of the best fit Schechter function faint-end slopes of the galaxy LF in voids are not well constrained. Estimates range from $\alpha = -1.18 \pm 0.13$ for a small sample of galaxies brighter than $M_r = -14.5$ (Hoyle et al., 2005) to $\alpha = -0.98 \pm 0.02$ for galaxies brighter than $M_r = -17$ (Tempel et al., 2011) to $\alpha = -1.36 \pm 0.05$ for galaxies brighter than $M_r = -17$ (McNaught-Roberts et al., 2014). In the dwarf ($M_r > -17$) regime, Hoyle et al. (2005) find that the faint-end slope remains the same between void galaxies and those in denser regions. The best fit LF faint-end slopes of galaxy groups vary from $\alpha \sim -1.0$ to -1.2 where the faint-end slope steepens with increasing group mass (Eke et al., 2004; Tully, 2005; Yang et al., 2009). As for dwarf galaxies in groups, Tully (2005) finds that more dynamically evolved regions have steeper faint-end slopes. The faint-end slopes of composite LFs for clusters yield slopes ranging from $\alpha \sim -1.25$ to -1.4 (Valotto et al., 1997; De Propris et al., 2003; Durret et al., 2011; McNaught-Roberts et al., 2014; Martinet et al., 2014b). Additionally, Tempel et al. (2011) find that elliptical galaxies dominate the LF in high-density regions. This corroborates the luminosity-morphology-density relation of Park et al. (2007) and the work of Hoyle et al. (2012) who find that galaxies in the most underdense voids are primarily bluer, late-type galaxies. The overall trend for nearby groups and clusters seems to be that the faint-end slope steepens with increasing density. Where the void galaxy LF faint-end slope fits in to this trend is currently uncertain. To date, studies using large ($> 10^4$) sample sizes have not probed the void LF down to the dwarf regime ($M_r > -17$).

In this chapter, we will investigate the optical LF of void galaxies down to $M_r = -13$. The dwarf faintest end of the LF that we probe could be plagued by low-surface brightness selection effects. Blanton et al. (2005b) estimate the LF of extremely low luminosity galaxies, but do not explore the environmental effects. These authors also examine the effects of low-surface brightness selection in the extremely low luminosity sample and find that accounting for low surface brightness selection effects steepens the global LF faint-end slope from $\alpha \sim -1.3$ to $\alpha \sim -1.5$.

To avoid the optical selection bias against low surface brightness galaxies, we would like to determine the effects on the optical LF of a sample of H I selected galaxies. Zwaan et al. (2001) estimate the LF using an H I selected sample from the Arecibo H I Strip Survey (AHISS), an approach that is free from optical selection biases. These authors find the LF of AHISS detections are in good agreement with those of late-type galaxies. However, Zwaan et al. (2001) have a sample size of only 60 H I detections. For the first time, we have a statistically significant sample of matched optical and H I data with which we can estimate the optical galaxy LF.

Blind H I surveys typically detect bluer galaxies than optically selected surveys with large values of the inverse concentration index which is characteristic of late-type galaxies. Given the known similarities between the void galaxies (Hoyle et al., 2012; Croton & Farrar, 2008) and H I selected galaxies (Toribio & Solanes, 2009; Huang et al., 2012a) (e.g. blue, late-type, high-specific star formation rates), we expect to find a larger fraction of void galaxies in our H I selected sample (Moorman et al., 2014) and less environmental dependence on the optical LF of H I selected samples than found for optically selected samples. Namely, a smaller shift in characteristic magnitudes and similar faint-end slope between void and wall LFs. Thus, we will also test for environmental dependencies on the optical LF of H I selected galaxies.

ΛCDM simulations predict a steep ($\alpha \sim -1.8$) power law slope at the faint end of the dark matter halo mass function (Mathis & White, 2002; Klypin et al., 2011). Halo occupation distribution models provide a statistical description of the number of luminous galaxies that occupy a halo of given mass: massive halos host a "central" galaxies as well as less luminous "satellites," while very low mass halos may host, at most, one central galaxy. ΛCDM simulations predict that the characteristic mass of the dark matter halo mass function shifts toward lower mass in low density regions (Goldberg et al., 2005). Together, these results imply that faint galaxies in voids are likely to be"central" galaxies in their own halos, while faint galaxies in denser regions are likely to be satellites of more luminous galaxies. Additionally, the hydrodynamic simulations used in Sawala et al. (2014) which were tailored to match the conditions of the Local Group imply that luminous, low-mass halos near "central" halos were probably once larger halos that formed stars in the early Universe and have

since been tidally stripped by neighboring halos. These results imply a relatively steep faint-end slope in dense regions. Other simulations predict varying environmental effects on the faint-end slope of the galaxy LF. For instance, Mathis & White (2002) predict a steeper faint-end slope in low-density regions, while Cui et al. (2011) predict that the faint-end slope in low-density regions is similar to that of high-density regions. Therefore, accurately measuring the shape of the faint-end of the LF provides strong constraints for formation models of dwarf galaxies.

The observed galaxy LF slope is significantly shallower ($\alpha \sim -1.3$) than the predicted low-mass halo slope. For theory to match observations, the incorporation of feedback and photoionization effects is required in simulations to suppress star formation in galaxies at both the faint and bright ends. Current simulations (e.g. the Millennium Simulation, Springel et al. (2005)) have incorporated star formation quenching effects such that the outcome of the predicted LF matches current measurements of the observed LF. However, if the current measurements are underestimating the "true" faint-end slope of the galaxy LF as predicted by Blanton et al. (2005b), then the simulations may need to scale back the effects of feedback and photoionization to account for the presence of LSB galaxies.

In this chapter, we present the environmental effects on the LF of optically selected galaxies from the SDSS DR7 and H I selected galaxies from the ALFALFA Survey. In Section 3.2 we briefly discuss the data, void identification method, and compare the properties of H I and optically selected samples. In Section 3.3 we discuss the methods used. We present the optical LF of void and wall galaxies from SDSS DR7 galaxies as well as the void and wall LFs of H I detections from the ALFALFA Survey in Section 3.4. Here, we also discuss any differences between the optical LFs of H I and optically selected galaxies. We discuss the conclusions of our work in Section 3.5. Throughout this chapter, we assume $\Omega_m = 0.26$ and $\Omega_\Lambda = 0.74$ when calculating comoving coordinates and absolute magnitudes.

3.2 Data

3.2.1 SDSS DR7

The Sloan Digital Sky Survey (SDSS) (Fukugita et al., 1996; Gunn et al., 1998; Lupton et al., 2001; Strauss et al., 2002; Blanton et al., 2003a) is a wide-field multi-filter imaging and spectroscopic survey covering a quarter of the northern Galactic Hemisphere in the five band SDSS system – u, g, r, i, and z. Once each image is classified, follow up spectroscopy is done on galaxies with r-band magnitude $r < 17.77$. Spectra obtained through the SDSS are taken using two double fiber-fed spectrographs and fiber plug plates covering a portion of the sky 1.49° in radius with minimum fiber separation of 55 arcseconds.

For the optical data in this work, we utilize the Korea Institute for Advanced Study Value-Added Galaxy Catalog (KIAS-VAGC) of Choi et al. (2010). The KIAS-VAGC catalog is based on the SDSS Data Release 7 (DR7) (Abazajian et al., 2009) spectroscopic targets in the main galaxy sample and contains 707,817 galaxies.

3.2.2 ALFALFA

The Arecibo Legacy Fast ALFA (ALFALFA) Survey (Giovanelli et al., 2005b,a) is a large-area, blind extragalactic H I survey with sensitivity limits allowing for the detection of galaxies with H I masses down to $M_{HI} = 10^8 M_\odot$ out to 40 Mpc. The most recent release of the ALFALFA Survey ($\alpha.40$; Haynes et al., 2011), covers ∼2800 deg^2 across two regions in the northern Galactic Hemisphere, called the Spring Sky, (07^h30^m <R.A.< 16^h30^m, 04° < Dec < 16° and 24° < Dec < 28°), and two in the southern Galactic Hemisphere, called the Fall Sky, (22^h <R.A.< 03^h, 14° < Dec < 16° and 24° < Dec < 32°). The H I detections in this catalog are categorized as either Code 1, 2, or 9. Code 1 objects are reliable detections with high S/N (> 6.5); Code 2 objects have S/N< 6.5 and coincide with optical counterparts with known redshift similar to the H I detected redshift; and Code 9 objects are high velocity clouds.

To obtain optical properties of the H I sources, we use the cross-reference catalog of 12,468 ALFALFA H I sources with the most probable optical counterpart from the SDSS DR7 supplied by Haynes et al. (2011). Because we are interested in each galaxy's environment, we must limit our

sample to objects found in the region accessible to the DR7 void catalog of Pan et al. (2012), the NGC region. We limit our sample to Code 1 detections within $z \leq 0.05$, due to radio frequency interference beyond this redshift range.

For our detections, we query the SDSS DR7 database to obtain all information needed for the analysis in this work, such as color, inverse concentration index, absolute magnitude, and surface brightness. Because we compare optically selected galaxy LFs to H I selected galaxy LFs, we must remain consistent in how we determine absolute magnitudes, M_r. Therefore, we K-correct the magnitudes and band-shift each H I source's M_r to $z = 0.1$ using K-correct Version 4.4 (Blanton & Roweis, 2007) as done in the KIAS-VAGC. Because not all ALFALFA detections have optical spectroscopy, we adopt the 21 cm redshift for determining each galaxy's comoving distance and r-band absolute magnitude.

3.2.3 Creating the Void Samples

We classify all of our galaxies as void or wall detections by comparing the comoving coordinates of each to the void catalog of Pan et al. (2012). This void catalog uses the galaxy-based void finding algorithm of Hoyle & Vogeley (2002), VoidFinder (also, see El-Ad & Piran (1997)). We briefly discuss the algorithm here: VoidFinder grows spheres in underdense regions of a map populated by a volume-limited sample. We require each underdense sphere to live completely within the survey mask and have a minimum radius of $10h^{-1}$Mpc to be considered a true void. Because we require each sphere to lie completely within the mask, we risk misclassifying true void galaxies along the edges as wall galaxies. From the optically selected sample, we identify $75,063$ (21%) void galaxies and $274,436$ (77%) wall galaxies within $z < 0.107$. The remaining galaxies (2%) lie along the survey edges and are excluded due to the potential misclassification issues.

Similarly, for the H I selected sample, we positionally compare each H I detection's comoving coordinates to the void catalog. We identify $2,611$ (35%) void detections, $4,566$ (60%) wall detections, and 390 (5%) detections located near the survey edges.

For the sake of comparing the effects of the selection biases between the SDSS and ALFALFA samples, we make an optically selected subsample which we call $\mathrm{SDSS_{nearby}}$. For $\mathrm{SDSS_{nearby}}$, we limit

ourselves to galaxies within $z < 0.05$. We further limit the sample to galaxies within 07^h30^m <R.A.< 16^h30^m, 04° < Dec < 16° and 24° < Dec < 28° to ensure we only use galaxies within the same volume as our ALFALFA sample. We compare the magnitude-limited ($r < 17.6$) $\mathrm{SDSS_{nearby}}$ galaxy locations to the void catalog of Pan et al. (2012). We identify 7,058 (25%) void galaxies, 20,148 (73%) wall galaxies, and 537 (2%) galaxies living near the survey edges. The reader should keep in mind that a "void" sample from an H I survey and a "void" sample obtained from an optical survey contain fundamentally different galaxies.

3.2.4 Comparing The H I and Optically Selected Samples

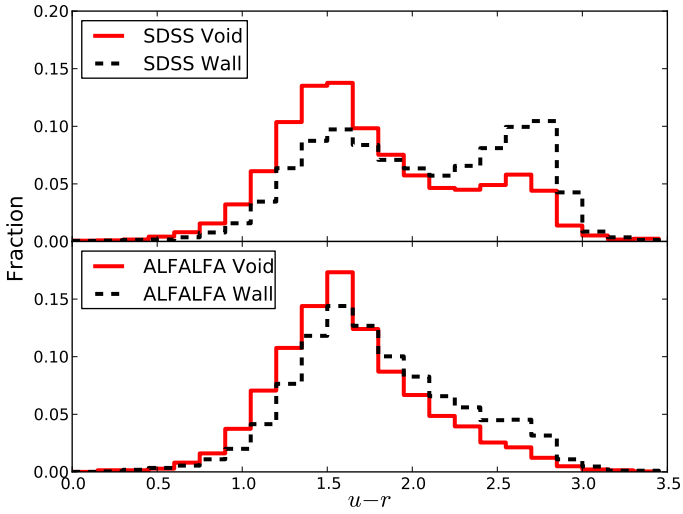

Figure 3.1 Color distribution of $\mathrm{SDSS_{nearby}}$ (upper) and ALFALFA (lower) void (red) and wall (black) galaxies. The $\mathrm{SDSS_{nearby}}$ sample contains 7,058 void galaxies and 20,148 wall galaxies. The ALFALFA sample contains 2,611 void detections and 4,566 wall detections. Both SDSS distributions appear bi-modal, with a less prevalent red sequence peak in the void distribution as evident in the results of Hoyle et al. (2012). The ALFALFA color distributions do not appear to be as bimodal as the SDSS distributions do, because H I selection is biased against luminous, red galaxies. We see a hint of the red sequence in the H I selected wall distribution, but the void distribution appears to follow a skewed unimodal distribution originating from the blue cloud. For both surveys, void galaxies are generally bluer than wall galaxies.

Previous studies on the types of galaxies typically found by blind-H I surveys reveal late-type, mostly blue galaxies with high star formation rates and specific star formation rates (Toribio & Solanes, 2009). Huang et al. (2012a) provide an in-depth comparison of optically and H I selected samples and show that galaxies detected in H I tend to have low star formation efficiencies. Here

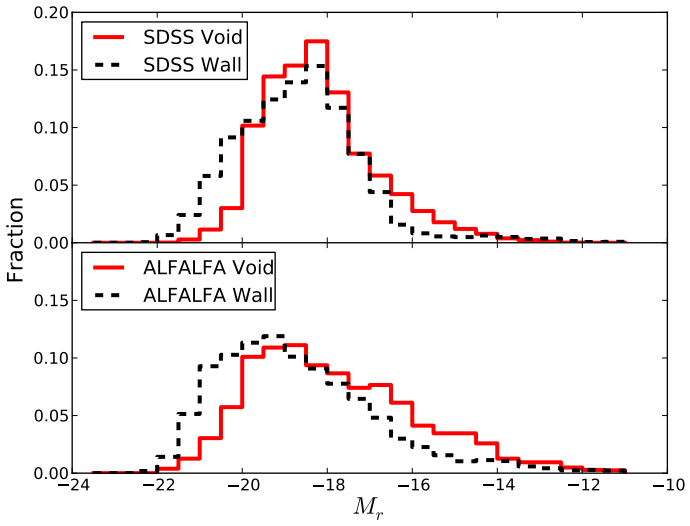

Figure 3.2 Magnitude distribution of $\mathrm{SDSS_{nearby}}$ (upper) and ALFALFA (lower) void (red) and wall (black) galaxies. The $\mathrm{SDSS_{nearby}}$ sample contains 7,058 void galaxies and 20,148 wall galaxies. The ALFALFA sample contains 2,611 void detections and 4,566 wall detections. Consistent with previous work (Hoyle et al. 2012), we see that the SDSS void r-band magnitude distribution shifts to fainter galaxies. In agreement with this trend, H I selected void galaxies tend to be fainter than their counterparts in denser regions.

we briefly compare the environmental differences of an H I selected sample from the ALFALFA Survey and an optically selected sample from the SDSS catalog covering the same volume of sky ($\mathrm{SDSS_{nearby}}$).

In Figure 3.1 we compare the optical $u-r$ color distribution of $\mathrm{SDSS_{nearby}}$ (upper) and ALFALFA (lower) galaxies. We obtain galaxy colors using SDSS model magnitudes. The feature that is most evident is the deficiency of red galaxies in the ALFALFA sample compared to the SDSS sample. The void and wall SDSS color distributions are bimodal with the second peak appearing as a result of the highly populated red sequence, whereas the H I color distributions are unimodal with only a slight presence of the red sequence in the ALFALFA wall sample. While a majority of the ALFALFA detections are blue, we notice the void population on average tends to be *bluer* than the wall population. Hoyle et al. (2012) notice a similar trend towards bluer colors in the SDSS void sample. In both survey samples, we notice significantly fewer red galaxies in the void populations than those in walls.

In Figure 3.2 we present the r-band absolute magnitude distributions of the $\mathrm{SDSS_{nearby}}$ (upper) and ALFALFA (lower) samples. As shown in Hoyle et al. (2012), we see a shift toward fainter magnitudes in the SDSS void sample. The H I void galaxy sample detects relatively more dwarf galaxies than the optically selected sample. This is because the SDSS spectroscopic main galaxy sample is biased against faint, low-surface brightness, patchy galaxies, which are more easily detectable in an H I survey. Because of the relative abundance of dwarf galaxies in the H I sample we suspect the LF of ALFALFA galaxies will have a much steeper slope than the optically selected sample. We also see that the H I selected wall galaxies are slightly brighter than the typical optically selected wall galaxies on average. A typical galaxy in a wall will experience gas stripping phenomena (tidal stripping, mergers, ram pressure stripping, etc.), thereby reducing the H I fraction of its baryonic content. This reduced H I fraction will contain just enough H I to be detected by a radio survey for only the largest/brightest galaxies in the walls. We suspect the shift towards brighter galaxies in the mean of the distribution of the ALFALFA wall sample compared to the $\mathrm{SDSS_{nearby}}$ wall sample will result in the ALFALFA wall LF having a somewhat brighter characteristic magnitude than that of $\mathrm{SDSS_{nearby}}$.

As galaxies evolve, they are thought to move from the blue cloud to the red sequence after star formation has been quenched. Galaxies in voids are typically less evolved–and, therefore, fainter and more gaseous–than similar sized galaxies in walls. This makes void galaxies easy targets for radio surveys. As we will show later in Section 3.4.3, ALFALFA prefers less evolved galaxies regardless of environment.

3.3 Method

3.3.1 The SWML Method

The LF is a measure of the number of galaxies per Mpc^3 in a magnitude range dM_r centered at magnitude M_r. For each measurement of the LF, we find the best fit parameters of a Schechter (1976) function of the form

$$\Phi(M_r) = 0.4 \ln 10 \Phi^* 10^{0.4(M^*-M_r)(\alpha+1)} \times \exp\left(-10^{0.4(M^*-M_r)}\right). \tag{3.1}$$

We estimate the LF of our SDSS and ALFALFA void and wall samples using the stepwise maximum likelihood (SWML) method of Efstathiou et al. (1988). The SWML method does not retain information about the normalization of the LF; therefore, we adjust the amplitude according to the number density of the particular sample of interest. We estimate the best-fit Schechter parameters (the normalization factor Φ^*, the characteristic magnitude M^*, and the faint-end slope α) to our functions over the magnitude range $-22.0 < M_r < -13.0$ using a least squares estimator.

3.3.2 Errors

We estimate errors for each optical LF from three sources. The first source is Poisson error which account for $\sim$ 70 percent of the uncertainties in each bin. These errors affect the brightest and faintest ends more so than the intermediate magnitude bins, because we have less information in the outermost bins. That is, extremely bright galaxies are uncommon in the Universe and the faintest galaxies are difficult to detect beyond the very nearby Universe.

The second source is the error in each bin introduced from the SWML method, described in Efstathiou et al. (1988). These errors account for about 30 percent of the total bin uncertainties. As with the Poisson errors, we have less information about the galaxy distribution in the brightest and faintest bins, making the uncertainties larger in these bins.

The third source is an error estimate accounting for the inhomogeneity of large-scale structure, using the jackknife method of Efron (1982). For this source of error, we divide our region of interest into 18 subregions, and calculate the LF of the galaxy sample excluding one of the 18 regions for each iteration. We estimate the variance in each bin after all iterations. The jackknife errors account for less than 1 percent of the total error. This suggests that the SWML method is relatively robust against large-scale structure.

3.4 Results

3.4.1 LF of Void Galaxies in an Optically Selected Sample

We calculate the LF of our SDSS void and wall galaxies down to $M_r \sim -13$ using the methods outlined in Section 3.3. In Figure 3.3, we present our estimates of the void (red) and wall (black)

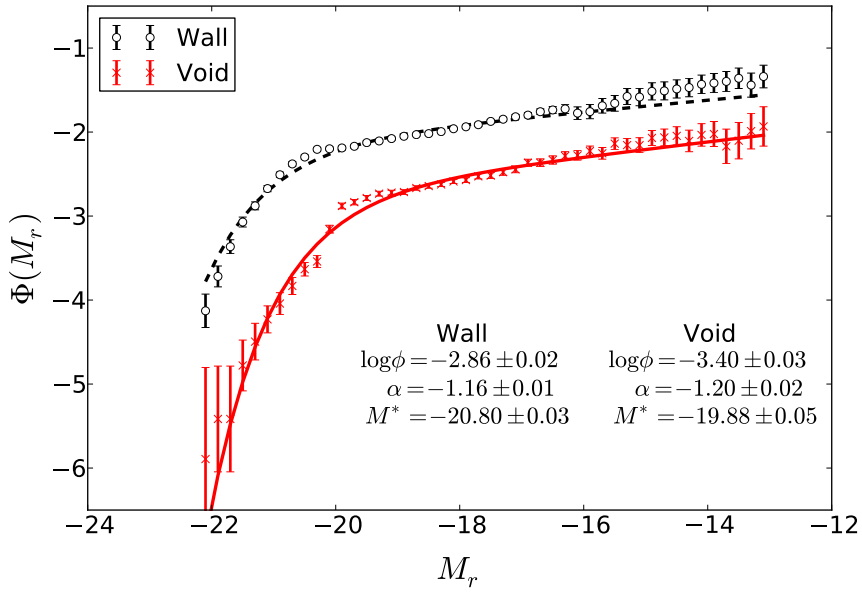

Figure 3.3 LF of SDSS void (red) and wall (black) galaxies. We find a shift towards fainter galaxies by almost a full magnitude. Consistent with previous studies, we do not find a statistically significant difference in the faint-end slopes.

galaxy LFs with the best fitting Schechter functions. The parameters associated with the best fit Schechter functions are: $\log \Phi^* = -3.40 \pm 0.03$ log(Mpc^{-3}), $M^* = -19.88 \pm 0.05$, and $\alpha = -1.20 \pm 0.02$ for void galaxies, and $\log \Phi^* = -2.86 \pm 0.02$ log(Mpc^{-3}), $M^* = -20.80 \pm 0.03$, and $\alpha = -1.16 \pm 0.01$ for wall galaxies. An explanation of uncertainties may be found in Section 3.3.2. Much like the void/wall LF results found using a previous partial data release of the SDSS (Hoyle et al., 2005), we find about a one magnitude shift in M^* towards fainter galaxies in voids. It is obvious from Figure 3.3 that the faint-end slopes of both the void and wall LFs are underestimated. For a more accurate estimation of the faint-end slopes, we fit a power law to the LF values fainter than $M_r = -18$. These power law slopes correspond to a slope of $\alpha = -1.25 \pm 0.02$ for void galaxies and $\alpha = -1.27 \pm 0.02$ for wall galaxies. There is no statistically significant difference between the slopes of the void and wall LFs down to $M_r \sim -13$, indicating that there is no relative excess of void dwarfs compared to the wall distribution. This faint-end slope result is consistent with the predictions of Cui et al. (2011), whose simulations show that the faint ends of the LF should remain the same between the most underdense and overdense regions. This conflicts with the predictions of

Mathis & White (2002), although these authors neglect SNe feedback and background UV radiation which should be included when calculating the infall rate of cold gas for low mass halos. The faint end of the void and wall LFs starts to stray from a classic Schechter function once we reach the dwarf regime ($M_r > -17$). This variation doesn't appear in the analysis of Tempel et al. (2011), because the authors exclude galaxies fainter than $M_r = -17$. Excluding these dwarf galaxies from our analysis, we find a faint-end slope that closely matches that of Tempel et al. (2011).

We notice a feature at the bright end ($M_r = -20.1$) of both the void and wall LFs: the void LF drops in amplitude, while the wall LF increases in amplitude. These features are an artifact of the void identification process. The void catalog is defined by a volume-limited sample corresponding to galaxies with $M_r < -20.1$. By defining the void catalog using galaxies brighter than this magnitude, we will see a significant decrease in the number of bright ($M_r < -20.1$) void galaxies and an increase in the number of bright wall galaxies.

Comparing to Previous Observations and Simulations

We have measured the galaxy LF in both voids and walls, where the wall environment is effectively an average over all higher density regions. Comparing the void and wall galaxy LFs reveals an expected shift towards fainter galaxies in voids, but does not reveal any dependence of the faint-end slope on large-scale underdensities. Our finding that the void faint-end slope matches the wall faint-end slope is similar to the trend found in Moorman et al. (2014) in which we find the low-mass slope of the void HIMF closely matches the low-mass slope of the wall HIMF. We suspect that the void faint-end slope closely matches the LF slope of all galaxies in denser regions averaged together (wall galaxies) for the following reason. Rojas et al. (2004) and Hoyle et al. (2012) show that void galaxies are generally blue, late-type galaxies, and Tempel et al. (2011) show that the faint-end slope of late-type galaxies does not vary with environment. Thus, one might expect the faint-end slope of the void galaxy LF to be an average of the slopes of LFs across denser environments where we find both early- and late-type galaxies.

Comparing our void LF results with previous work on the LFs of galaxy groups and clusters reveals a non-monotonic trend in α with environment. We find the void regions have a faint-end

slope around $\alpha = -1.2$, which is consistent with an earlier result in Hoyle et al. (2005). Croton et al. (2005) find that galaxies in regions with density contrast $-0.5 < \rho < 0$ (isolated galaxies not associated with voids) have a flattened faint-end slope of $\alpha \sim -1.0$. Galaxies in denser environments, such as galaxy groups, tend to have flat faint-end slopes in the $\alpha \sim -1.0$ to -1.2 range, where the slopes increase with increasing group mass (Eke et al., 2004; Yang et al., 2009). The faint-end slope of the composite LFs of galaxy clusters tend to range from $\alpha \sim -1.2$ to -1.4 (Valotto et al., 1997; De Propris et al., 2003; Croton et al., 2005; McNaught-Roberts et al., 2014). Put together, the overall trend of the faint-end slope with environment is average for voids, flattens for "field" galaxies, steepens with increasing mass in groups, and either remains constant or steepens further when the large-scale density increases to the cluster regime.

The steepening trend among denser regions is consistent with predictions from the hydrodynamic simulations of Sawala et al. (2014), who find that dwarf halos closer to central galaxies typically had higher masses in the earlier Universe, making the probability of star formation more likely. That is, galaxies are more likely to form in halos near denser regions than in isolated halos in the field. The steepening of α with increasing density from the field to clusters corroborates this prediction.

3.4.2 LF of Void Galaxies in an H I Selected Sample

As mentioned earlier, the predicted halo mass function has a steep slope of $\alpha = -1.8$, whereas the observed LFs (estimated here and in other works) have much shallower slopes of $\alpha \sim -1.2$ to -1.3. Blanton et al. (2005b) show that the faint end of the LF can be steepened to $\alpha \sim -1.5$ with the inclusion of low luminosity/low surface brightness galaxies. To avoid the optical selection bias against low surface brightness galaxies, we estimate the optical LF of a sample of H I selected galaxies from the ALFALFA sample.

We divide the ALFALFA galaxy sample into void and wall galaxies and estimate the r-band LF presented in Figure 3.4. It is clear from the figure that the H I selected LFs are not well fitted by a simple Schechter function, but for the sake of comparison between the LFs in this work and others, we provide the best fitting parameters to a Schechter function found using a least squares estimator. For the void sample, we estimate the best fitting Schechter parameters to be $\log \Phi^* = -4.43 \pm 0.09$

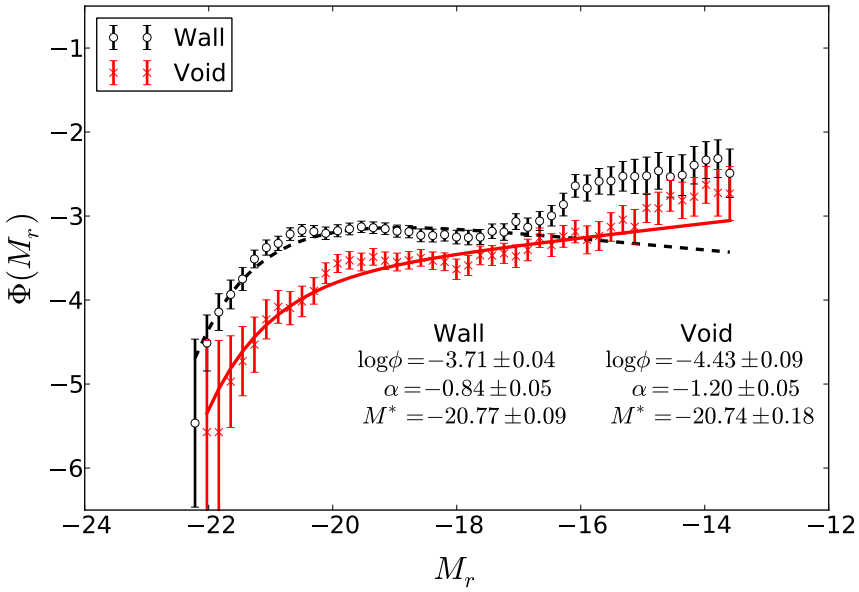

Figure 3.4 LF of H I selected void (red) and wall (black) galaxies from α.40 Spring Sky. Both void and wall LFs are poorly fit by a simple Schechter function as shown by the curves depicting the best fit Schechter functions found via a least squares estimator.

log(Mpc^{-3}), $M^* = -20.74 \pm 0.18$, and $\alpha = -1.20 \pm 0.05$. For the wall galaxy sample, we estimate $\log \Phi^* = -3.71 \pm 0.04$ log(Mpc^{-3}), $M^* = -20.77 \pm 0.09$, and $\alpha = -0.84 \pm 0.05$. See Section 3.3.2 for an explanation of uncertainties. The curves in Figure 3.4 show the Schechter functions associated with these best-fit parameters; however, the Schechter fits underestimate both the bright and faint ends of the ALFALFA LFs.

At the bright end, the best-fit Schechter function predicts the characteristic magnitudes of both the void and wall samples to be too bright. To get a realistic sense of the shift in M^* between voids and walls, we fit only the bright end ($-22 \leq M_r \leq -18$) of the LFs revealing a shift in M^* towards fainter magnitudes in voids by about one half of a magnitude (see the left panel of Figure 3.5). The direction of this shift is consistent with the shift in the dark matter halo mass function of extended Press-Schechter theory (Goldberg et al., 2005). The magnitude of the shift is significantly less than the shift in the predicted halo mass function as well as the shift in M^* of the SDSS LF found in the previous section. The reason for this smaller shift is that typically the brightest galaxies in denser regions have burnt through their cool gas, lost their gas during mergers, and/or had it stripped away

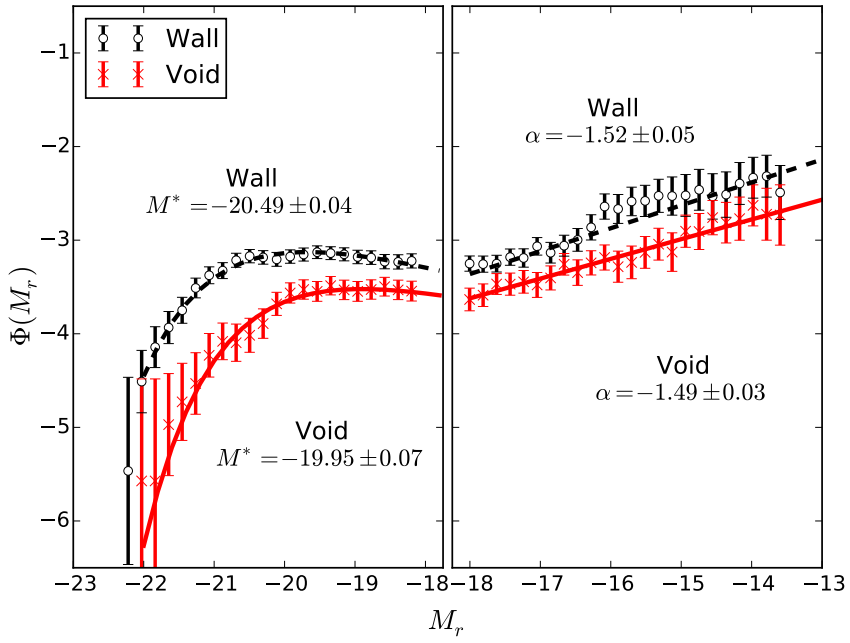

Figure 3.5 Separately fit LF parameters of the brightest and faintest H I selected void (red) and wall (black) galaxies from $\alpha.40$ Spring Sky. We identify the M^* parameter by fitting a Schechter function only to the bright ($M_r < -18$) end of the LF to reveal the true shift in the characteristic magnitude between voids and walls. The curves to the left of $M_r = -18$ represent the Schechter fits to the bright galaxy distribution. We separately fit a power law to the faint end of the LF. The lines plotted at the faint end represent the best fit slopes.

via tidal stripping, ram pressure stripping, etc. Therefore, a survey looking for cool neutral gas will detect the brightest galaxies within denser regions far less frequently than an optically selected sample. While an optically selected spectroscopic sample may be biased against faint, low-surface brightness galaxies, an H I selected sample is biased against massive, red galaxies.

At the faint end, the best fitting Schechter function also severely underestimates the faint-end slopes of the void and wall LFs, estimating a much shallower slope than actually observed. To more accurately determine the faint-end slopes, we fit a power law function to only the faint ends ($-18 < M_r \leq -13$) of the LFs. The new faint-end slopes of the H I selected LFs (shown in the right panel of Figure 3.5) are $\alpha = -1.49 \pm 0.03$ for voids and $\alpha = -1.52 \pm 0.05$ for walls. We see no statistically significant difference in the faint-end slopes of the void and wall LFs. The faint-end slopes of the ALFALFA void and wall LFs appear to be independent of large-scale environment. We suspect this is largely due to the relatively large number of late-type galaxies (which generally

Table 3.1 Best fit power law and Schechter function parameters to the optical LFs of the SDSS and ALFALFA samples across environments. Each LF was split into a bright end and faint end, separated at $M_{\rm r} = -18$. Each bright end was fit by a Schechter function; from this function, we extract the characteristic magnitude parameter, M_r^*. Each faint end ($M_r > -18$) was fit by a power law function. From this fit, we extract the faint-end slope parameter, α.

Sample	LSS	M_r^*	α
SDSS	void	-19.32±0.03	-1.25±0.02
SDSS	wall	-20.54±0.02	-1.27±0.02
$\rm SDSS_{nearby}$	void	-19.30±0.06	-1.31±0.04
$\rm SDSS_{nearby}$	wall	-20.55±0.03	-1.23±0.03
ALFALFA	void	-19.95±0.07	-1.49±0.03
ALFALFA	wall	-20.49±0.04	-1.52±0.05

dominate the faint-end of the LF) present in the ALFALFA sample compared to massive, elliptical galaxies. Tempel et al. (2011) find the LF of spiral galaxies is independent of environment, while the faint-end slope of the observed elliptical galaxy LF steepens with increasing large-scale densities.

To more directly compare the void and wall distributions of the H I and optically selected samples, we need to compute the optical LF of SDSS and ALFALFA galaxies over the same volume of sky. Therefore, we measure the LF of the $\rm SDSS_{nearby}$ sample and estimate its characteristic magnitude and faint-end slope in the following way. For each sample (SDSS, $\rm SDSS_{nearby}$, and ALFALFA), we split each LF into a bright and faint end, divided at $M_r = -18$. The bright end is fit with a Schechter function, from which we obtain the sample's characteristic magnitude, M^*. Each faint end is separately fit with a power law, from which we obtain the faint-end slope of each LF. We provide these fits to the data in Table 3.1. Note the M^* and α parameters in the table are not the same related parameters estimated in equation (3.1).

Two interesting comparisons arise from this table. The first comes from comparing the full SDSS and $\rm SDSS_{nearby}$ fits, which gives us information on how the selected volume affects the shape of the LF. We find it interesting that reducing the area and redshift affects the void faint-end slope. The faint-end slopes of the full SDSS sample are more accurate, because we are averaging over more structure. The large-scale structure within the nearby volume may be atypical of the full Universe. The second comparison worth making is between the ALFALFA and $\rm SDSS_{nearby}$ fits, which gives us

information on how sample selection affects the shape of the LF. We see that using an H I selected sample produces a much steeper faint-end slope than an optically selected sample. This is due mostly to the inclusion of extremely low luminosity galaxies in H I surveys. The SDSS photometry affects the main galaxy sample target selection. The selection process is biased against low-surface brightness galaxies, so these faint galaxies are excluded from our optical sample. (Refer to Figure 3.2 for a comparison of the M_r distributions of the two samples.) The power law fits to the faint-end slopes match closely those shown in Blanton et al. (2005b) who investigate the effects of extremely low luminosity galaxies on the faint-end slope of the galaxy LF. Again, these authors find that the slopes increase from $\alpha = -1.3$ to $\alpha = -1.5$ when adjusting for the incompleteness of the SDSS spectroscopic sample at low surface brightnesses.

3.4.3 Comparing the Optically and H I Selected LFs

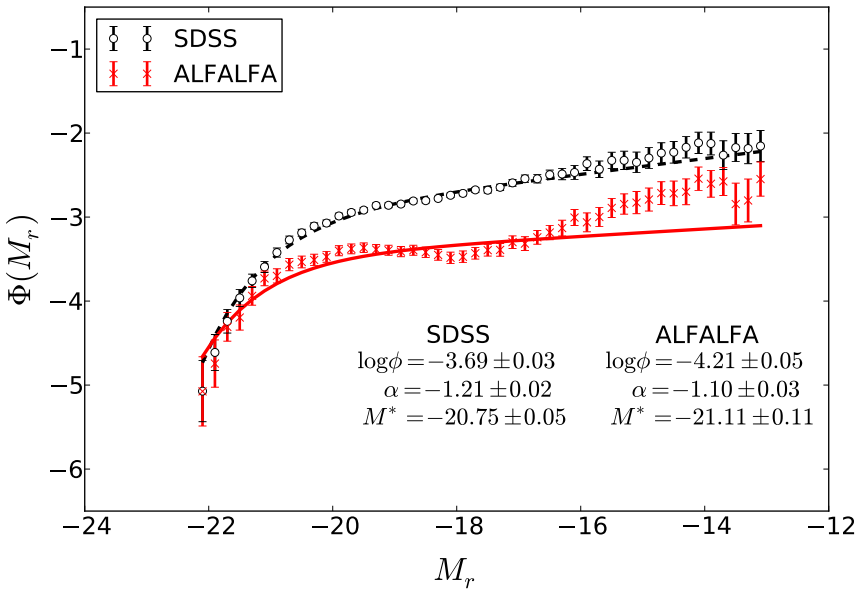

Figure 3.6 LF of optically selected galaxies from $\text{SDSS}_{\text{nearby}}$ with the best-fit Schechter function (black) and the LF of H I selected galaxies from the $\alpha.40$ Spring Sky with the best-fit Schechter function (red).

In Figure 3.6, we present the global LF of the Spring Sky subsample of the $\alpha.40$ data set as well as that of $\text{SDSS}_{\text{nearby}}$ sample. We see in this figure, as well as the previous subsection, that the optical LF of H I selected galaxies has a clearly different shape than that of the optically selected

galaxies. The optically selected LF is reasonably well fitted by a Schechter function with estimated parameters $\log \Phi^* = -3.69 \pm 0.03$ log(Mpc^{-3}), $M^* = -20.75 \pm 0.05$, and $\alpha = -1.21 \pm 0.02$. It is clear from the figure that the H I selected global LF is not fit well by a Schechter function. The best fit Schechter parameters are $\log \Phi^* = -4.21 \pm 0.05$ log(Mpc^{-3}), $M^* = -21.11 \pm 0.11$, and $\alpha = -1.10 \pm 0.03$. One of the most notable aspects of the H I selected LF is a broad, dip-like feature around $M_r = -18$ followed by a sharp upturn at fainter magnitudes. Evidence of a similar dip and upturn is seen in Zwaan et al. (2001) in the LF of H I selected galaxies from the Arecibo H I Strip Survey, though the authors only use a sample of 60 H I sources and attribute the features of the faint-end slope to low number statistics. For the first time, we show statistically significant evidence for a population of LSB dwarf galaxies present in the H I selected optical galaxy LF.

We suspect that the wide dip present in the ALFALFA LF is the result of a linear combination of different types of optically selected galaxies, i.e. dwarfy-starbursting galaxies at the faint end and gas-rich spirals at the bright end. In the next section, we will investigate different combinations of optically selected galaxies that may produce similar features and further split the H I sample to see which properties of the galaxies may be causing these features. Additionally, we wish to note that Papastergis et al. (2012) see a similar, albeit much shallower, dip feature in the baryonic mass function of ALFALFA galaxies. While these two phenomena may be related, it does not explain the severity of the dip seen in the ALFALFA galaxy LF.

Following the previous subsection, we fit the bright and faint ends separately with a Schechter function and power law, respectively. Again, the bright/faint division takes place at $M_r = -18$, where we see the dip-like feature. The characteristic magnitude of the H I selected sample brighter than $M_r = -18$ is $M^* = -20.48 \pm 0.04$. The faint-end slope, estimated via a power law fit to the LF fainter than $M_r = -18$, is $\alpha = -1.47 \pm 0.02$. As mentioned above, the dramatic steepening of the faint-end slope of the H I selected LF is most likely due to the inclusion of extremely low luminosity/LSB galaxies (Blanton et al., 2005b). Figure 3.7 shows the presence of a population of LSB galaxies in our ALFALFA sample that do not appear in the spectroscopic SDSS sample. The SDSS spectroscopic sample is biased against these very faint galaxies, thus we do not see such

a drastic upturn of the optically selected LF. Zwaan et al. (2001) find that gaseous LSB galaxies make up only 5±2 per cent of the luminosity density, suggesting that there shouldn't be low surface brightness effects from an H I survey, but these galaxies dominate the shape of the LF at the very faint end steepening the slope by $\Delta\alpha \sim 0.26$.

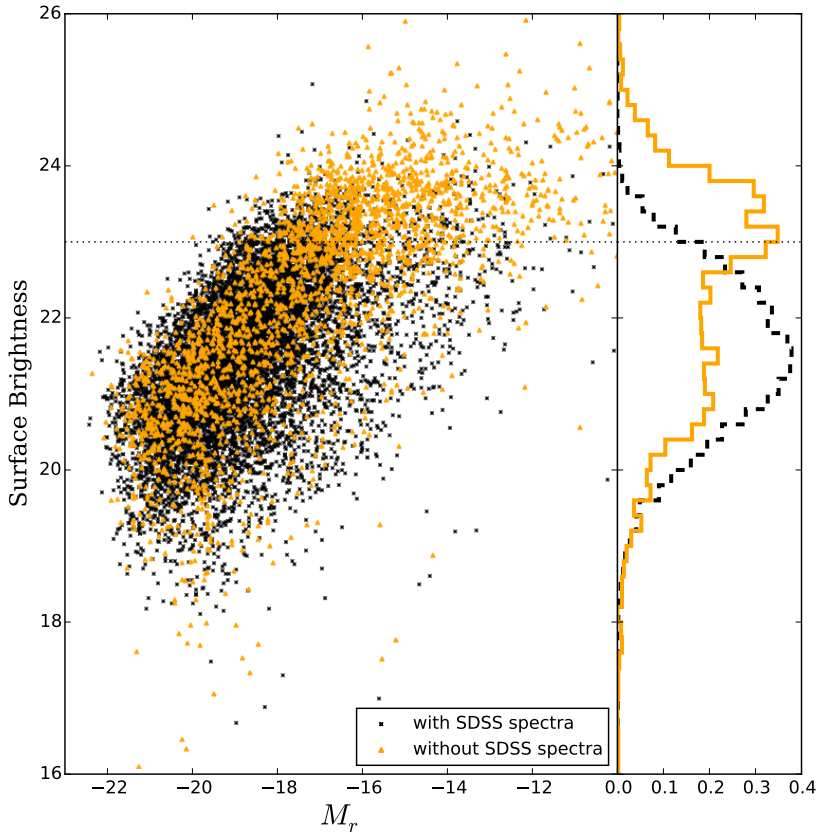

Figure 3.7 Distribution of ALFALFA galaxies with (black) and without (orange) SDSS spectra in SB–M_r space. ALFALFA contains a significant population of LSB dwarf galaxies not present in the SDSS main galaxy spectroscopic survey. The histogram (right panel) depicts the normalized SB distribution of ALFALFA galaxies with (dashed black) and without (orange) SDSS spectra. The dotted line denotes the LSB limit of Blanton et al. (2005b), in which galaxies with SB > 23 are considered to be LSB detections.

Subsets of the Optically Selected LF

Given the dramatic differences in the overall shapes of the ALFALFA and $\mathrm{SDSS_{nearby}}$ LFs, we would like to determine if the unique shape of the ALFALFA LF is reproducible using a combination of populations from the $\mathrm{SDSS_{nearby}}$ sample. Knowing that most galaxies in an H I survey tend to be blue, late-type galaxies, we first split the $\mathrm{SDSS_{nearby}}$ sample into blue and red galaxies using the

color cut from Moorman et al. (2014): $u - r = -0.09M_r + 0.46$, where M_r is an object's r-band absolute magnitude. We consider a galaxy with $u-r$ color less than the value given by the equation to be blue, otherwise the galaxy is considered red. Our resulting subsamples contain 16,548 blue galaxies and 11,147 red galaxies. We estimate the LF of blue and red samples, and, surprisingly, find that the red galaxy LF produces a dip similar to, albeit much shallower than, that of the ALFALFA sample. See Figure 3.8 for the LFs of optically selected blue and red galaxies.

Suspecting that the red sample is composed of both large elliptical galaxies as well as edge-on spirals reddened by dust, we split the $\mathrm{SDSS_{nearby}}$ red sample into two categories of morphological type. We make morphological cuts based on a galaxy's inverse concentration index (ICI), which is shown to be correlated with morphological type (Shimasaku et al., 2001). The ICI is defined to be $c_{in} = R_{50}/R_{90}$, where R_{50} and R_{90} are the radii containing 50% and 90% of the integrated Petrosian flux of a galaxy. In Figure 3.9 we present the normalized distribution of each sample's color vs. morphological type via the galaxies' inverse concentration indices. It is clear from the figure that ALFALFA tends to detect less evolved galaxies than SDSS, regardless of environment. Within the $\mathrm{SDSS_{nearby}}$ sample, it appears that the void galaxies span the range of inverse concentration indices of ICI=0.2-0.6, whereas the wall galaxies are primarily early-type galaxies (ICI<0.42).

From the $\mathrm{SDSS_{nearby}}$ sample, we have 8127 red elliptical galaxies and 3020 reddened spiral galaxies. As expected, we see, in Figure 3.10, that splitting the red sample by ICI produces two distinct functions. The early-type galaxies have a relatively flat distribution with a small dip-like feature present around $M_r = -18$, while the late-type galaxies are well fitted by a Schechter function with a faint-end slope similar to that of the global SDSS sample. The red, late-type galaxy LF has a similar characteristic magnitude to the blue galaxy LF, but has a shallower slope. Zwaan et al. (2001) show that their H I selected LF closely matches that of late-type galaxies found in optical surveys. We find that this is not the case for the ALFALFA LF, because of the significant population of massive gas-rich galaxies mentioned in Huang et al. (2012a). See Figure 3.11 comparing the ALFALFA LF and the $\mathrm{SDSS_{nearby}}$ late-type galaxy LF.

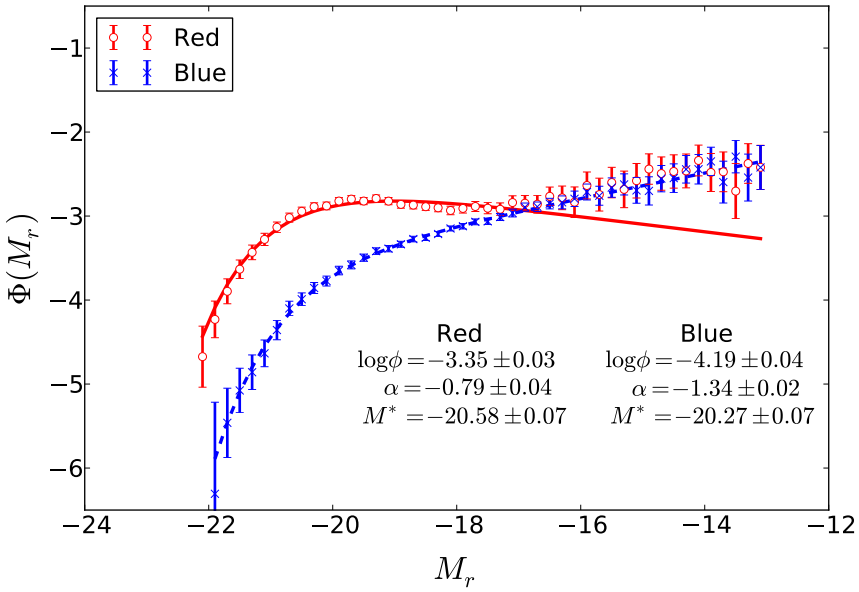

Figure 3.8 LF of red and blue optically selected galaxies from SDSS DR7 with best-fit Schechter functions. The red galaxy LF shows similar features to that of the H I sample.

Subsets of the H I Selected LF

No known H I selection effects could be responsible for producing such a wide dip in the galaxy LF. In attempts to directly determine what populations of galaxies could be influencing the shape of the H I selected optical LF, we divide the ALFALFA sample by color into red (1,376) and blue (6,234) galaxies and compute the LFs. As shown in Figure 3.12, the dip in the LF remains present in the H I selected red galaxy sample, and we see a much less prevalent inflection at the same magnitude for the H I selected blue galaxy sample. Splitting the red and blue distributions by morphological type, based on ICI, does not reveal the origin of the dip feature present in the ALFALFA LF. That is, no subsample of ALFALFA galaxies removes the dip feature from the LF.

3.5 Conclusions

Using the SDSS DR7 void catalog obtained from Pan et al. (2012), the KIAS-VAGC SDSS DR7 galaxy catalog from Choi et al. (2010), and the ALFALFA $\alpha.40$ catalog from Haynes et al. (2011), we measure the optical LF of 75,063 optically selected void galaxies with r-band magnitudes ranging from $-22.0 < M_r < -13.0$ and 2,611 H I selected void galaxies with r-band magnitudes ranging from

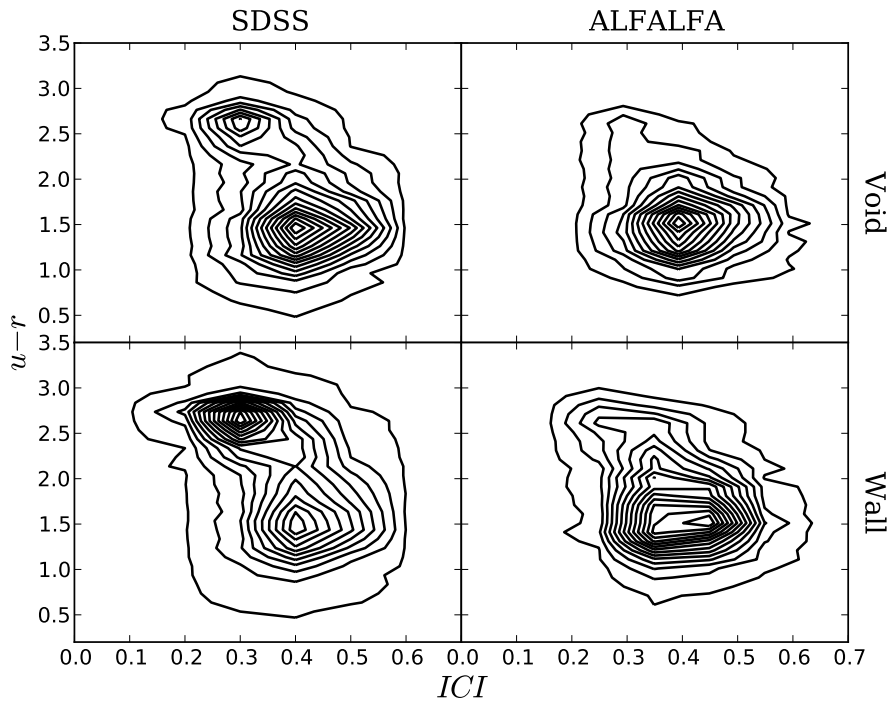

Figure 3.9 Normalized inverse concentration index vs. color density contours of void (top row) and wall (bottom row) galaxies in $\mathrm{SDSS_{nearby}}$ (left column) and ALFALFA (right rolumn). Both void and wall samples in SDSS contain both late- and early-type galaxies. The void galaxies are preferentially later-type, while the wall galaxies are primarily more evolved. Void and wall detections in ALFALFA both prefer blue, late-type galaxies.

$-22.0 < M_r < -13.0$. We find that sample selection plays a large role in determining the shape of the LF. Within a given data set, the large-scale environment affects the value of the characteristic magnitude of the LF, in that the characteristic magnitude shifts toward fainter values in cosmic voids. The environmental effects on the faint-end slope vary with the volume over which we look.

We find that the LF of void galaxies from the full SDSS sample is well fitted by a Schechter function with parameters $\log \Phi^* = -3.40 \pm 0.03$ $\log(\mathrm{Mpc}^{-3})$, $M^* = -19.88 \pm 0.05$, and $\alpha = -1.20 \pm 0.02$. For galaxies residing in higher density regions, we find the best fit Schechter parameters to be $\log \Phi^* = -2.86 \pm 0.02$ $\log(\mathrm{Mpc}^{-3})$, $M^* = -20.80 \pm 0.03$, and $\alpha = -1.16 \pm 0.01$. Our findings suggest that the location of the LF is dependent on environment. That is, the characteristic magnitude, M^*, shifts to fainter magnitudes in voids. For the optically selected sample, the shift in M^* is about one magnitude, consistent with an earlier partial SDSS data release (Hoyle et al., 2005). The direction

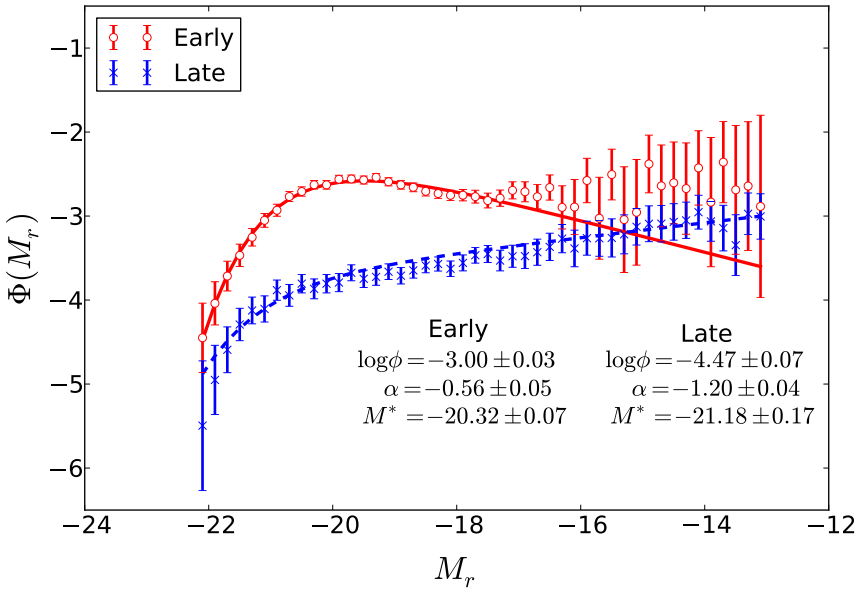

Figure 3.10 LF of red optically selected galaxies from $\text{SDSS}_{\text{nearby}}$ with best-fit Schechter functions split by morphology, as determined by the inverse concentration index. The early-type population has a relatively flat distribution and consists primarily of large elliptical galaxies. The late-type population has distribution that is well fitted by a Schechter function with a faint-end slope similar to that of the global sample.

of the shift is consistent with extended Press-Schechter theory which states that the dark matter mass function should shift to lower masses in underdense regions (Goldberg et al., 2005). When we fit Schechter functions to the void and wall LFs over the range $-22.0 < M_r < -13.0$, we see a small environmental dependence on the faint-end slope Schechter function parameter. However, the best fitting Schechter function underestimates the faint-end slope of the void and wall optical LFs. To account for this, we fit a power law to only the faint ends of the void and wall LFs (refer back to Table 3.1). We find that the true faint-end slope of the optically selected void galaxy LF is the same as that of the wall galaxy LF. It is important to note that the faint-end slope of the LF varies among isolated galaxies, groups, and clusters. The faint-end slope of the void LF matches the faint-end slope of all dense regions averaged together.

Limiting the SDSS sample to the volume over which $a.40$ and SDSS overlap ($\text{SDSS}_{\text{nearby}}$), yields similar results to the full SDSS sample, regarding M^*. That is, the characteristic magnitude in voids shifts fainter by about a full magnitude. However, we do see an environmental dependence on the

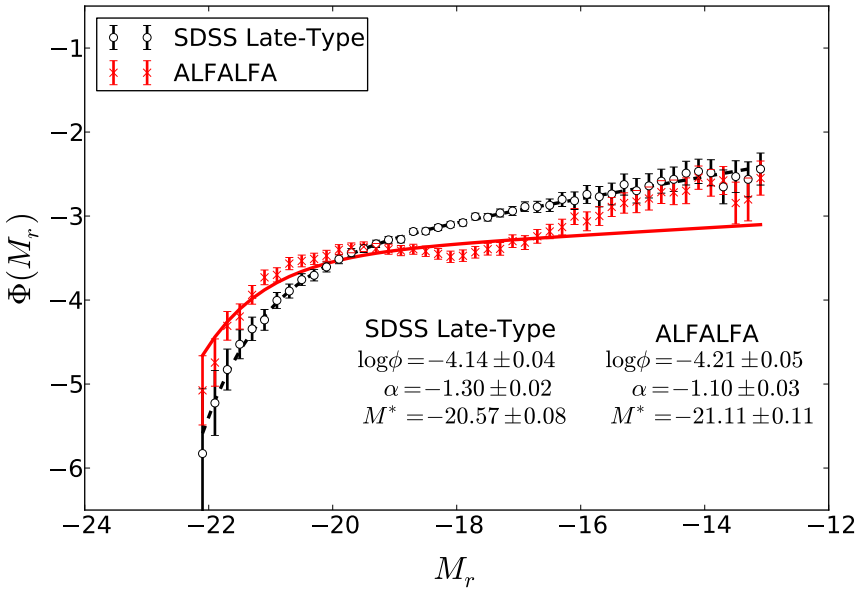

Figure 3.11 LFs of ALFALFA galaxies with best-fit Schechter functions (red) and $\mathrm{SDSS_{nearby}}$ late-type galaxies with best fit Schechter functions (black). Given that H I surveys tend to observe late-type galaxies, we would expect the ALFALFA LF to resemble the late-type $\mathrm{SDSS_{nearby}}$ LF. Surprisingly, this is not the case.

faint-end slope when we fit a power law to the void and wall faint-end slopes. Over this reduced volume, the faint-end slope of void galaxies, estimated by a power law fit to the faint end, steepens to $\alpha = -1.31 \pm 0.04$ as opposed to $\alpha = -1.23 \pm 0.03$ in walls. The difference in faint-end slopes in the $\mathrm{SDSS_{nearby}}$ sample is due to the fact that we are not averaging over as much structure as in the full SDSS sample. The large-scale structure within the nearby volume is likely not representative of the full volume of the local Universe; thus, we suspect the full SDSS LF estimates are better representatives of the actual void and wall LFs of the local Universe. The estimated faint-end slopes of galaxy LFs are highly dependent on the volume over which we observe, and we provide these results solely to compare the effects of sample selection on the optical LF.

The optical LF of ALFALFA galaxies within the $\alpha.40$ Spring Sky region has a very wide, dip-like feature around $M_r = -18$; thus, the ALFALFA optical LF is not well fitted by a Schechter function. We are currently unsure of the origin of the dip-like feature in the ALFALFA LF, but we suspect there may be a connection between the inclusion of massive, gas-rich galaxies in the ALFALFA

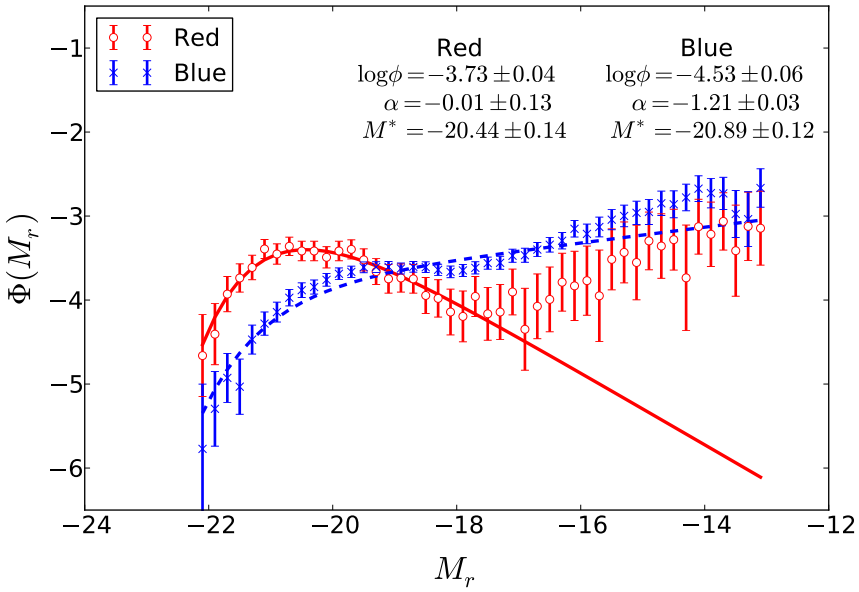

Figure 3.12 LF of red and blue H I selected galaxies from ALFALFA with best-fit Schechter functions. Both distributions feature a dip around $M_r = -18$. The red galaxy distribution is relatively flat and is dominated by large bright galaxies. The blue distribution has a steeper faint-end slope and is most likely dominated by dwarfy star-bursting galaxies.

sample and the bizarre shape. We do point out, however, that this feature cannot be explained by a simple combination of populations of optically selected galaxies. Splitting the H I sample by color, via SDSS model magnitudes, and morphological type, via the inverse concentration index, reveals a significant population of late-type reddish galaxies. While the red elliptical galaxy LF from the $\text{SDSS}_{\text{nearby}}$ sample produced a relatively small dip around $M_r = -18$, the red elliptical population in ALFALFA is small compared to other galaxy types. Additionally, the dip feature is also seen in the ALFALFA blue galaxy LF. Thus, it is improbable that the red elliptical distribution alone caused the shape. The magnitude range over which we find this feature corresponds to a stellar mass range of $\log(M_*/M_\odot) \sim 8.5 - 9.5$. Huang et al. (2012a) and Kreckel et al. (2012) find that specific star formation rates begin to decrease more substantially in galaxies with stellar masses greater than $M_*/M_\odot \sim 10^{9.5}$, but this does not explain the presence of the dip in the ALFALFA optical LF.

To estimate the ALFALFA void and wall galaxy LFs, we separately fit exponential cut-offs to the bright ends ($M_r \leq -18$) and power law slopes to the faint ends ($M_r > -18$). The best fit

characteristic magnitude in voids is $M^* = -19.95 \pm 0.07$, and $M^* = -20.49 \pm 0.04$ for walls. We find a shift towards fainter magnitudes in voids of $\Delta M \sim 0.5$. This magnitude shift is much smaller than the full magnitude shift found in either SDSS sample, because H I surveys detect bright galaxies in denser regions far less frequently than optical surveys. The separately fit faint-end slopes of the ALFALFA galaxy LFs are: $\alpha = -1.49 \pm 0.03$ for voids and $\alpha = -1.52 \pm 0.05$ for walls. Unlike the LFs of $\mathrm{SDSS_{nearby}}$ galaxies over the same volume, we find no evidence for an environmental dependence on the faint-end slope parameter. This is likely because the H I selected sample primarily detects late-type galaxies, whose LFs were shown by Tempel et al. (2011) to be independent of large-scale environment.

We also see a much steeper faint-end slope than for the $\mathrm{SDSS_{nearby}}$ sample. The effect of LSB galaxies present in the ALFALFA sample steepens the faint end of the optical LF closer to $\alpha \sim -1.5$ as predicted in Blanton et al. (2005b). We believe this result is evidence that the "true" faint-end slope of the optical LF is around $\alpha \sim -1.5$. Thus, simulations may need to scale back the effects of feedback and photoionization to account for the presence of LSB galaxies. We also note that the presence of LSB galaxies in the ALFALFA sample is not the cause of the intriguing dip feature in the ALFALFA optical LF.

Acknowledgements

The authors would like to acknowledge the work of the entire ALFALFA collaboration team in observing, flagging, and extracting the catalog of galaxies used in this work. This study was supported by NSF grant 1410525. The ALFALFA team at Cornell is supported by NSF grants AST-0607007 and AST-1107390 to RG and MPH and by grants from the Brinson Foundation.

Funding for the creation and distribution of the SDSS Archive has been provided by the Alfred P. Sloan Foundation, the Participating Institutions, the National Aeronautics and Space Administration, the National Science Foundation, the U.S. Department of Energy, the Japanese Monbukagakusho, and the Max Planck Society. The SDSS Web site is http://www.sdss.org/.

The SDSS is managed by the Astrophysical Research Consortium (ARC) for the Participating Institutions. The Participating Institutions are The University of Chicago, Fermilab, the Institute for

Advanced Study, the Japan Participation Group, The Johns Hopkins University, the Korean Scientist Group, Los Alamos National Laboratory, the Max-Planck-Institute for Astronomy (MPIA), the Max-Planck-Institute for Astrophysics (MPA), New Mexico State University, University of Pittsburgh, Princeton University, the United States Naval Observatory, and the University of Washington.

Chapter 4: On the Star Formation Properties of Void Galaxies

Abstract

We measure the star formation properties of two large samples of galaxies from the SDSS in large-scale cosmic voids on time scales of 10 Myr and 100 Myr, using Hα emission line strengths and GALEX *FUV* fluxes, respectively. The first sample consists of 109,818 optically selected galaxies. We find that void galaxies in this sample have higher specific star formation rates (SSFRs; star formation rates per unit stellar mass) than similar stellar mass galaxies in denser regions. The second sample is a subset of the optically selected sample containing 8070 galaxies with reliable S/N H I detections from ALFALFA. For the H I detected sample, SSFRs are similar regardless of large-scale environment. Investigating only the H I detected dwarf galaxies reveals a trend towards higher SSFRs in voids. Furthermore, we estimate the star formation rate per unit H I mass, known as the star formation efficiency (SFE) of a galaxy, as a function of environment. For the overall H I detected population, we notice no environmental dependence. Limiting the sample to dwarf galaxies again reveals a trend towards higher SFEs in voids. These results suggest that void environments provide a nurturing environment for dwarf galaxy evolution.

4.1 Introduction

Large-scale, cosmic voids make up about 60% of the volume of our Universe (Geller & Huchra, 1989; da Costa et al., 1988; Pan et al., 2012). While not completely empty, these voids are underdense enough that gas-stripping galaxy interactions are exceptionally rare, making these voids a unique environment for studying the formation and evolution of galaxies. According to Λ Cold Dark Matter (ΛCDM) simulations (e.g. Hoeft et al. (2006)), voids should have a density of low-mass halos of about 1/10th the cosmic mean. Karachentsev et al. (2004) find that the measured density of observed bright galaxies in the Local Void closely matches this prediction, but the density of dwarf galaxies in the Local Void is measured to be 1/100th that of the cosmic mean.

An explanation for this lack of low-mass, faint galaxies is that void galaxies may have their star formation suppressed (e.g. Koposov et al., 2009). One critical test of comparison between simulations and real data is through the relation of the predicted dark matter halo mass function and the observed galaxy luminosity and/or mass functions. Both simulations and semi-analytic models apply methods of star formation suppression to simulated dwarf "galaxies" in attempt to more closely match observations. Semi-analytic models (e.g. Benson et al. (2002)) suggest that reionization could suppress the dwarf galaxies. On the other hand, Hoeft et al. (2006) find in hydrodynamic simulations that adding in effects of UV photo-heating before and after reionization is not enough to match the slope of the observed mass function. Simulations more targeted at determining effects of large-scale environment on galaxies include the high resolution hydrodynamical simulations of void and cluster environments by Cen (2011). This adaptive mesh refinement simulation is the strongest predictor of void dwarf galaxy properties to date. The simulation predicts void dwarf galaxies at $z = 0$ will have high specific star formation rates. It predicts that these void dwarf galaxies are able to continue forming stars, because the entropy of the gas in voids is below the threshold at which the galaxies' cooling times exceeds a Hubble time.

Previous studies based on galaxy surveys suggest that galaxies within voids have higher star formation rates per stellar mass, called specific star formation rate (SSFR), than galaxies in walls. Rojas et al. (2005) use a sample of ~ 1000 underdense SDSS galaxies, corresponding to $\delta\rho/\rho < -0.6$, and find that void galaxies have higher SSFRs given their stellar mass. Von Benda-Beckmann & Müller (2008) find stronger star formation suppression in the field than in voids using a sample of faint galaxies from the 2dFGRS. These authors also find that galaxies towards void centers have a weak tendency to have higher rates of star formation. Using a collection of 60 targeted H I imaged galaxies from the Void Galaxy Survey (VGS; Stanonik et al., 2009; Kreckel et al., 2011, 2012), Kreckel et al. (2012) find SSFRs of their void galaxies to be similar to SSFRs of galaxies from GALEX Arecibo SDSS Survey (GASS; Catinella et al., 2010) in average environments. Examining a large sample of galaxies from the SDSS DR7, Ricciardelli et al. (2014) compare galaxies from the "maximal spheres" of voids to a sample of galaxies within 1.5 times the radius of the "maximal

spheres" of the voids, called "shell" galaxies. Results of environment are certainly sensitive to the definition of environment used within the work. Icke (1984) and van de Weygaert & van Kampen (1993) show that voids evolve to become more spherical with time; however, current measurements of actual voids from Pan (2011) show that voids are more ellipsoidal with a tendency to be prolate. Assuming voids are non-spherical bodies comprised of multiple spheres to create an ellipsoidal shape, the "maximal sphere" of a void, as seen in Ricciardelli et al. (2014), is the sphere with the maximum radius within a single void. Thus, the "shell" sample contains a mixture of outer-edge void galaxies as well as those just beyond the outskirts of the void (i.e. a sample likely containing both void and non-void galaxies). It is, therefore, unsurprising that Ricciardelli et al. (2014) find no environmental dependence on SSFR. Overall, it seems that void galaxies tend to have higher SSFRs than galaxies in average density regions.

Galaxies in voids have relatively higher SSFRs than galaxies in denser regions (Rojas et al., 2005; von Benda-Beckmann & Müller, 2008). Thus, we wonder if there is a trend in how efficiently galaxies are converting their gas into stars across environments, allowing void dwarf galaxies to continue their star formation at late times. The efficiency at which a galaxy transforms its gas into stars is called Star Formation Efficiency (SFE) and is defined as the SFR normalized by the H I mass of the galaxy (SFE=SFR/M_{HI}). To determine how effectively galaxies are forming stars from their gas, we require an H I mass for each galaxy. We should first determine what effects an H I selection imposes on the results of SFRs before making environmental comparisons. H I surveys typically detect blue, gaseous, actively star forming galaxies. Huang et al. (2012a) find that selecting only H I detections results in overall higher SSFRs than an optically selected sample. This is due primarily to the removal of most passive galaxies from the optically selected sample. Kreckel et al. (2012) study the efficiency of galaxies in the VGS and find two galaxies with which they can compare to similar stellar mass galaxies in denser regions. These two galaxies happen to have higher SFEs than the GASS galaxies to which they compare their observations. This hints that void galaxies *may* have higher SFEs than galaxies in average environments.

In this paper, we present the environmental effects on the specific star formation rate and the

star formation efficiency of dwarf galaxies in voids using optical data from the SDSS DR8, H I data from the ALFALFA Survey, and UV data from GALEX. For the first time, we determine the large-scale environmental impact on the star formation properties of dwarf galaxies down to $M_r = -13$. Throughout this work, we assume $\Omega_m = 0.26$ and $\Omega_\Lambda = 0.74$ when calculating comoving coordinates.

4.2 NASA-Sloan Atlas

The parent data set that we use in this work is the NASA-Sloan Atlas (NSA) version (Blanton et al., 2011). The NSA is a collection of galaxies in the local Universe ($z \leq 0.055$) based primarily on the Sloan Digital Sky Survey Data Release 8 (SDSS DR8) spectroscopic catalog (York et al., 2000; Aihara et al., 2011) and contains about 140,000 galaxies within the footprint of SDSS DR8. The catalog contains galaxy parameters and images from a combination of several catalogs across multiple wavelengths: SDSS DR8, NASA Extragalactic Database, Six-degree Field Galaxy Redshift Survey, Two-degree Field Galaxy Redshift Survey, ZCAT, WISE, 2MASS, GALEX, and ALFALFA. The NSA catalog re-analyzes the SDSS photometry in u, g, r, i, and z bands using the background subtraction methods described in Blanton et al. (2011). The photometry is redone to help eliminate the contamination of a dwarf galaxy sample by shredded or deblended galaxies as well as to improve background subtraction procedures for large galaxies. The spectroscopic data is also re-analyzed using methods of Yan (2011) and Yan & Blanton (2012). Distances within this catalog are obtained using the local velocity flow model of Willick et al. (1997). Stellar masses in the catalog were estimated from K-correction fits (Blanton & Roweis, 2007).

4.2.1 SDSS DR8

To determine SFRs on time scales of 10 Myr, we need optical spectra, which we obtain from the SDSS DR8 parameters provided within the NSA. The SDSS is a wide-field multi-band imaging and spectroscopic survey that uses drift scanning to map about a quarter of the northern sky. SDSS employs the 2.5m telescope at Apache Point Observatory in New Mexico, allowing it to cover $\sim 10^4$ deg^2 of the northern hemisphere in the five band SDSS system–u, g, r, i, and z (Fukugita et al., 1996; Gunn et al., 1998). Galaxies with Petrosian r-band magnitude $r < 17.77$ are selected for

spectroscopic follow up (Lupton et al., 2001; Strauss et al., 2002). SDSS spectra are taken using two double fiber-fed spectrographs and fiber plug plates covering a portion of the sky 1.49° in radius with a minimum fiber separation of 55 arcseconds (Blanton et al., 2003a). The SDSS DR8 spectra used in the NSA were reduced using the Princeton spectroscopic reduction pipeline. Flux measurements for this catalog were estimated using the code from Yan (2011) that calibrates the flux by matching the synthetic r-band magnitude to the apparent r-band fiber magnitude and subtracts the stellar continuum modeled in Bruzual & Charlot (2003). These methods are detailed in Yan (2011) and Yan & Blanton (2012).

4.2.2 GALEX

In order to determine SFRs on timescales of 100 Myr, we need photometric information in the far and near ultraviolet bands (FUV and NUV, respectively). To obtain this information, we utilize data from the Galaxy Evolution Explorer (GALEX) (Martin et al., 2005). GALEX is an 0.5m orbiting space telescope that images the sky in FUV and NUV photometric bands across 10 billion years of cosmic history. Portions of the GALEX GR6 footprint overlap with the northern sky surveyed in SDSS DR8. In this work, we use the cross-matched NSA-GALEX GR6 catalog provided by the NSA team to obtain all UV parameters.

4.2.3 ALFALFA

To determine whether galaxies in voids are more efficient at forming stars than galaxies of similar size in denser regions, we need estimates of each galaxy's H I mass. We utilize the Arecibo Legacy Fast ALFA (ALFALFA) Survey (Giovanelli et al., 2005b,a) to obtain H I information for our galaxies. ALFALFA is a large-area, blind extragalactic H I survey that will detect over 30,000 sources out to $z \sim 0.06$ with a median redshift of $z \sim 0.027$, over 7000 deg^2 of sky upon completion. ALFALFA has a 5σ detection limit of 0.72 Jy km s^{-1} for a source with a profile width of 200 km s^{-1} (Giovanelli et al., 2005b) allowing for the detection of sources with H I mass down to $M_{HI} = 10^8 M_\odot$ out to 40 Mpc.

Specifically, we use the most recent release of the ALFALFA Survey, $\alpha.40$ (Haynes et al., 2011),

which covers ∼2800 deg^2. For this work, we are interested in sources lying in the Northern Galactic Hemisphere within $z = 0.05$. The $\alpha.40$ catalog overlaps this region in two strips in the R.A. range 07^h30^m <R.A.< 16^h30^m: 04° < Dec< 16° and 24° < Dec < 28°. This region contains 8,070 H I detections within this volume. Each detection in the catalog is flagged as either Code 1, 2, or 9. Code 1 objects are reliable detections with S/N > 6.5; Code 2 objects have S/N< 4.5, but coincide with optical counterparts with known redshift similar to H I detection redshift; and Code 9 objects correspond to high velocity clouds. In this work, we only consider Code 1 and Code 2 detections. We use the H I masses from this catalog (which utilize the heliocentric distances provided in the catalog assuming $h = 0.7$) and use the NSA catalog for estimates of all other properties such as position, distance, and color. Because a blind H I survey is biased towards detecting blue, faint, gaseous galaxies and because the survey volume covered by ALFALFA is substantially smaller than the full NSA survey volume, only a small fraction of galaxies in the NSA catalog have H I information. Thus, we will separately track the effects of using an H I selected sample starting in Section 4.4.

4.3 Determining Environment

4.3.1 Creating the Void and Wall Samples

We identify the large-scale environment of our sources by comparing the comoving coordinates of each galaxy to the void catalog of Pan et al. (2012). This void catalog uses VoidFinder, the galaxy-based void finding algorithm of Hoyle & Vogeley (2002); El-Ad & Piran (1997). The algorithm grows spheres in the most underdense regions of a volume limited distribution of galaxies. Each sphere must live fully within the SDSS DR7 survey mask and must have radius $R \geq 10\mathrm{h}^{-1}\mathrm{Mpc}$. We exclude galaxies living along the edge of the survey, because we cannot determine the true large-scale structure of galaxies on the survey boundaries (see Pan et al. (2012), Hoyle et al. (2012), or Moorman et al. (2014) for a more detailed explanation). Galaxies identified as residing in a void are called void galaxies; those outside of voids are deemed wall galaxies. From the galaxies within $z < 0.05$ and Hα lines in the NSA catalog, we identify 34,548 (31%) void galaxies, 70,950 (65%) wall galaxies, and 4,320 (4%) galaxies lying on the edge of the survey mask.

Galaxies in voids have been shown to be fainter by a factor of 2.5 in the M_r luminosity function

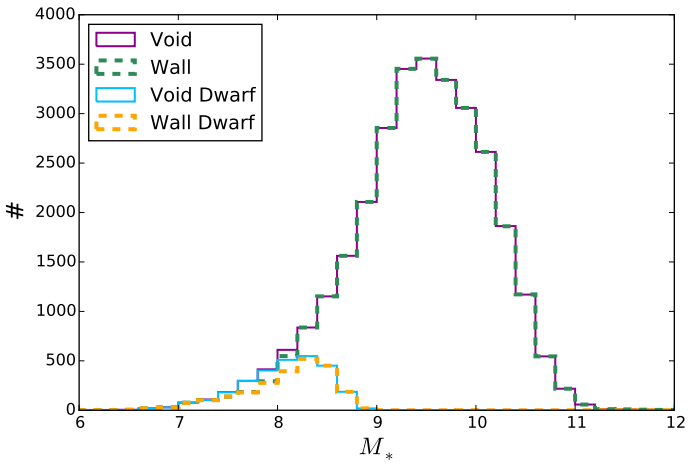

Figure 4.1 Distribution of stellar masses of the void and wall galaxies in the NSA full and dwarf samples. The wall galaxies are down-sampled so that the stellar mass distributions of voids and walls match. Because the void stellar mass distribution is naturally shifted towards lower masses, we lack the number of wall galaxies to match the void distribution, especially for the dwarf sample.

(Hoyle et al. 2005 and Moorman et al. 2015, submitted) and less massive by a factor of 1.4 in H I mass function (Moorman et al., 2014). Additionally, dark matter halo mass function estimates have been predicted to shift towards lower masses in voids in Goldberg & Vogeley (2004). This dependence of the mass/luminosity function on large-scale environment is now firmly established. See, for example, Alpaslan et al. (2015) who show that stellar mass is a strong predictor of galaxy properties. To test for environmental trends in addition to that effect, we compare samples of galaxies in voids and walls that are constructed to have the same stellar same distribution. In this analysis, we wish to ensure that any differences we may see are not due to the shift in the overall brightness or mass differences between void and wall galaxies. To remove this bias towards more massive, brighter galaxies in walls, we randomly sample galaxies from the wall distribution such that the new stellar mass distribution of the wall galaxies matches that of the void galaxies. See Figure 4.1 for the stellar mass-matched NSA full and dwarf distribution. As mentioned above, void galaxies are typically less massive than wall galaxies. Therefore, in some of the lowest mass bins, we have more void galaxies than wall galaxies. When we downsample the wall distribution, the lack of a sufficient sample of wall galaxies in these bins causes a very minor mismatch in the stellar mass distribution at masses lower than $\log(M_*) \sim 8$. Downsampling the wall galaxy sample to match

the stellar mass distribution of void galaxies also removes the bias towards brighter galaxies in the walls as seen in the left panel of Figure 4.2. In the right panel of Figure 4.2, we see the effects of down-sampling the walls on $u-r$ color. Compared to the original optical color distributions seen in the walls (scaled by 0.75 and depicted as a gray dotted line in the figure), we see a decreased ratio of red to blue galaxies in walls, although not as low as that of the void sample. Similarly, stellar mass matching the wall dwarf distribution to match the void dwarf stellar mass distribution decreases the red galaxy population in the wall dwarf sample. (For wall dwarfs, we provide the original wall dwarf distribution as a scaled gray dotted line in the figure.)

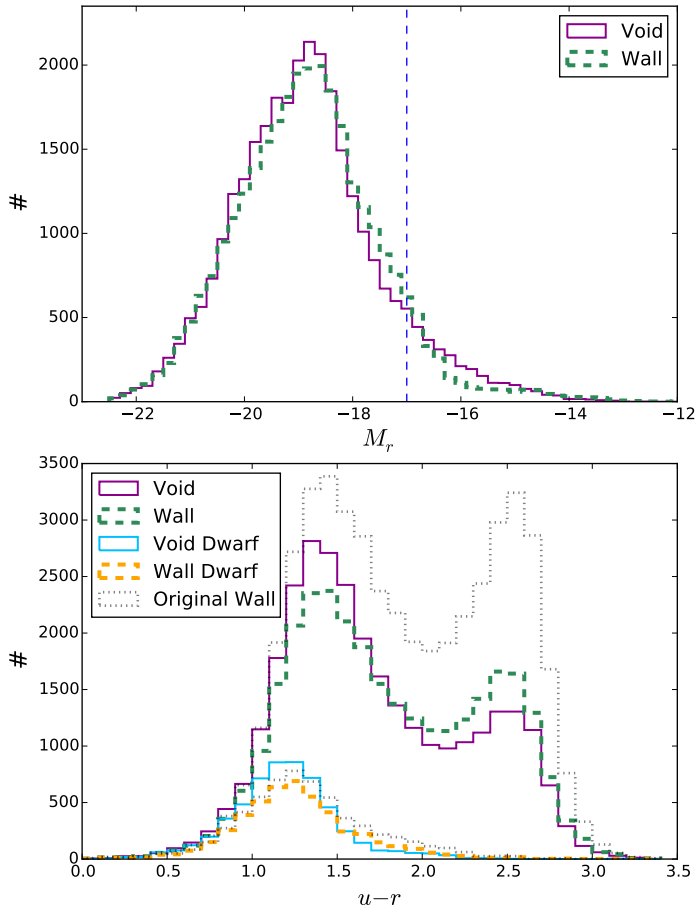

Figure 4.2 Left: Distribution of absolute magnitude M_r of void and wall samples that have the same stellar mass distribution. The bias towards brighter galaxies in walls is largely removed. The blue dashed line indicates the division between dwarf galaxies and brighter galaxies. Right: Distribution of $u-r$ color of void and wall samples that have the same stellar mass distribution. The number of red galaxies within the walls is reduced, but there is still a higher ratio of red to blue galaxies in walls than voids. For clarity, the dwarf distributions have been amplified by a factor of 2.

Of the galaxies with matched H I information, we have 2,737 (34%) void galaxies and 5,154 (64%) wall galaxies within $z < 0.05$. The remaining (2%) lie along the survey edges and are excluded due to the potential misclassification issues. We apply the same stellar mass-matched requirements to the H I sample as discussed earlier. The stellar mass matching has similar effects on the H I sample distributions. The M_r distributions are more similar, and the wall distributions become less red overall. By its nature, the H I sample primarily selects primarily blue, gas-rich galaxies (Toribio et al., 2011b; Huang et al., 2012a). Given these H I selection effects and the effects of stellar mass matching, we may have removed any environmental dependence, so we do not expect that we will see much of a difference between the star formation properties of the H I selected void and wall galaxies.

4.3.2 Creating the Small-Scale Density Samples

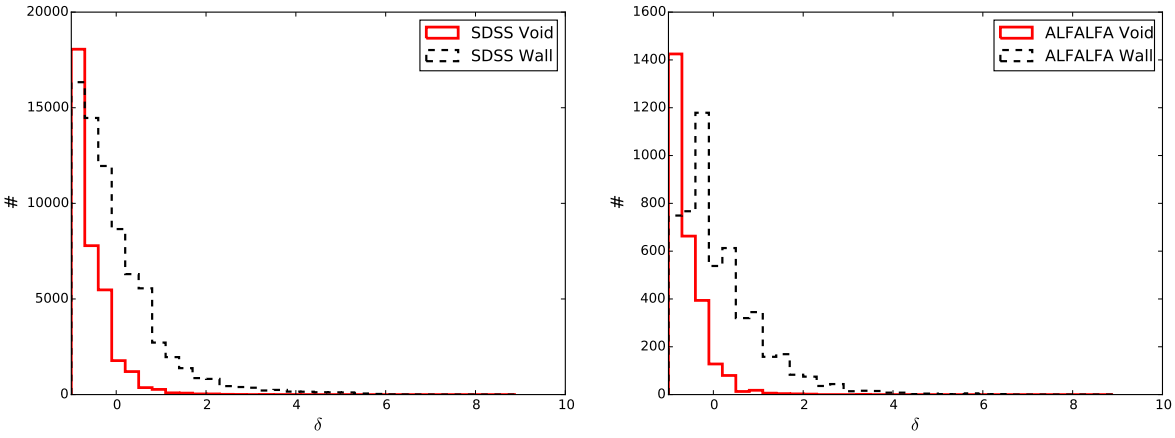

Figure 4.3 Distribution of relative local densities for void and wall galaxies in the NSA (left) and ALFALFA (right) samples. Void and wall galaxies were selected using a volume-limited sample based on $M_r = -20.1$, whereas the small scale densities were calculated using a volume-limited sample based on $M_r = -18.5$. We see that wall galaxies range anywhere from isolated to clustered regions. Our void galaxies are grouped together with relatively fainter galaxies ($-20.1 < M_r < -18.5$) within the voids on smaller scales than are probed by the void catalog.

Previous work indicates that star formation properties may be influenced by local density. For example, Elbaz et al. (2007) find that galaxy SSFRs decrease with stellar mass and increase with density at $z \sim 1$. Huang et al. (2012b) find that low H I mass ALFALFA detections ($M_{HI} < 10^{7.7}$) in the Virgo Cluster have gas depletion time scales less than a Hubble time. This implies that either the dwarf galaxies are undergoing gas-stripping interactions (common to galaxy clusters) or

the highest density regions are somehow enhancing SFEs.

In Section 4.6, we study the effects of local density on SFE in ALFALFA galaxies. We estimate the small-scale densities of each galaxy within the volume covered by VoidFinder, based on a volume-limited sample from the SDSS DR7 KIAS-VAGC (Choi et al., 2010) catalog. We create a volume-limited sample with an absolute magnitude cut of $M_r = -18.5$ corresponding to a redshift cut of $z = 0.06$ to ensure that we completely enclose the NSA volume ($z_{max} = 0.055$). We apply a nearest-neighbors algorithm to the volume-limited sample with a smoothing scale of ~ 2.5 h^{-1}Mpc to approximate the local density, ρ, within the volume covered. We then evaluate the relative local density (density contrast), $\delta = (\rho - \bar{\rho})/\bar{\rho}$, of each galaxy in the NSA catalog mentioned above. Figure 4.3 shows the distribution of our void and wall galaxies as a function of small-scale density contrast, δ. The relative densities of the void galaxies found using the void catalog primarily lie in regions less dense than the mean, but there may be filaments or groups of $M_r \leq -18.5$ galaxies within the voids increasing the relative density of void galaxies. Additionally, we find wall galaxies with small δ that are isolated galaxies not located in large-scale voids.

4.4 Estimating Star Formation Rates

To determine if large-scale environment affects star formation in galaxies, and on what time scales, we measure the star formation rate (SFR) of galaxies using two independent methods. The first method, described in detail in Salim et al. (2007) uses FUV photometry. The timescales of UV bright stars corresponds to $\sim$ 100 Myr; therefore, this method best estimates the star formation rates of galaxies over the past $\sim$ 100 Myr. The second method is described in Lee et al. (2009) and measures SFRs using Hα spectral lines. Only massive (> 10 $M_\odot$), young (< 20 Myr) stars significantly contribute to the integrated ionizing flux of a galaxy; thus, the Hα method provides a good estimate of SFRs on short timescales ($\sim$ 10 Myr). Both of these methods use the star formation relations of Kennicutt (1998). We briefly describe the methods in this section.

4.4.1 *FUV* Method

We measure the SFRs of galaxies over the last 100 Myr using the GALEX photometric *FUV* fluxes from the NSA catalog. *FUV* photometry is sensitive to dust; therefore, we correct the rest frame *FUV* fluxes for dust attenuation. We do so via the empirical equations found from SED fitting of GALEX galaxies in Salim et al. (2007). These authors find the effects of dust are stronger for red ($NUV - r \geq 4$) galaxies than blue ($NUV - r < 4$) galaxies. Thus red galaxies are corrected by

$$A_{FUV} = \begin{cases} 3.32(FUV - NUV) + 0.22 & FUV - NUV \leq 0.95 \\ 3.37 & FUV - NUV > 0.95 \end{cases}, \tag{4.1}$$

and blue galaxies are corrected by

$$A_{FUV} = \begin{cases} 2.99(FUV - NUV) + 0.27 & F - N \leq 0.90 \\ 2.96 & F - N > 0.90 \end{cases}. \tag{4.2}$$

Here, A_{FUV} is the dust attenuation correction for SFRs obtained using the *FUV* method. For galaxies with dust attenuation corrections falling below zero, we set the correction to $A_{FUV} = 0$, to ensure that we are not artificially adding dust back into the system. We apply this correction to the rest-frame flux, f^0, in the following way:

$$f_{FUV} = f^0 10^{A_{FUV}/2.5}. \tag{4.3}$$

From the dust corrected *FUV* fluxes, f_{FUV}, we calculate the *FUV* luminosities via

$$L_{FUV} = 4\pi D_L^2 f_{FUV}, \tag{4.4}$$

where D_L is the luminosity distance. Following Salim et al. (2007), we then apply the Kennicutt (1998) SFR relation with a factor to better match the stellar evolution models of Bruzual & Charlot

(2003),

$$SFR = 1.08 \times 10^{-28} L_{FUV}, \tag{4.5}$$

to obtain the average SFR in units of $M_{\odot}\mathrm{yr}^{-1}$ over the past ~ 100 Myr.

4.4.2 Hα Method

For an estimate of galaxy SFRs on more recent time scales, we calculate the Hα luminosity and apply the Kennicutt (1998) SFR relation similar to equation (4.5):

$$SFR = 7.9 \times 10^{-41.28} L_{\mathrm{H}\alpha} \tag{4.6}$$

to obtain the average SFR in units of $M_{\odot}\mathrm{yr}^{-1}$ over the past $\sim$ 10 Myr. Here, $L_{\mathrm{H}\alpha}$ is the Hα luminosity obtained from

$$L_{\mathrm{H}\alpha} = 4\pi D_L^2 f_{\mathrm{H}\alpha}, \tag{4.7}$$

where $f_{\mathrm{H}\alpha}$ is the dust-corrected Hα flux and D_L is the luminosity distance. As with the FUV method above, we must make dust attenuation corrections to the Hα SFR estimates. To do so, we use the correction suggested in Lee et al. (2009):

$$A_{\mathrm{H}\alpha} = 5.91 \log(\mathrm{H}\alpha/\mathrm{H}\beta) - 2.70. \tag{4.8}$$

Additionally, we make an aperture correction to the Hα luminosity to adjust for the fiber diameter being smaller than the size of the galaxy observed. We use the correction of Hopkins et al. (2003) adjusting the Hα luminosity by a factor of r_{Petro}/r_{fiber}. Here, r_{Petro} is the r-band Petrosian magnitude of the full galaxy, and r_{fiber} is the r-band magnitude within the fiber.

4.4.3 Star Formation Rates

We calculate the SFR for both methods mentioned above for all galaxies in our data set. In this work, we investigate the differences of the star formation properties based on environment and sample selection of the following samples: all galaxies identifiable as a void or wall galaxy (hereafter,

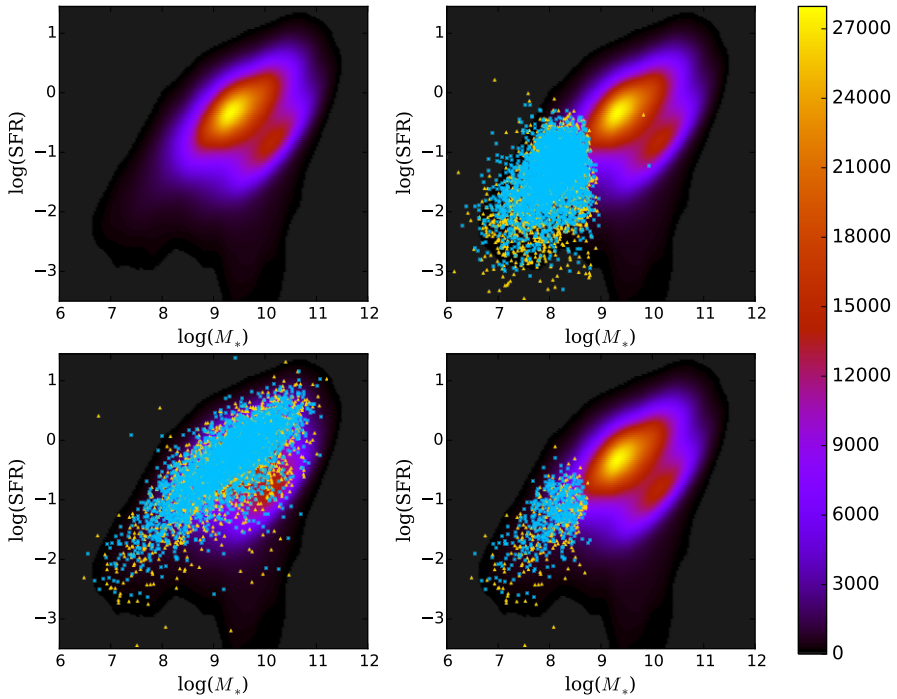

Figure 4.4 Upper Left: Color contours depict the logged stellar mass, log(M_*), vs log(SFR$_{FUV}$) distribution for all NSA galaxies. The colorbar depicts the number of galaxies in the sample in this space. Upper Right: Depicts location of NSA Dwarf void (blue crosses) and stellar mass-matched wall (gold triangles) galaxies overplotted on the full NSA distribution. SFR is closely correlated with mass; therefore, it is unsurprising that dwarf galaxies tend to have low SFRs. Most dwarf galaxies in the NSA are star forming with a small fraction appearing in an extension of the passive sequence. Lower Left: All ALFALFA void and stellar mass-matched wall galaxies. ALFALFA typically detects active star forming galaxies, mostly avoiding the passive galaxy region in the plot. Lower Right: ALFALFA Dwarf void and stellar mass-matched wall galaxies. These galaxies lie almost exclusively in the star forming sequence.

NSA), all dwarf galaxies identifiable as a void or wall galaxy (NSA Dwarf), galaxies within the aforementioned NSA sample with ALFALFA H I masses measured with S/N>4.5 (ALFALFA), and galaxies within the NSA Dwarf sample with corresponding H I clouds with S/N>4.5 (ALFALFA Dwarf).

We investigate the effects of sample selection on SFR by comparing the location of galaxy subsamples within log(SFR$_{FUV}$)–stellar mass (logM_*) space to the full galaxy catalog in Figure 4.4. Again, the NSA sample is a superset of all other galaxy samples used in this work (i.e. the NSA Dwarf, ALFALFA, and ALFALFA Dwarf samples). The upper left panel of Figure 4.4 depicts a density contour of the NSA sample in a log(SFR$_{FUV}$) vs. log(M_*) diagram. We see a clear bimodal-

ity in the diagram, indicating the existence of both an "active" (higher SFR) population depicted by the main peak in the contour diagram, and a "passive" (lower SFR) population depicted by the smaller peak to the lower right of the main peak. In the lower left panel, we select galaxies within the NSA catalog with H I emission lines strong enough to be detected by ALFALFA. We divide the ALFALFA detections into void (blue crosses) and wall (yellow triangles) galaxies and overplot them on the NSA density contour in the log(SFR) vs. log(M_*) space. This panel shows the overall effects of H I selection on galaxy SFR. We notice that we lose most evidence of bimodality in the distribution. This confirms that H I surveys tend to detect galaxies that are actively forming stars today. These findings corroborate the work of Huang et al. (2012a), who mention that the ALFALFA galaxies have higher SFRs than optically selected samples from the SDSS. We see some evidence at the high stellar mass end that a population of quiescent galaxies exists that contain just enough gas to be detected by ALFALFA.

SFR is correlated with stellar mass; therefore it is no surprise that selecting only the dwarf galaxies (right column of Figure 4.4) produces lower SFRs than the average galaxies in the full catalogs. Plotting Figure 4.4 using the Hα method rather than the FUV method we find similar results on the sample selection effects and dwarf selection effects; thus, we will not plot the Hα estimated SFR distributions here.

4.5 Specific Star Formation Rates

To account for the correlation between the SFR and mass of a galaxy, we normalize the SFR of each object by its stellar mass to obtain its specific SFR (SSFR=SFR/M_*), which is a measure of the SFR per unit mass. Figure 4.5 depicts the location of each galaxy sample within the SSFR$_{FUV}$ vs. stellar mass plane. The upper left panel shows the density contour of the NSA sample. The passive galaxy sequence is seen primarily as an extension from the main active sequence moving towards lower SSFRs around log(M_*) $\sim$ 10 and continuing towards the bottom edge of the figure. This density contour is replotted in the background of each subplot of the figure for the sake of comparing how sample selection affects the SSFRs. In the lower left panel, we divide the ALFALFA detections into void (blue crosses) and wall (yellow triangles) galaxies and scatter them over the

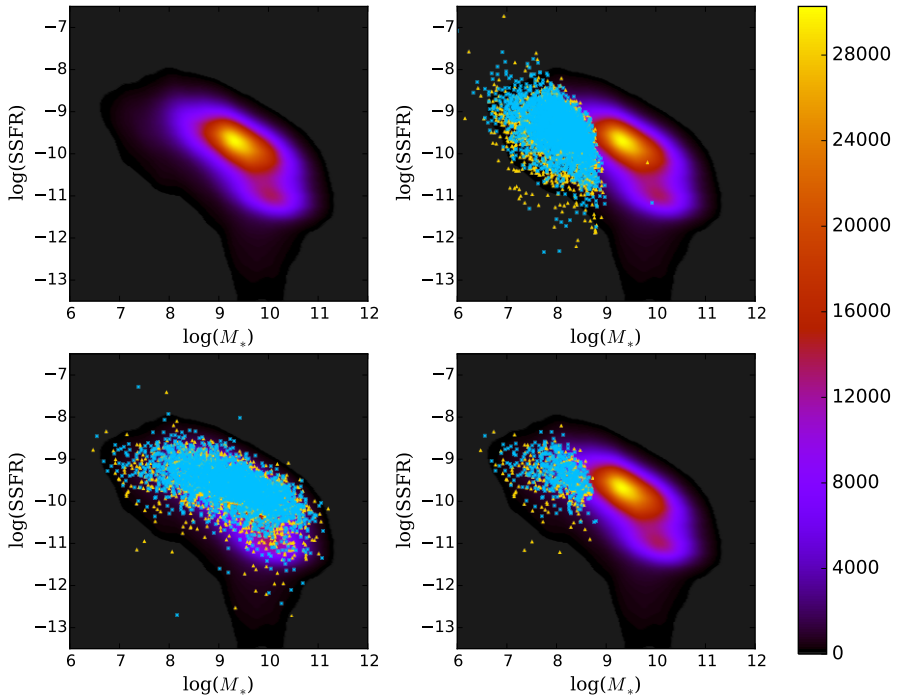

Figure 4.5 Upper Left: Color contours depict the logged stellar mass, $\log(M_*)$, vs $\log(\mathrm{SSFR}_{FUV})$ distribution for all NSA galaxies. The colorbar depicts the number of galaxies in the sample in this space. Upper Right: NSA Dwarf void (blue crosses) and wall (gold triangles) galaxies overplotted on the full NSA distribution. The wall dwarf galaxies have been downsampled so that the wall dwarf galaxy stellar mass distribution matches the stellar mass distribution of void dwarf galaxies. Dwarf galaxies tend to have relatively high SFRs given their size. A majority of dwarf galaxies lie in the active star forming region in this space. Lower Left: All ALFALFA void and stellar mass-matched wall galaxies. As seen with the SFR distributions, ALFALFA typically detects active star forming galaxies, avoiding the passive galaxy region in the plot. Lower Right: ALFALFA void dwarf and stellar mass-matched wall dwarf galaxies. These galaxies are actively forming stars at relatively high rates.

NSA density contour in the SSFR vs. stellar mass space. This panel shows the overall effects of H I selection on galaxy SSFR. As seen in Section 4.4.3, we find the ALFALFA sample lies primarily in the star forming sequence and is sparse in the passive galaxy region. Huang et al. (2012a) find a similar result for all ALFALFA galaxies.

In the right column of Figure 4.5, we select out only the dwarf galaxies ($M_r \geq -17$) within the NSA (top right) catalog and overplot them on the full NSA density contours. We find that, as a whole, dwarf galaxies tend to lie primarily in the active star forming sequence, with a few trailing into the passive region. Dwarf galaxies have higher SSFRs than average galaxies as predicted by the high resolution simulations of Cen (2011). We then select out the dwarf galaxies that have H I

emissions large enough to be detected in ALFALFA. We plot these galaxies in the bottom right panel of Figure 4.5, and find that the H I selection cuts out almost all of the dwarf galaxies lying in the passive galaxy region.

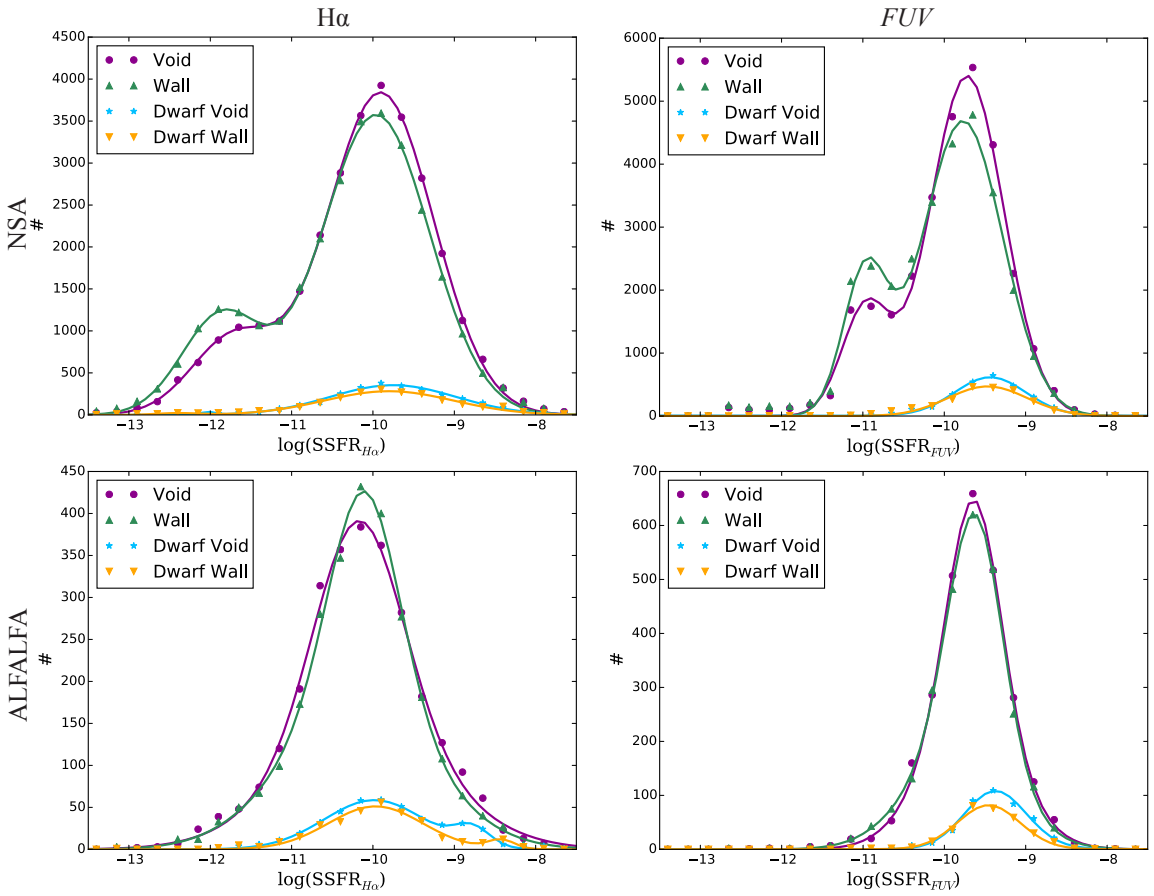

Figure 4.6 SSFR distribution of void and stellar mass-matched wall galaxies measured via Hα and *FUV* methods for NSA, NSA Dwarf, ALFALFA, and ALFALFA Dwarf samples. Lines denote the best-fit summed Gaussian. Upper Left: NSA SSFR distributions via the Hα method. Void galaxies have higher SSFRs than wall galaxies in the full sample as well as the dwarf sample. Upper Right: NSA SSFR distributions via the *FUV* method. Again, the void galaxies have higher SSFRs than wall galaxies in the full sample as well as the dwarf sample. Lower Left: ALFALFA SSFR distributions via the Hα method. Due to H I selection effects, we do not see evidence of the passive galaxy sequence. We notice no difference in the full void and wall distributions. A peak in the high-SSFR end of the void dwarf distribution reveals a population of star-bursting void dwarf galaxies. Lower Right: ALFALFA SSFR distributions via the *FUV* method. There is no significant difference between the full void and wall samples. The void dwarf distribution appears to be shifted towards higher SSFRs, but this shift is due to the lack of wall detections in the nearby ALFALFA sample.

To clearly distinguish between the large-scale environmental effects on the SSFR, in Figure 4.6 we present the void and wall distributions of both *FUV* and Hα SSFRs for the NSA and ALFALFA

Table 4.1. Gaussian fits to the SSFRs

Sample	type	method	A_1	μ_1	σ_1	A_2	μ_2	σ_2
NSA	void	Hα	3841	-9.906	0.651	926	-11.707	0.518
NSA	wall	Hα	3576	-9.961	0.658	1194	-11.858	0.489
NSA Dwarf	void	Hα	355	-9.752	0.773	33	-12.029	0.078
NSA Dwarf	wall	Hα	282	-9.803	0.793	21	-12.401	0.261
NSA	void	*FUV*	5406	-9.719	0.454	1727	-10.963	0.294
NSA	wall	*FUV*	4691	-9.769	0.489	2269	-10.970	0.272
NSA Dwarf	void	*FUV*	612	-9.434	0.438	—	—	—
NSA Dwarf	wall	*FUV*	471	-9.467	0.488	—	—	—
ALFALFA	void	Hα	263	-10.177	0.540	129	-10.110	0.991
ALFALFA	wall	Hα	167	-10.199	0.896	260	-10.104	0.429
ALFALFA Dwarf	void	Hα	59	-9.984	0.618	22	-8.781	0.215
ALFALFA Dwarf	wall	Hα	51	-9.968	0.579	11	-8.423	0.163
ALFALFA	void	*FUV*	416	-9.633	0.323	233	-9.697	0.561
ALFALFA	wall	*FUV*	449	-9.616	0.331	181	-9.814	0.618
ALFALFA Dwarf	void	*FUV*	104	-9.378	0.376	5	-9.114	0.570
ALFALFA Dwarf	wall	*FUV*	81	-9.456	0.383	1	-8.218	3.131

samples fitted with two summed Gaussians:

$$f(x) = \frac{A_1}{\sigma_1\sqrt{2\pi}} e^{-\frac{(x-\mu_1)^2}{2\sigma_1^2}} + \frac{A_2}{\sigma_2\sqrt{2\pi}} e^{-\frac{(x-\mu_2)^2}{2\sigma_2^2}}. \tag{4.9}$$

Here, A is the amplitude, μ is the mean, and σ is the standard deviation of each 1-D gaussian. See Table 4.1 for the parameter values for each sample.

The left column in the Figure 4.6 plots SSFR distributions averaged over the last $\sim$ 10 Myr, estimated using the Hα line. The right column plots the SSFR distributions averaged over the last $\sim$ 100 Myr, estimated using the *FUV* photometry. The top row shows the stellar mass-matched NSA data, and the bottom row shows the stellar mass-matched ALFALFA data. It is obvious from the top left panel of Figure 4.6, that void galaxies have higher SSFRs than wall galaxies in both the active (13% shift) and passive (41% shift) regions based on the Hα estimates. For the NSA Dwarf sample, the void galaxy distribution has an 11% shift towards higher SSFRs than stellar mass-matched wall dwarf galaxies when using the Hα method.

In the upper right panel of Figure 4.6, we measure the *FUV* SSFR for NSA galaxies and find that void galaxies have higher SSFRs than stellar mass-matched wall galaxies in both the active (13%)

and passive (41%) populations. The NSA Dwarf void galaxies also experience higher SSFRs based on the FUV method by $\sim 7\%$. Based on the FUV method, we find that 90% of void dwarf galaxies and 85% of wall dwarf galaxies have SSFRs high enough to double their stellar mass in a Hubble time (corresponding to log(SSFR)> -10.1 $M_{\odot}\mathrm{yr}^{-1}$). Computing the Kolmogorov-Smirnov (K-S) test statistic on the mass-matched void and wall SSFR distributions on both time scales returns a p-value of identically 0.0 for the NSA void and stellar mass-matched wall samples as well as for the NSA Dwarf void and stellar mass-matched wall samples. Thus, we can reject the null hypothesis that the void and stellar mass-matched wall galaxies from these two sets were drawn from the same distribution.

4.5.1 Tracking the Sample Selection Effects

SSFRs are highly anti-correlated with $NUV - r$ color (r_s=-0.923 for the NSA sample and r_s=-0.875 for the ALFALFA sample). That is, bluer galaxies tend to have the higher SSFRs. Of course, there are always exceptions, such as the population of dust-reddened spiral galaxies detected by ALFALFA (see Chapter 3). Edge-on, blue spiral galaxies will have high SSFRs, but will generally appear redder than they truly are due to dust in the galaxy absorbing and scattering photons with shorter wavelengths. Because of the bias towards blue galaxies in the H I samples, we will see hardly any difference between the SSFRs of void and wall galaxies. The H I detection SSFRs, on average, should be higher than for an optically selected sample because we are lacking galaxies from the red, passive galaxy sequence. While the average SSFRs are higher, comparing only the active star-forming sequence of ALFALFA to that of NSA reveals a shift towards lower SSFRs in H I surveys. This is unsurprising given that the ALFALFA blue cloud is shifted towards redder colors than the SDSS blue cloud (see Figure 3.1).

In the bottom row of Figure 4.6, there are no discernible differences between the full ALFALFA void and ALFALFA stellar mass-matched wall SSFR distributions on either time scale. Estimating a shift in the void and wall distributions based on the summed Gaussian fits, we find only a 5% shift towards lower Hα SSFRs with a broader distribution in voids than walls (see Table 4.1 for fits). In the bottom right panel, we find a $< 1\%$ shift towards higher FUV SSFRs and no width differences

in the distributions, implying that the SSFRs of H I selected galaxies are not dependent on large scale structure based on the FUV method. The K-S test results in $p_{K-S} = 0.09$ for Hα SSFRs and $p_{K-S} = 0.14$ for FUV SSFRs, meaning that we cannot reject that the ALFALFA void and wall samples were drawn from the same distribution on either time scale.

Limiting our scope to the ALFALFA Dwarf sample, we find in the Hα SSFR distribution that the main peak of the void sample, centered on log(SSFR)~ -10, is shifted only by $\sim 4\%$ towards lower SSFRs than the main peak of the wall galaxy distribution. Both the void and wall ALFALFA Dwarf samples have secondary peaks at the high end of the Hα SSFR distribution not apparent in any other sample. This is indicative of a population of star bursting dwarf galaxies that has been active very recently (10 Myr) especially in voids. The wall galaxies, however, seem to be lacking a sample of high Hα SSFRs around $-9.2 <$log(SSFR)< -8.4 where the secondary void peak is strongest. This effect is due to: 1) ALFALFA's bias towards detecting galaxies preferentially found in voids and 2) the presence of large-scale voids in the foreground of the ALFALFA volume. Fortunately, the nearby void presence allows us to study the star formation properties of a substantial number of highly active, gas-rich, void dwarf galaxies; however, we are lacking a comparable wall sample with which we may compare these properties. At higher SSFRs, the wall dwarf distribution increases again, to closely match the void distribution around log(SSFR) ~ -8.5. Due to these high-SSFR features, a K-S test yields $p_{K-S} = 0.005$, indicating that we should reject that these samples are drawn from the same population. The differences in distributions are due to a lack of a nearby ALFALFA Dwarf wall population, rather than SSFRs varying with environment.

On longer time scales ($\sim$ 100 Myr), the ALFALFA Dwarf void galaxies are shifted towards higher FUV SSFRs by 23% with $p_{K-S} = 0.002$. Based on this test statistic, we should reject that the void and wall ALFALFA Dwarf detections were drawn from the same distribution. It might be tempting to assume that void galaxies form stars at substantially higher rates than wall galaxies; however, as seen with the Hα method, the wall dwarf galaxy sample is largely affected by the presence of nearby cosmic voids in the $\alpha.40$ volume. The lack of wall galaxies on the high end of the FUV SSFR distribution is due to exactly that. Keeping this caveat in mind, we expect that we will find

Table 4.2. Gaussian fits to the SFEs

Sample	type	method	A_1	μ_1	σ_1	A_2	μ_2	σ_2
ALFALFA	void	Hα	500	-10.530	0.646	-3	-11.558	1.138
ALFALFA	wall	Hα	499	-10.492	0.607	7	-7.618	1.894
ALFALFA Dwarf	void	Hα	72	-10.611	0.701	-2	-5.956	0.521
ALFALFA Dwarf	wall	Hα	66	-10.776	0.493	13	-9.488	0.374
ALFALFA	void	*FUV*	874	-9.986	0.361	—	—	—
ALFALFA	wall	*FUV*	805	-9.989	0.3759	—	—	—
ALFALFA Dwarf	void	*FUV*	125	-10.038	0.339	28	-10.658	0.284
ALFALFA Dwarf	wall	*FUV*	43	-10.281	0.240	56	-10.082	0.498

the star formation efficiency of ALFALFA void and wall galaxies to be very similar for both the Hα and *FUV* methods. We also suspect the ALFALFA Dwarf galaxies will vary only slightly on short time scales and will not vary with environment on longer time scales with the exception of the lack of wall galaxies in the nearby Universe. Compared to the NSA Dwarf SSFR$_{FUV}$ distribution, the ALFALFA Dwarf galaxies have higher SSFRs on average with 94% of void dwarfs and 93% of wall dwarfs having SSFRs high enough to double their stellar mass within a Hubble time.

4.6 Star Formation Efficiency

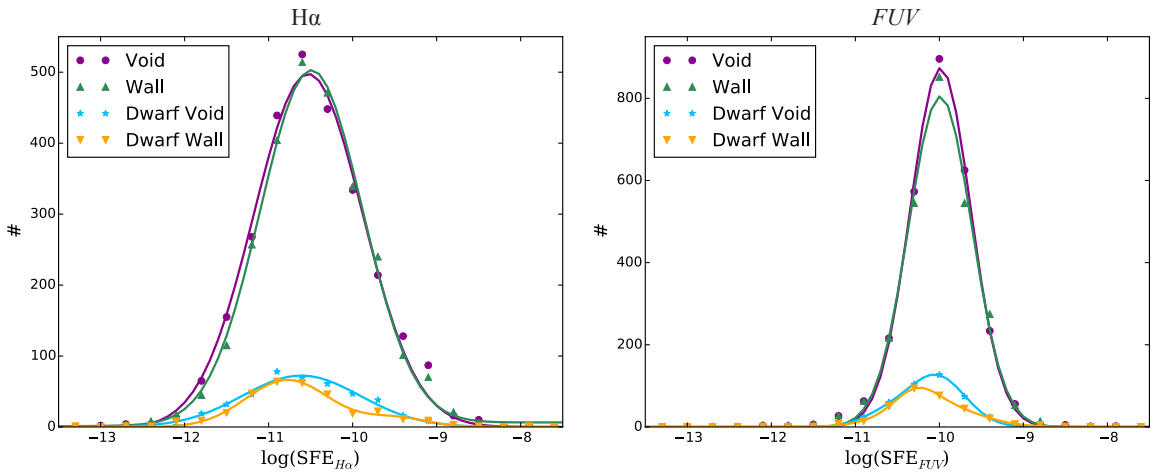

Figure 4.7 Left: Distribution of the Hα SFE of all void and wall galaxies as well as the dwarf void and wall galaxies. Right: Distribution of the *FUV* SFE of all void and wall galaxies as well as the dwarf void and wall galaxies. There is no discernible difference between the full void and wall SFE distributions of ALFALFA galaxies on either timescale. Isolating the ALFALFA dwarf galaxies reveals a slight trend towards higher SFEs in void galaxies.

A measure of how efficiently galaxies are transforming their gas into stars is the SFR normalized by the H I mass, termed the galaxy's star formation efficiency (SFE = SFR/M_{HI}). In Figure 4.7 we present the SFE distribution of the full ALFALFA void and wall samples and the ALFALFA dwarf void and wall samples for both the Hα method (left panel) and FUV (right panel). The lines plotted represent the best-fit summed Gaussians (see equation 4.9) with parameters shown in Table 4.2. In the Hα distribution, we find a small (9%) shift towards lower SFEs and a broader distribution in ALFALFA void galaxies compared to walls. As with the ALFALFA Dwarf SSFR$_{\mathrm{H}\alpha}$ distributions, the SFE$_{\mathrm{H}\alpha}$ wall distribution is lacking at the high SFE end (log(SFE)~ -10). This is primarily due to the same large-scale structure (LSS) and H I selection effects discussed in the previous section. We also find similar results between the SFE$_{FUV}$ and SSFR$_{FUV}$, in that there is no difference in the ALFALFA void and wall distributions and there is a lack of ALFALFA Dwarf wall galaxies at high SSFRs. Again, this lack of wall galaxies is likely due to the prominence of nearby voids within the ALFALFA α.40 volume. The K-S test statistics ($p_{full} = 0.13$ and $p_{dwarf} = 0.17$ for the Hα method and $p_{full} = 0.24$ and $p_{dwarf} = 0.11$ for the FUV method) indicate that we cannot reject that the samples were drawn from the same distribution.

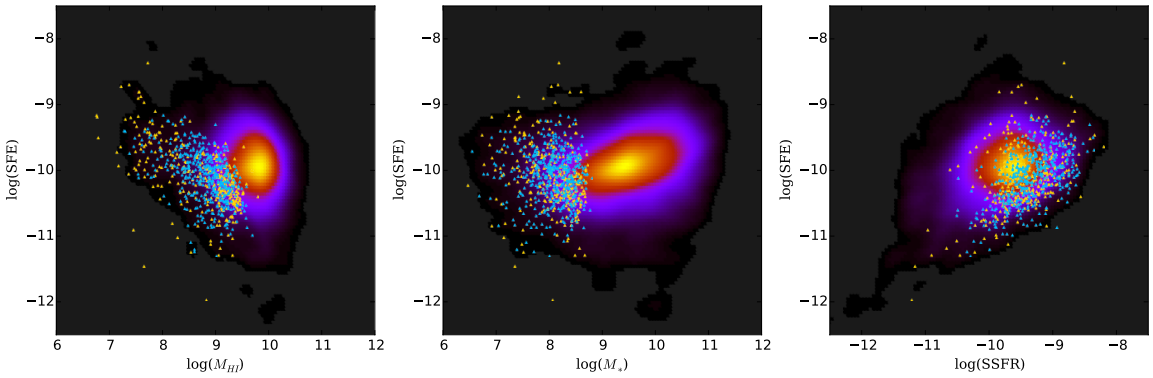

Figure 4.8 Left to right: ALFALFA galaxy SFEs as a function of M_{HI}, M_*, and SSFR. Color contours represent the full ALFALFA sample, while the ALFALFA void dwarf (blue crosses) and ALFALFA wall dwarf (gold triangles) populations are overplotted. The wall dwarf galaxies were sampled so that the wall dwarf stellar mass distribution matched the void dwarf stellar mass distribution. We notice a population of wall dwarf galaxies with very high SFEs.

Figure 4.8 presents the distribution of SFEs as a function of M_{HI}, M_*, and SSFR. ALFALFA Dwarf void galaxies (blue crosses) and wall galaxies (gold triangles) are overplotted on the colored-

contour of the full ALFALFA sample in each space. We see evidence of a population of ~ 10 low-H I mass dwarf galaxies with relatively high SFEs in walls. Figure 4.9 shows the M_* vs M_{HI} distribution of the ALFALFA dwarf galaxies. Huang et al. (2012a) and Kreckel et al. (2012) show that ALFALFA galaxies are predominately H I mass dominated below $\log(M_*) \sim 9.5$ (falling below the dashed line in the figure) and stellar mass dominated at larger M_*. The high SFE wall galaxies fall below the $M_{HI} = M_*$ line, indicating that they have lower gas mass fractions than typical ALFALFA galaxies of similar stellar mass. We note that the void and wall dwarf galaxies plotted in Figure 4.9 are stellar mass-matched, so the shift towards lower M_{HI} at a given M_* is important. Galaxies with low gas fractions typically show the following traits: low SFRs, low SSFRs, high SFEs, high metallicities, high extinctions, redder, and more evolved. These particular galaxies do have lower a SFR and SSFR, and a higher SFE, but they appear to be just as blue as the rest of the ALFALFA dwarf population and half of them are late-type while the other half are early-type as judged by the galaxies inverse concentration index. These galaxies live in relatively high local density regions as determined by the KDE estimator discussed in Section 4.3 (see Figure 4.10 for SFEs as a function of local density).

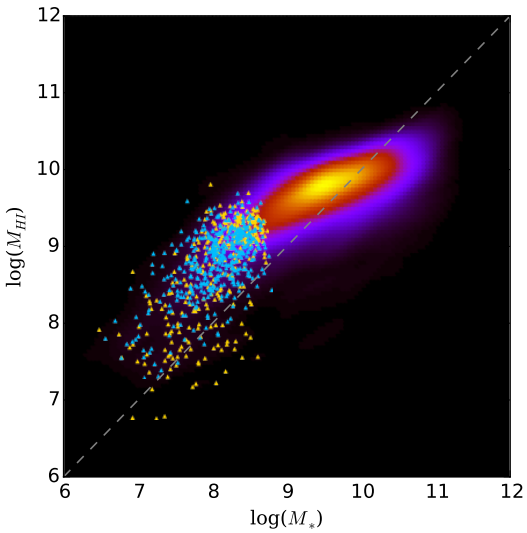

Figure 4.9 Color contours show M_* vs M_{HI} of the full ALFALFA sample. ALFALFA void dwarf (blue crosses) and stellar mass-matched wall dwarf (gold triangles) galaxies are overplotted. We see that at a given stellar mass, void dwarf galaxies have higher H I masses than wall dwarf galaxies. This implies that void dwarf galaxies have lower SFEs than similar stellar mass galaxies in walls.

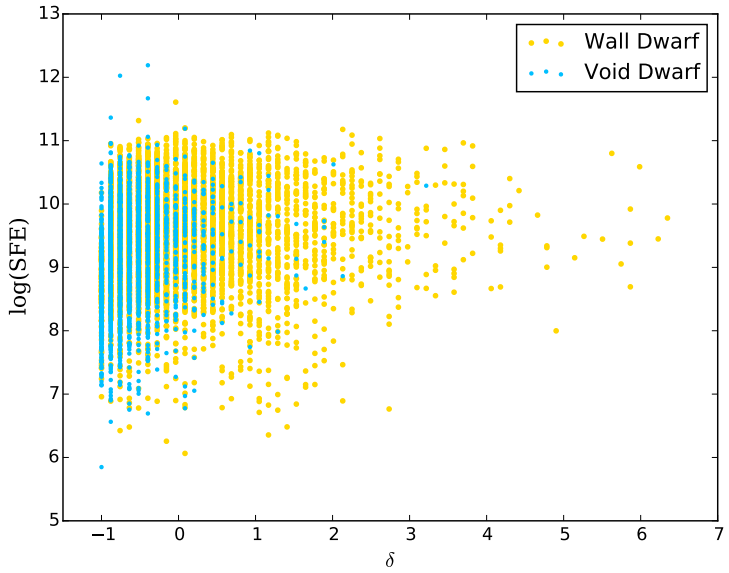

Figure 4.10 SFEs for void dwarf (blue) and stellar mass-matched wall dwarf (gold) galaxies in the ALFALFA Dwarf sample as a function of local density. We find that void galaxies are more isolated than wall galaxies. Wall dwarf galaxies detected in ALFALFA rarely appear in extremely dense environments.

Measured on both time scales, the SFE distribution of void dwarf galaxies appears broader than that of wall dwarf galaxies. As previously mentioned, the SFEs of void dwarfs are shifted higher due to presence of nearby voids in the $\alpha.40$ volume. There is also a smaller shift towards lower SFEs that is not due to the prominence of voids in the survey volume. The broadened distribution towards lower SFEs could be indicative of *marginally* lower SFEs in void dwarf galaxies. Perhaps this means the void environment does provide a sheltered life for dwarf galaxies, allowing them to retain their H I gas allowing for fueling over longer periods.

4.7 Comparison to Previous Results

Our results are consistent with previous studies regarding the variation of galaxy SSFRs with large-scale environment which suggest that galaxies in underdense environments have higher SSFRs than those in denser regions. Rojas et al. (2005) measure the SSFR of galaxies from an earlier data release of the SDSS and find that at fixed luminosity, void galaxies have higher SSFRs than wall galaxies. They also find that SFRs are very similar or slightly lower for void galaxies than wall galaxies,

but this is expected, because void galaxies are generally less massive and SFRs are correlated with galaxy mass. Similarly, using a sample of faint galaxies from the 2dFGRS, von Benda-Beckmann & Müller (2008) find stronger star formation suppression in the field than in voids via the color-SSFR relation. That is, they find that galaxy colors are redder in fields than in voids. Because SSFR and color are strongly correlated, these authors make the claim that SSFRs must be lower in fields.

At first glance, the recent results of Ricciardelli et al. (2014) appear to contradict our results, although this is likely a consquence of how the authors define "void" in their work. Ricciardelli et al. (2014) estimate the SSFR of "void" and "shell" galaxies within the SDSS DR7. These authors find that the average SSFR does *not* vary with large-scale structure. These results do not necessarily contradict our results because the definitions of LSS used in that work vary from what we define in this work. The "void" galaxy sample used in Ricciardelli et al. (2014) is a sample of galaxies that live only in the void centers. That is, the authors use a void catalog that only includes the maximal sphere of each void. (See the discussion in Section 4.1 for a definition of maximal sphere.) This allows the authors to use only galaxies in the void centers; however, they are comparing their void sample to a "shell" sample that likely contains void galaxies from the outskirts of the voids. Pan et al. (2012) show that the density profiles of voids are flat out to the edges, therefore properties of galaxies should not vary with void centric distance. The "shells" used in this paper are spherical shells from the maximal sphere radius, R_{void}, to $1.5R_{void}$. If all voids were perfectly spherical, this would work well to distinguish galaxies in underdense versus dense regions, but Pan (2011) shows that voids in the nearby Universe are more ellipsoidal than spherical, with a tendency towards bring prolate. By accounting for only the maximal spheres of a void, these authors are using a sample littered with both void and wall galaxies as the "shell" sample. Comparing properties of void galaxies with a population that likely has a significant number of void galaxies mixed in, they would not notice a difference. It is clear from their distributions that they are lacking a large portion of quiescent galaxies that are present in our sample. Consistent with our findings, these authors find that the proportion of star forming galaxies in voids is higher and the fraction of passive galaxies are higher in denser regions.

The SSFR trends seen in our work also agree with the high-resolution void simulation of Cen (2011), who predicts that void galaxies will have higher SSFRs than galaxies in denser regions. Cen (2011) also finds a trend of increasing SSFRs with decreasing stellar mass. As we move into the dwarf regime, we find that galaxies with lower M_* have higher SSFRs, with most (90% void dwarf galaxies and 85% of wall dwarf galaxies) having SSFRs high enough to double the stellar mass within a Hubble time, according to the FUV method.

Our results on the SSFRs of ALFALFA galaxies are also in agreement with the results of Kreckel et al. (2012) regarding the environmental dependence of SSFR in an H I selected sample. Kreckel et al. (2012) use the Void Galaxy Survey (VGS), a targeted H I imaging survey, to map the H I in galaxies in known voids in the nearby Universe. They compare 60 void galaxies from the VGS to a control sample of galaxies in average environments in a similar stellar mass range from the GALEX Arecibo SDSS Survey (GASS) catalog. They find that the SSFRs of H I selected void galaxies are similar to SSFRs of galaxies in denser regions. While we find higher SSFRs in void galaxies for our NSA sample, the void and stellar mass-matched wall SSFRs of ALFALFA galaxies are very similar. Beygu et al. (2015) also use the VGS and find no difference in SSFR between VGS void galaxies and galaxies of similar stellar mass in denser environments (JCMT field galaxies, LV isolated and field galaxies, and ALFALFA Virgo cluster galaxies).

Most works to date investigating the environmental dependence of star formation efficiencies have focused on clusters or isolated galaxies rather than on large-scale void environments. One work that does focus on the LSS dependence of SFEs is that of Kreckel et al. (2012), who find only two galaxies within the VGS with $M_* > 10^{10} M_\odot$ which they could compare to the GASS galaxies in denser regions. These two galaxies happened to higher SFEs ($10^{-8.6}\mathrm{yr}^{-1}$ and $10^{-9.1}\mathrm{yr}^{-1}$) than $M_* > 10^{10} M_\odot$ GASS galaxies which had an average SFE of $10^{-9.5}\mathrm{yr}^{-1}$ in this stellar mass range. Kreckel et al. (2012) further compare the VGS SFEs to a volume-limited sample of 447 ALFLFA galaxies ($\log(M_{HI}) > 9$ within $0.007 < z < 0.024$). The 447 ALFALFA control galaxies live in average density regions ($1 < \delta + 1 < 10$) and are crossmatched to SDSS DR7 using cross-matching techniques found in Toribio et al. (2011b). The authors find hints (via a weak trend) that the VGS

galaxies display higher SFEs than the volume-limited ALFALFA subset, but do not suggest that these results are significant. Our results for the full ALFALFA sample do not indicate that void galaxies, on the whole, are more effective at forming stars with their gas. Further investigation of the VGS void galaxies by Beygu et al. (2015) reveals no difference in SFE between VGS void galaxies and galaxies of similar stellar mass in denser regions (JCMT field galaxies, LV isolated and field galaxies, and ALFALFA Virgo cluster galaxies).

Investigating the ALFALFA Dwarf SFE distributions, we find a feature at the high-SFE end caused by a relative abundance of voids in the nearby volume. The low-end appears to have relatively more void galaxies than wall galaxies. This could be indicative of lower SFEs in voids, but is not statistically significant. If it is the case that void galaxies have lower SFEs, this would be in agreement with the work of Bigiel et al. (2010) who find that the H I column is correlated with SFE and is dependent on local environment. It may be the case that even small-scale groups of galaxies within voids provide a more isolated environment (i.e. lower δ) than even the most isolated of galaxies outside of voids. See Figure 4.10 which shows that void dwarf galaxies are significantly more isolated than wall dwarf galaxies.

4.8 Conclusions

We examine the effects of both large-scale and local environment on star formation properties of these two samples, focusing particularly on the faintest galaxies ($M_r \geq -17$). We utilize the NASA Sloan Atlas (NSA) which offers a set of cross-matched objects within the SDSS DR8-GALEX-ALFALFA footprint. From the NSA sample, we extract 113,145 galaxies with optical and UV information, and 8070 galaxies with information from all three catalogs. We determine the large-scale environment in which each galaxy lives using the void catalog of Pan et al. (2012) splitting the galaxies into "void galaxies" and "wall galaxies." We match the stellar mass distributions of void and wall galaxies and find the following results.

- Void galaxies have higher SSFRs than wall galaxies overall as well as in the dwarf ($M_r \geq -17$) regime. This holds true on timescales of both $\sim$ 10 (Hα) and $\sim$ 100 (FUV) Myr. This

reproduces the trend towards higher SSFRs for bright void galaxies and reveals that the shift towards higher SSFRs in cosmic voids extends down to magnitudes as faint as $M_r = -13$.

- When we limit our sample to those containing enough H I to be detected by ALFALFA, we remove the passive galaxy population. After stellar mass matching the void and wall ALFALFA galaxies, we notice no difference in the SSFR distributions. This further supports the findings that ALFALFA detects primarily blue, star forming galaxies.

- Comparing only the active star forming sequences in the NSA and ALFALFA catalogs shows a shift towards lower SSFRs in ALFALFA. This reiterates the finding in Chapter 3 (Moorman et al. 2015 submitted) that the blue cloud in ALFALFA is somewhat redder than the blue cloud of the optically selected sample.

- Investigating the dwarf galaxy population within the NSA and ALFALFA samples, we find that dwarf galaxies have higher SSFRs and lower SFEs than typical brighter galaxies. This indicates that dwarf galaxies are likely to be star-bursting galaxies with very recent star formation. The lower SFEs could also imply that dwarf galaxies are able to retain their gas more easily than brighter galaxies.

- A peak in the ALFALFA Dwarf void galaxy log(SSFR$_{Ha}$) distribution and a trough in the wall dwarf distribution at ~ -8.75 points to the presence of a void-rich volume in the nearby $\alpha.40$ survey.

- We do not find statistical evidence indicating whether or not H I detected, stellar mass-matched void and wall dwarf galaxies have similar SFEs. Assuming that the two samples *are* drawn from the same distribution, it would appear that the wall dwarf sample is lacking galaxies around log(SFE)~ -10. Dwarf galaxies have been forming stars at relatively high rates in recent times (10Myr) but due to survey sensitivities, we can only see dwarf galaxies in the local Universe. Due to the presence of a nearby void within the ALFALFA $\alpha.40$ volume, we have a substantial sample of gas rich void dwarf galaxies, but are unable to make a comparison of the properties as a function of LSS.

Chapter 5: Conclusions/Future Work

5.1 Discussion

Studying the formation and evolution of dwarf galaxies across environments is interesting, because their relatively shallow potential wells make them sensitive to astrophysical effects that may be more prominent in one environment over another. The assembly histories of dwarf galaxies are predicted by high-resolution, hydrodynamic simulations (Lackner et al., 2012) to be very different than brighter, more-massive galaxies. Therefore, a comparison of the properties of dwarf galaxies in voids versus those in denser regions is important. Most studies to date focusing on resolving the discrepancy between the predicted halo mass function and the observed density of dwarf galaxies have dealt primarily with properties of dwarf galaxies in dense regions. Studying the properties of dwarf galaxies in voids is more difficult than studying wall dwarf galaxies because survey sensitivity limits allow for dwarf detections only nearby and we do not live in a void. With the advent of large redshift surveys and surveys sensitive to galaxies down to $M_r = -13$, we now have a statistically significant catalog of crossmatched optical, H I, and UV data for dwarf galaxies in voids. We contribute to the literature an analysis of the properties of dwarf galaxies in large-scale, cosmic voids. Within the sections that follow, we present our results on the H I mass function (HIMF), optical luminosity function (LF), and star formation properties of void dwarf galaxies in the context of the questions that motivated this thesis.

Before we delve into the results, we should point out that sample selection (H I versus optically selected galaxies) is important and must be considered when interpreting our results, and before making statements regarding the effects of environment on galaxies. Blind H I surveys primarily detect galaxies that are faint, blue, and later-type—properties shared with typical denizens of voids—and tend to avoid massive, bright, early-type, red galaxies, characteristically found in walls. Maps of the Universe produced using optical and infrared surveys trace the same large-scale structure; maps produced using H I surveys identify the same voids, but do not trace denser regions as well. Thus, we

find higher fractions of void galaxies in the ALFALFA sample. Although blind H I surveys are biased against galaxies typically found in clusters, we still find H I selected galaxies follow environmental trends similar to those found in optical surveys. That is, void galaxies from blind H I surveys are *bluer* and *fainter* than wall galaxies from the same survey.

5.2 Does the void environment affect the formation/evolution of galaxies?

Voids produce less massive and fainter galaxies than denser environments. Large-scale voids provide a unique environment for galaxies to form and evolve relatively undisturbed. The relative infrequency of galaxy mergers in cosmic voids results in fainter, less massive galaxies than found in denser regions. Thus, it is no surprise that we find a shift in the HIMF towards lower masses in voids in Chapter 2. We find a shift of $\Delta \log(M_{HI}) = 0.14$ (a factor of 1.4) rather than the much larger shifts seen in e.g. optical LFs of optically selected samples, because ALFALFA is biased against bright, early-type, passive galaxies commonly detected in clusters by optical surveys. Haynes et al. (1984) find that massive cluster galaxies tend to be H I deficient. In terms of magnitudes, we find the optical LF shifts towards fainter magnitudes in voids by a full magnitude (a factor of 2.5) for optically selected galaxies in Chapter 3, confirming the results of previous works on the shift in characteristic magnitude between void and wall galaxies. We measure a shift in the optical LF of ALFALFA galaxies of only $\Delta M_r \sim 0.5$ towards fainter magnitudes in voids. The shift of the ALFALFA LF is much smaller than that of the SDSS LF, because of the bias in the ALFALFA survey against bright, early-type, cluster galaxies.

Voids contain fewer galaxies than walls. We find that there are fewer dwarf galaxies in voids compared to walls. When we compare the HIMF of void and wall galaxies, we find a lower amplitude for void galaxies (see Table 2.1). Integrating under the void and wall HIMF curves reveals fewer galaxies per $h^{-3}\mathrm{Mpc}^3$ in voids for the ALFALFA Survey. Similarly, the amplitude of the optical LF of SDSS void galaxies is smaller than the amplitude of the optical LF of SDSS wall galaxies. Integrating under the void and wall LFs produces fewer void galaxies than wall galaxies per $h^{-3}\mathrm{Mpc}^3$ for the SDSS.

The relative abundance of dwarfs compared to brighter galaxies does not vary between voids and

walls. We estimate similar low-mass end slopes in the void and wall HIMFs. Although there is variation in the low-mass slope when comparing small-scale environmental differences (i.e. groups versus clusters), there is not a pronounced difference between voids and walls, where walls include a variety of small scale dense environments. This is interesting, because there are strong feedback effects in the Universe that should be more pronounced in denser regions. Additionally, the hydrodynamic simulations of Cen (2011) indicate that the gas in voids should have lower entropy than the gas in clusters. Gas in voids should then more easily condense and cool onto galaxies, allowing for the possibility of higher star formation rates in voids. Therefore, we find it puzzling that the low-mass slopes of the void and wall HIMFs are so similar. Additionally, we find the faint-end slopes of the void and wall LF to be nearly the same. Again, the faint-end slope of the LF seems to vary on smaller density scales. The similar faint-end slopes across the void and wall environments are consistent with predictions of the luminosity function from hydrodynamic simulations (e.g. GIMIC; Crain et al. 2009) and semi-analytic models (Bower et al., 2006) down to $M_r = -16$. See Cui et al. (2011) for a comparison of these predictions against the global SDSS LF from Blanton et al. (2001). A challenge to ΛCDM theory is to determine how feedback mechanisms vary the faint-end slopes of LFs across small-scale densities.

5.3 Are there low-luminosity galaxies in voids to match the low-mass halos predicted by LCDM?

We find no evidence of a population of low-luminosity galaxies in voids numerous enough to match the low-mass halos predicted by ΛCDM . The HIMF of void galaxies from the ALFALFA survey has a low-mass slope of $\alpha \sim -1.35$, a value similar to the global HIMF for ALFALFA. Similarly, the SDSS LF faint-end slope for void galaxies has a slope of $\alpha \sim -1.25$; this value is also in agreement with previous estimates of the global SDSS LF. Thus, the low-mass-end slope of the void HIMF of H I selected galaxies and the faint-end slope of the void LF of optically selected galaxies are not steep enough to match the predicted number of low-mass dark matter halos (DMHs).

The inclusion of low-surface-brightness galaxies steepens the faint-end slope of the observed optical LF, but not enough to match the predicted number of low-mass DMHs. Blanton et al. (2005b) find

that correcting the global SDSS LF for the effects of low-surface-brightness (LSB) galaxies should steepen the faint-end slope up to $\alpha \sim -1.5$. An H I selected catalog should be free from optical surface brightness selection effects; therefore, we estimate the effects of H I selection on the optical LF. We find the optical LF of ALFALFA detections steepens the faint-end slope from $\alpha = -1.25$ for the SDSS optical LF to $\alpha = -1.49$. The contribution of LSB galaxies to the faint-end slope of the optical LF is substantial. Spectroscopic measurements of fainter galaxies should be taken to include LSB galaxies in estimates of the LF. This will give us a more accurate estimate of the true optical LF faint-end slope.

We do not observe a population of gas-rich, optically-faint galaxies in void centers. The high-resolution, hydrodynamic simulation of Kreckel et al. (2011) predict the presence of ultra-low-luminosity galaxies residing in void centers. Using the ALFALFA survey, which contains a larger population of LSB galaxies, we do not find an excess of $M_r \geq -14$ galaxies in the centers of our cosmic voids. Figure 5.1 compares the magnitude distribution of galaxies predicted to reside in a simulated void center by Kreckel et al. (2011) (depicted as the blue dashed line in the upper panel) to the stacked magnitude distribution of ALFALFA detections observed in void centers (depicted by the solid blue line in the lower panel). We scale each void by its effective radius R_{eff} and define the void centers as the sphere of radius $r/R_{eff} \leq 0.3$. Although Pan (2011) finds that Ly-α absorbers in voids preferentially reside in void centers, we do not observe a population of optically-faint or gas-rich galaxies in void centers. Figure 5.2 compares the voidcentric distances of ALFALFA detections to the voidcentric distances of the Ly-α absorbers in Pan (2011). We find that ALFALFA detections actually prefer the outer edges of voids rather than the void centers.

5.4 Can the mismatch in observed dwarf counts and predicted low-mass halo counts be reconciled by suppressing star formation in dwarf galaxies in simulations?

The mismatch between theory and observation can be reconciled by the inclusion of star formation suppression effects, and hydrodynamic simulations may need to scale back the effects they currently employ. To better match observations, theorists tune hydrodynamic simulation parameters to match

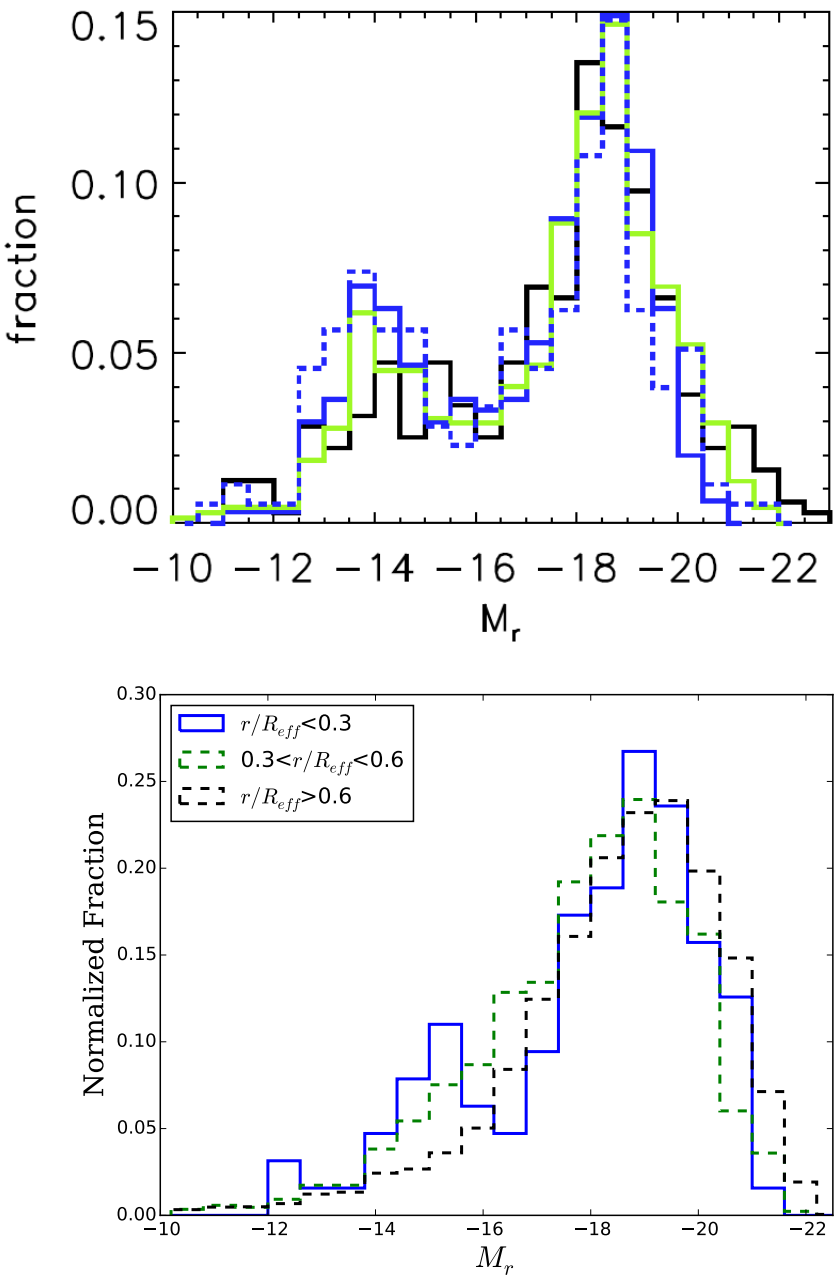

Figure 5.1 Top: The blue dashed line represents the absolute magnitude distribution of galaxies in void centers from Kreckel et al. (2011). There is an excess of dwarf galaxies with $-15 \leq M_r \leq -12$ in the center of one simulated void. Bottom: The solid blue line represents the magnitude distribution of ALFALFA galaxies within the inner sphere of each void stacked together. The radius of the inner sphere is 1/3 of the effective radius (R_{eff}) of each void. We see a population of faint galaxies within the centers; however, these galaxies are not as faint as the ultra-low-luminosities predicted by Kreckel et al. (2011).

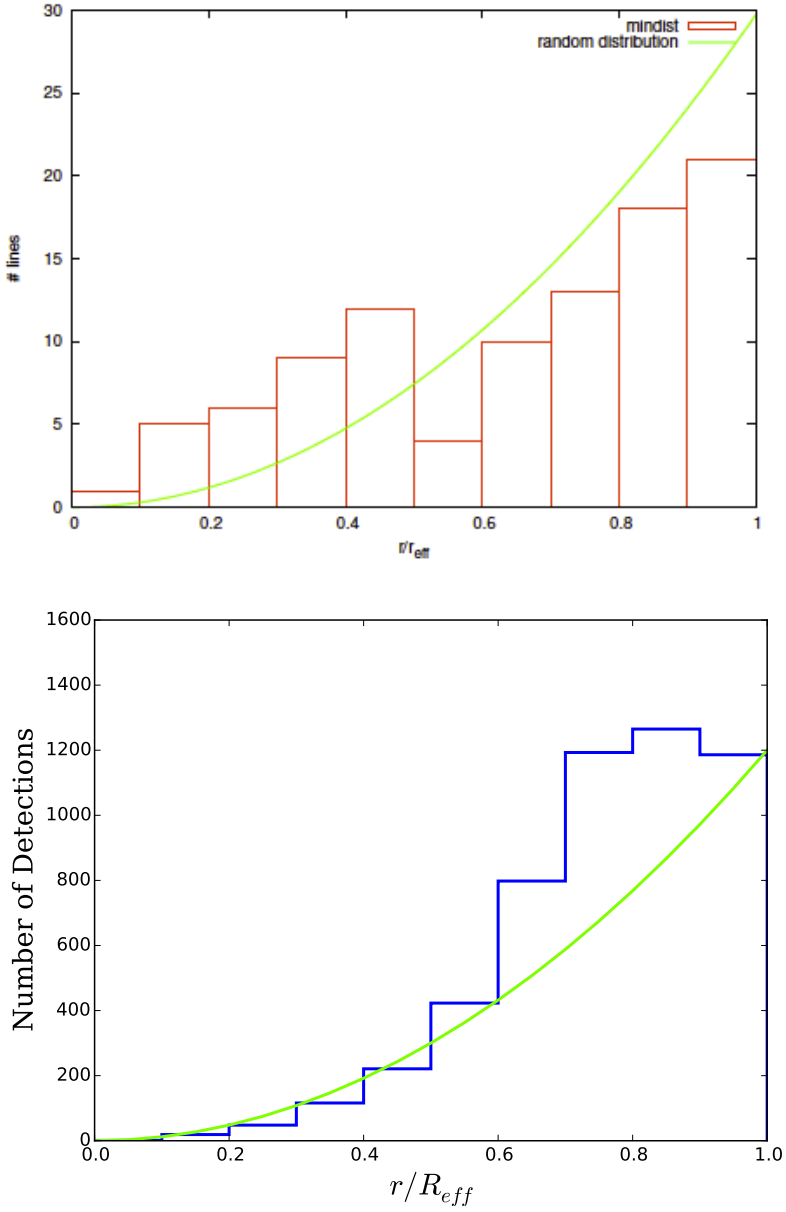

Figure 5.2 Top: Number distribution of Ly-α absorbers in voids as a function of distance from the void center from Pan (2011). The green line represents a random distribution following an $N(r) \propto r^2$ distribution. Pan (2011) finds that Ly-α absorbers prefer the void centers. Bottom: Number distribution of ALFALFA galaxies as a function of voidcentric distance. Following Pan (2011), we provide an $N(r) \propto r^2$ distribution to which we may compare the void galaxy distribution. Rather than a preference for residing in void centers, we find an excess of H I detections towards the outer shells of voids.

fundamental galaxy properties (i.e. the galaxy LF, color distribution, magnitude distribution, etc.). Most simulations (see, for example, Croton et al. 2006; Bower et al. 2006; Hoeft & Gottlöber 2010 and Cen 2011) incorporate star formation suppression effects from various sources to decrease the number of predicted dwarf halos to match the number density of galaxies predicted by the faint-end slope of the optical LF. Semi-analytic models (SAMs) (Bower et al., 2006; De Lucia & Blaizot, 2007) and hydrodynamic simulations (Crain et al. 2009) with resolutions high enough to detect galaxies down to $M_r = -16$ estimate low mass slopes similar to those of Blanton et al. (2001) ($\alpha = -1.2$). We find in Chapter 3 that the inclusion of LSB galaxies–from H I selected samples–substantially steepens the slope of the optical LF to $\alpha \sim -1.5$. The implication of this steeper slope is that there *is* a population of optically-faint galaxies that has not been accounted for in simulations that have adjusted their parameters to reproduce the shallow slope of the optically-selected LF. Thus, future hydrodynamic simulations and SAMs likely do not need to suppress star formation as much as suggested by the shallow faint-end slope of previous estimates of the optical LF.

Predictions of void dwarf galaxy properties in simulations that apply star formation suppression effects produce results consistent with reality. The agreement between simulated and observed galaxy properties reinforces the fact that star formation suppression effects are needed in simulations. Relatively few simulations have the resolution to predict properties of galaxies down into the dwarf regime. To date, the best predictor of dwarf galaxy properties is the high-resolution, hydrodynamic simulation of Cen (2011) which includes star formation suppression effects from the UV background (with a model for shielding of UV radiation by H I) and supernova feedback. They do not include feedback effects from AGN, but this effect primarily serves to suppress star formation in the brightest galaxies; therefore, it is not important to our analysis. We compare the results of this simulation to our dwarf galaxy SFR results in Chapter 4, and determine that the predictions of void dwarf galaxies in this simulation are consistent with properties of actual void dwarf galaxies. Void galaxies have higher specific star formation rates (SSFRs) than wall galaxies. This was previously known for brighter galaxies in voids (e.g. Rojas et al., 2005). Our results reveal that this trend continues into the dwarf galaxy regime down to $M_r = -13$. Void dwarf galaxies have higher SSFRs than

brighter void galaxies. Our estimates are consistent with the results of the high-resolution, hydrodynamic simulations of Cen (2011), which predict higher SSFRs in void dwarf galaxies than galaxies in denser regions. Cen (2011) further predict that the entropy of gas in voids is much lower than in denser regions, allowing the gas to condense and cool and further fuel star formation. Given the decreasing trend of SSFR with stellar mass, the low stellar masses of dwarf galaxies, and the low entropy in voids, void dwarf galaxies have SSFRs large enough that they could double their current stellar mass within a Hubble time. Most dwarf galaxies in our sample have SSFRs above the rate at which they should double their stellar mass in a Hubble time. We find a higher fraction of ALFALFA dwarf galaxies have rates above this threshold, because dwarf galaxies detected in H I tend to be gas dominated. A challenge to galaxy formation theory is to incorporate star formation suppression mechanisms in simulations in such a way that dwarf galaxies have higher SSFRs than brighter galaxies *and* void galaxies have higher SSFRs than wall galaxies.

We find that dwarf galaxies have lower SFEs than brighter galaxies; this may indicate the need for the inclusion of star formation suppression effects in dwarf galaxies in simulations. At face value, the lower SFEs in dwarf galaxies implies that the mechanisms driving star formation in dim galaxies are not as efficient as those driving star formation in brighter galaxies. Of the galaxies that do have enough gas to be detected by ALFALFA, we find that the efficiency of void dwarf galaxies is similar to wall dwarf galaxies with similar stellar masses. A caveat here is that we are only considering a special subset of galaxies; this is not a general statement about all galaxies. Blind H I surveys are biased against cluster environments, and stellar mass has a strong environmental dependence. Here we are only analyzing H I selected galaxies with high S/N, and we downsample the wall galaxies such that the void and wall stellar mass distributions match. Once we demand large H I S/N and control for stellar mass, we have likely removed any environmental dependence from the samples, so this result is not surprising. In Chapter 4, we see only a *small hint* that SFEs are lower in voids. H I selected dwarf galaxies are dominated by their H I mass, more so for void dwarf galaxies than wall dwarf galaxies. *If* void dwarfs are, indeed, less efficient at converting their gas to stars, this could imply stronger star formation suppression needs to be applied to void dwarfs than wall dwarfs. A

challenge to simulations is to explain what feedback mechanisms are suppressing star formation such that dwarf galaxies have lower SFEs and higher SSFRs than brighter galaxies galaxies.

5.5 Suggestions for Future Work

Void galaxies are predicted to be less massive than wall galaxies by DM simulations, and have been observed to be much fainter. We find the shift of the characteristic mass/magnitude between void and wall galaxies in the HIMF/LF of H I selected galaxies is significantly smaller than the shift found for the galaxy LF of optically selected galaxies. We wonder how much of the shift in H I masses is due to the shift in the characteristic mass/magnitude towards lower masses/magnitudes in voids. A next step might be to calculate the differences in the void and wall HIMFs for galaxies within similar stellar or dynamical mass ranges. This would give us a better indication of how the void environment affects the shape of the HIMF and the overall H I gas content of galaxies.

In principle, we can more directly probe the observed galaxy mass function via the velocity width function (WF) rather than using the LF or HIMF. However, due to large uncertainties in the void and wall WFs, we can not make any substantial claims about the environmental impact of the typical rotational velocities of the H I clouds. Unfortunately, relating the WF to the galaxy mass function is fraught with difficulties in interpretation. Simulations predict the halo circular velocity function (see Chapter 2 for references), which is not easily computed from the H I-detected WF. Papastergis et al. (2011) explore the relation between the observed WF and the predicted circular velocity function, but this relation requires many assumptions about the halo-galaxy relation and about the distribution of high velocity width galaxies which ALFALFA is biased against. Exploring these relations to determine the large-scale environmental impact on the galaxy mass function is beyond the scope of this work. To better ascertain the environmental effect on the true rotational velocities of ALFALFA galaxies, one could correct the H I-line width (W_{50}) values for galactic inclination via SDSS photometry and convert the corrected widths to rotational velocities. Care must be taken in estimating dynamical masses from H I disks, because gas stripping effects often remove H I from the outskirts of galaxies such that the H I disk does not extend to the edges of the rotation curve. This would lead to an underestimation of the halo mass.

In Chapter 3, we find that the ALFALFA LF has a broad dip centered around $M_r \sim -18$. To date, we are unaware of the origins of this feature. We know that it is not solely due to the survey volume covered by the $\alpha.40$ catalog, because the SDSS LF analyzed over the same volume does not produce a wide dip in the optical LF. Additionally, we do not find a type of galaxy prominent in the ALFALFA population that reproduces this feature. That is, we find a similar dip in the LF of optically selected red, late-type galaxies, but these galaxy properties are uncharacteristic of typical galaxies associated with ALFALFA detections. Processing of the full ALFALFA data is incomplete at present and inclusion of the remainder of the ALFALFA catalog in the LF analysis may provide insight to the source of the feature. Analyzing the LF of future, deeper, wider-area blind H I surveys may remove the feature from the H I selected galaxy optical LF.

In the halo occupation distribution (HOD) model, galaxies are considered either central galaxies or satellites of central galaxies. In denser regions, dwarf galaxies are often satellites within the halo of central galaxies, whereas void dwarf galaxies are often central galaxies themselves. Thus, void dwarf galaxies should have a very different local environment than wall dwarf galaxies. From this, we expect the properties of void and wall dwarf galaxies should be very different. We have not measured how local environment of void and wall dwarf galaxies affects their properties. An interesting question is: What fraction of dwarf galaxies in voids and walls are central galaxies in the HOD picture, and how does local environment affect their properties?

Maps of the matter distribution in the local Universe, as seen in IR and optical surveys trace the same large-scale structure. H I surveys identify the same large-scale voids, but undersample the walls due to the gas-stripping interactions prominent in denser environments. Based on the galaxy samples used in Chapter 4, ALFALFA detects 11% of stellar mass-matched void dwarf galaxies and only 7% of stellar mass-matched wall dwarf galaxies. There is a sample of wall dwarf galaxies (with similar stellar masses to those in voids) that ALFALFA is missing due to the H I masses of these dwarfs having S/N lower than the survey sensitivity of ALFALFA. Estimating an upper limit on H I masses for all dwarf galaxy non-detections may give us a better idea of the true shift in the SFE of void and wall galaxies. Assuming a void dwarf galaxy and wall dwarf galaxy have the same

stellar mass/magnitude, the void dwarf galaxy is more likely to retain its gas than the wall dwarf galaxy due to the prominence of gas-stripping phenomena in denser regions. This would give the void dwarf galaxy a lower SFE than the wall dwarf galaxy. Thus, we suspect that even with stellar mass-matching, we might find a shift towards lower SFEs in void dwarf galaxies, indicating the need for stronger star formation suppression in voids, bringing us closer to resolving the discrepancy between the predicted and observed densities of dwarf galaxies in voids.

Bibliography

Abazajian, K. N., Adelman-McCarthy, J. K., Agüeros, M. A., et al. 2009, ApJS, 182, 543

Abramson, L. E., Williams, R. J., Benson, A. J., Kollmeier, J. A., & Mulchaey, J. S. 2013, ArXiv e-prints, arXiv:1307.6555 [astro-ph.CO]

Aihara, H., Allende Prieto, C., An, D., et al. 2011, ApJS, 195, 26

Aikio, J., & Maehoenen, P. 1998, ApJ, 497, 534

Alpaslan, M., Robotham, A. S. G., Obreschkow, D., et al. 2014, MNRAS, 440, L106

Alpaslan, M., Driver, S., Robotham, A. S. G., et al. 2015, ArXiv e-prints, arXiv:1505.05518

Aragon-Calvo, M. A., & Szalay, A. S. 2013, MNRAS, 428, 3409

Aragon-Calvo, M. A., van de Weygaert, R., Araya-Melo, P. A., Platen, E., & Szalay, A. S. 2010, MNRAS, 404, L89

Basilakos, S., Plionis, M., Kovač, K., & Voglis, N. 2007, MNRAS, 378, 301

Benson, A. J., Hoyle, F., Torres, F., & Vogeley, M. S. 2003, MNRAS, 340, 160

Benson, A. J., Lacey, C., Baugh, C., Cole, S., & Frenk, C. 2002, in Astronomical Society of the Pacific Conference Series, Vol. 254, Extragalactic Gas at Low Redshift, ed. J. S. Mulchaey & J. T. Stocke, 354

Beygu, B., Kreckel, K., van de Weygaert, R., van der Hulst, J. M., & van Gorkom, J. H. 2013, AJ, 145, 120

Beygu, B., Kreckel, K., van der Hulst, J. M., et al. 2015, ArXiv e-prints, arXiv:1501.02577

Bigiel, F., Leroy, A., Walter, F., et al. 2010, AJ, 140, 1194

Blanton, M. R., Eisenstein, D., Hogg, D. W., Schlegel, D. J., & Brinkmann, J. 2005a, ApJ, 629, 143

Blanton, M. R., Kazin, E., Muna, D., Weaver, B. A., & Price-Whelan, A. 2011, AJ, 142, 31

Blanton, M. R., Lin, H., Lupton, R. H., et al. 2003a, AJ, 125, 2276

Blanton, M. R., Lupton, R. H., Schlegel, D. J., et al. 2005b, ApJ, 631, 208

Blanton, M. R., & Roweis, S. 2007, AJ, 133, 734

Blanton, M. R., Dalcanton, J., Eisenstein, D., et al. 2001, AJ, 121, 2358

Blanton, M. R., Hogg, D. W., Bahcall, N. A., et al. 2003b, ApJ, 592, 819

Blanton, M. R., Schlegel, D. J., Strauss, M. A., et al. 2005c, AJ, 129, 2562

Bond, J. R., Kofman, L., & Pogosyan, D. 1996, Nature, 380, 603

Bower, R. G., Benson, A. J., Malbon, R., et al. 2006, MNRAS, 370, 645

Boylan-Kolchin, M., Springel, V., White, S. D. M., Jenkins, A., & Lemson, G. 2009, MNRAS, 398, 1150

Bruzual, G., & Charlot, S. 2003, MNRAS, 344, 1000

Catinella, B., Schiminovich, D., Kauffmann, G., et al. 2010, MNRAS, 403, 683

Cen, R. 2011, ApJ, 741, 99

Choi, Y.-Y., Han, D.-H., & Kim, S. S. 2010, Journal of Korean Astronomical Society, 43, 191

Colberg, J. M., Pearce, F., Foster, C., et al. 2008, MNRAS, 387, 933

Colless, M., Dalton, G., Maddox, S., et al. 2001, MNRAS, 328, 1039

Conroy, C., Coil, A. L., White, M., et al. 2005, The Astrophysical Journal, 635, 990

Couchman, H. M. P., & Rees, M. J. 1986, MNRAS, 221, 53

Crain, R. A., Theuns, T., Dalla Vecchia, C., et al. 2009, MNRAS, 399, 1773

Croton, D. J., & Farrar, G. R. 2008, MNRAS, 386, 2285

Croton, D. J., Farrar, G. R., Norberg, P., et al. 2005, MNRAS, 356, 1155

Croton, D. J., Springel, V., White, S. D. M., et al. 2006, MNRAS, 365, 11

Cui, W., Springel, V., Yang, X., De Lucia, G., & Borgani, S. 2011, MNRAS, 416, 2997

da Costa, L. N., Pellegrini, P. S., Sargent, W. L. W., et al. 1988, ApJ, 327, 544

De Lucia, G., & Blaizot, J. 2007, MNRAS, 375, 2

De Propris, R., Colless, M., Driver, S. P., et al. 2003, MNRAS, 342, 725

Desai, V., Dalcanton, J. J., Reed, D., et al. 2004, MNRAS, 351, 265

Driver, S. P., Allen, P. D., Liske, J., & Graham, A. W. 2007, ApJ, 657, L85

Durret, F., Adami, C., & Laganá, T. F. 2011, in IAU Symposium, Vol. 277, IAU Symposium, ed. C. Carignan, F. Combes, & K. C. Freeman, 9

Efron, B. 1982, The Jackknife, the Bootstrap, and Other Resampling Plans (Philadelphia, PA: Society for Industrial and Applied Mathematics)

Efstathiou, G., Ellis, R. S., & Peterson, B. A. 1988, MNRAS, 232, 431

Eke, V. R., Frenk, C. S., Baugh, C. M., et al. 2004, MNRAS, 355, 769

El-Ad, H., & Piran, T. 1997, ApJ, 491, 421

—. 2000, MNRAS, 313, 553

El-Ad, H., Piran, T., & da Costa, L. N. 1997, MNRAS, 287, 790

Elbaz, D., Daddi, E., Le Borgne, D., et al. 2007, A&A, 468, 33

Elyiv, A. A., Karachentsev, I. D., Karachentseva, V. E., Melnyk, O. V., & Makarov, D. I. 2013, Astrophysical Bulletin, 68, 1

Fisher, K. B., Huchra, J. P., Strauss, M. A., et al. 1995, ApJS, 100, 69

Fukugita, M., Ichikawa, T., Gunn, J. E., et al. 1996, AJ, 111, 1748

Geha, M., Blanton, M. R., Yan, R., & Tinker, J. L. 2012, ApJ, 757, 85

Geller, M. J., & Huchra, J. P. 1989, Science, 246, 897

Giovanelli, R., & Haynes, M. P. 1985, AJ, 90, 2445

Giovanelli, R., Haynes, M. P., Kent, B. R., et al. 2005a, AJ, 130, 2598

—. 2005b, AJ, 130, 2613

—. 2007, AJ, 133, 2569

Giovanelli, R., Haynes, M. P., Adams, E. A. K., et al. 2013, AJ, 146, 15

Goldberg, D. M., Jones, T. D., Hoyle, F., et al. 2005, ApJ, 621, 643

Goldberg, D. M., & Vogeley, M. S. 2004, ApJ, 605, 1

Gottlöber, S., Łokas, E. L., Klypin, A., & Hoffman, Y. 2003, MNRAS, 344, 715

Grogin, N. A., & Geller, M. J. 1999, AJ, 118, 2561

Gunn, J. E., Carr, M., Rockosi, C., et al. 1998, AJ, 116, 3040

Haynes, M. P. 2008, in Astronomical Society of the Pacific Conference Series, Vol. 395, Frontiers of Astrophysics: A Celebration of NRAO's 50th Anniversary, ed. A. H. Bridle, J. J. Condon, & G. C. Hunt, 125

Haynes, M. P., Giovanelli, R., & Chincarini, G. L. 1984, ARA&A, 22, 445

Haynes, M. P., Giovanelli, R., Martin, A. M., et al. 2011, AJ, 142, 170

Hoeft, M., & Gottlöber, S. 2010, Advances in Astronomy, 2010, 87

Hoeft, M., Yepes, G., Gottlöber, S., & Springel, V. 2006, MNRAS, 371, 401

Hopkins, A. M., Miller, C. J., Nichol, R. C., et al. 2003, ApJ, 599, 971

Hoyle, F., Rojas, R. R., Vogeley, M. S., & Brinkmann, J. 2005, ApJ, 620, 618

Hoyle, F., & Vogeley, M. S. 2002, ApJ, 566, 641

—. 2004, ApJ, 607, 751

Hoyle, F., Vogeley, M. S., & Pan, D. 2012, MNRAS, 426, 3041

Huang, S., Haynes, M. P., Giovanelli, R., & Brinchmann, J. 2012a, ApJ, 756, 113

Huang, S., Haynes, M. P., Giovanelli, R., et al. 2012b, AJ, 143, 133

Icke, V. 1984, MNRAS, 206, 1P

Jones, D. H., Saunders, W., Colless, M., et al. 2004, MNRAS, 355, 747

Karachentsev, I. D., Karachentseva, V. E., Huchtmeier, W. K., & Makarov, D. I. 2004, AJ, 127, 2031

Karachentseva, V. E., Mitronova, S. N., Melnyk, O. V., & Karachentsev, I. D. 2010, Astrophysical Bulletin, 65, 1

Kauffmann, G., & Fairall, A. P. 1991, MNRAS, 248, 313

Kennicutt, Jr., R. C. 1998, ARA&A, 36, 189

Kent, B. R., Giovanelli, R., Haynes, M. P., et al. 2008, AJ, 136, 713

Klypin, A., Kravtsov, A. V., Valenzuela, O., & Prada, F. 1999, ApJ, 522, 82

Klypin, A. A., Trujillo-Gomez, S., & Primack, J. 2011, ApJ, 740, 102

Koposov, S. E., Yoo, J., Rix, H.-W., et al. 2009, ApJ, 696, 2179

Kovac, K. 2007, PhD thesis, University of Groningen

Kreckel, K., Joung, M. R., & Cen, R. 2011, ApJ, 735, 132

Kreckel, K., Platen, E., Aragón-Calvo, M. A., et al. 2012, AJ, 144, 16

Lackner, C. N., Cen, R., Ostriker, J. P., & Joung, M. R. 2012, MNRAS, 425, 641

Lee, J. C., Gil de Paz, A., Tremonti, C., et al. 2009, ApJ, 706, 599

Loveday, J. 2000, MNRAS, 312, 557

Loveday, J., Norberg, P., Baldry, I. K., et al. 2012, MNRAS, 420, 1239

Lupton, R., Gunn, J. E., Ivezić, Z., Knapp, G. R., & Kent, S. 2001, in Astronomical Society of the Pacific Conference Series, Vol. 238, Astronomical Data Analysis Software and Systems X, ed. F. R. Harnden, Jr., F. A. Primini, & H. E. Payne, 269

Madgwick, D. S., Lahav, O., Baldry, I. K., et al. 2002, MNRAS, 333, 133

Martin, A. M. 2011, PhD thesis, Cornell University, New York, USA

Martin, A. M., Giovanelli, R., Haynes, M. P., et al. 2009, ApJS, 183, 214

Martin, A. M., Papastergis, E., Giovanelli, R., et al. 2010, ApJ, 723, 1359

Martin, D. C., Fanson, J., Schiminovich, D., et al. 2005, ApJ, 619, L1

Martinet, M., Durret, F., Guennou, L., & Adami, C. 2014a, in SF2A-2014: Proceedings of the Annual meeting of the French Society of Astronomy and Astrophysics, ed. J. Ballet, F. Martins, F. Bournaud, R. Monier, & C. Reylé, 347

Martinet, N., Durret, F., Guennou, L., et al. 2014b, ArXiv e-prints, arXiv:1412.5821

Masters, K. L., Haynes, M. P., & Giovanelli, R. 2004, ApJ, 607, L115

Mathis, H., & White, S. D. M. 2002, MNRAS, 337, 1193

McNaught-Roberts, T., Norberg, P., Baugh, C., et al. 2014, MNRAS, 445, 2125

Melnyk, O. V., Karachentseva, V. E., Karachentsev, I. D., Makarov, D. I., & Chilingarian, I. V. 2009, Astrophysics, 52, 184

Meyer, M. J., Zwaan, M. A., Webster, R. L., et al. 2004, MNRAS, 350, 1195

Moorman, C. M., Vogeley, M. S., Hoyle, F., et al. 2014, MNRAS, 444, 3559

Neyrinck, M. C. 2008, MNRAS, 386, 2101

Pan, D. C. 2011, PhD thesis, Drexel University

Pan, D. C., Vogeley, M. S., Hoyle, F., Choi, Y.-Y., & Park, C. 2012, MNRAS, 421, 926

Papastergis, E., Cattaneo, A., Huang, S., Giovanelli, R., & Haynes, M. P. 2012, ApJ, 759, 138

Papastergis, E., Giovanelli, R., Haynes, M. P., Rodríguez-Puebla, A., & Jones, M. G. 2013, ApJ, 776, 43

Papastergis, E., Martin, A. M., Giovanelli, R., & Haynes, M. P. 2011, ApJ, 739, 38

Park, C., Choi, Y.-Y., Kim, J., et al. 2012, ApJ, 759, L7

Park, C., Choi, Y.-Y., Vogeley, M. S., et al. 2007, ApJ, 658, 898

Patiri, S. G., Prada, F., Holtzman, J., Klypin, A., & Betancort-Rijo, J. 2006, MNRAS, 372, 1710

Peebles, P. J. E. 2001, ApJ, 557, 495

Pisano, D. J., Barnes, D. G., Staveley-Smith, L., et al. 2011, ApJS, 197, 28

Plionis, M., & Basilakos, S. 2002, MNRAS, 330, 399

Press, W. H., & Schechter, P. 1974, ApJ, 187, 425

Ramos, B. H. F., Pellegrini, P. S., Benoist, C., et al. 2011, AJ, 142, 41

Ricciardelli, E., Cava, A., Varela, J., & Quilis, V. 2014, MNRAS, 445, 4045

Ricciardelli, E., Quilis, V., & Planelles, S. 2013, MNRAS, 434, 1192

Rieder, S., van de Weygaert, R., Cautun, M., Beygu, B., & Portegies Zwart, S. 2013, MNRAS, 435, 222

Rojas, R. R., Vogeley, M. S., Hoyle, F., & Brinkmann, J. 2004, ApJ, 617, 50

—. 2005, ApJ, 624, 571

Rosenberg, J. L., & Schneider, S. E. 2000, VizieR Online Data Catalog, 213, 177

—. 2002, ApJ, 567, 247

Saintonge, A., Giovanelli, R., Haynes, M. P., et al. 2008, AJ, 135, 588

Salim, S., Rich, R. M., Charlot, S., et al. 2007, ApJS, 173, 267

Saunders, W., Sutherland, W. J., Maddox, S. J., et al. 2000, MNRAS, 317, 55

Sawala, T., Frenk, C. S., Fattahi, A., et al. 2014, ArXiv e-prints, arXiv:1406.6362

Schaap, W. E., & van de Weygaert, R. 2000, A&A, 363, L29

Schechter, P. 1976, ApJ, 203, 297

Sheth, R. K., & van de Weygaert, R. 2004, MNRAS, 350, 517

Sheth, R. K., Bernardi, M., Schechter, P. L., et al. 2003, ApJ, 594, 225

Shimasaku, K., Fukugita, M., Doi, M., et al. 2001, AJ, 122, 1238

Sigad, Y., Kolatt, T. S., Bullock, J. S., et al. 2000, ArXiv Astrophysics e-prints, arXiv:astro-ph/0005323

Springel, V., White, S. D. M., Jenkins, A., et al. 2005, Nature, 435, 629

Springob, C. M., Haynes, M. P., & Giovanelli, R. 2005, ApJ, 621, 215

Stanonik, K., Platen, E., Aragón-Calvo, M. A., et al. 2009, ApJ, 696, L6

Stierwalt, S., Haynes, M. P., Giovanelli, R., et al. 2009, AJ, 138, 338

Strauss, M. A., Weinberg, D. H., Lupton, R. H., et al. 2002, AJ, 124, 1810

Sutter, P. M., Lavaux, G., Wandelt, B. D., & Weinberg, D. H. 2012, ApJ, 761, 44

Tassis, K., Kravtsov, A. V., & Gnedin, N. Y. 2008, ApJ, 672, 888

Tempel, E., Saar, E., Liivamägi, L. J., et al. 2011, A&A, 529, A53

Tinker, J. L., Conroy, C., Norberg, P., et al. 2008, ApJ, 686, 53

Toribio, M. C., & Solanes, J. M. 2009, AJ, 138, 1957

Toribio, M. C., Solanes, J. M., Giovanelli, R., Haynes, M. P., & Martin, A. M. 2011a, ApJ, 732, 93

Toribio, M. C., Solanes, J. M., Giovanelli, R., Haynes, M. P., & Masters, K. L. 2011b, ApJ, 732, 92

Tully, R. B. 2005, in IAU Colloq. 198: Near-fields cosmology with dwarf elliptical galaxies, ed. H. Jerjen & B. Binggeli, 331

Tully, R. B., & Fisher, J. R. 1977, A&A, 54, 661

Umemura, M., & Ikeuchi, S. 1984, Progress of Theoretical Physics, 72, 47

Valotto, C. A., Nicotra, M. A., Muriel, H., & Lambas, D. G. 1997, ApJ, 479, 90

van de Weygaert, R., Platen, E., Tigrak, E., et al. 2010, in Astronomical Society of the Pacific Conference Series, Vol. 421, Galaxies in Isolation: Exploring Nature Versus Nurture, ed. L. Verdes-Montenegro, A. Del Olmo, & J. Sulentic, 99

van de Weygaert, R., & van Kampen, E. 1993, MNRAS, 263, 481

Verheijen, M. A. W., Trentham, N., Tully, B., & Zwaan, M. 2001, in Astronomical Society of the Pacific Conference Series, Vol. 240, Gas and Galaxy Evolution, ed. J. E. Hibbard, M. Rupen, & J. H. van Gorkom, 507

von Benda-Beckmann, A. M., & Müller, V. 2008, MNRAS, 384, 1189

Warren, M. S., Abazajian, K., Holz, D. E., & Teodoro, L. 2006, ApJ, 646, 881

Waugh, M., Drinkwater, M. J., Webster, R. L., et al. 2002, MNRAS, 337, 641

Willick, J. A., Courteau, S., Faber, S. M., et al. 1997, ApJS, 109, 333

Yan, R. 2011, AJ, 142, 153

Yan, R., & Blanton, M. R. 2012, ApJ, 747, 61

Yang, X., Mo, H. J., & van den Bosch, F. C. 2009, ApJ, 695, 900

York, D. G., Adelman, J., Anderson, Jr., J. E., et al. 2000, AJ, 120, 1579

Zavala, J., Jing, Y. P., Faltenbacher, A., et al. 2009, ApJ, 700, 1779

Zwaan, M. A., Briggs, F. H., & Sprayberry, D. 2001, MNRAS, 327, 1249

Zwaan, M. A., Meyer, M. J., & Staveley-Smith, L. 2010, MNRAS, 403, 1969

Zwaan, M. A., Meyer, M. J., Staveley-Smith, L., & Webster, R. L. 2005, MNRAS, 359, L30

Vita

Crystal M. Moorman was born in Lynchburg, Virginia in July 1986. She grew up in Forest, Virginia attending Brookville High School. She graduated from Lynchburg College where she double majored, receiving a Bachelor of Science in Physics and Mathematics in December 2008. After teaching physics for a semester, she began her graduate work at Drexel University. At Drexel, she served as a Teaching Assistant from 2009 to 2014, and as a Research Fellow from 2014 to 2015. She received her Masters of Science in Physics from Drexel University in June 2011, and finished her Doctorate of Philosophy in Physics in July 2015.